Power Systems Development Facility

Technical Progress Report For Kellogg Brown & Root Transport Reactor Train With Siemens Westinghouse Particulate Control Device

TC04: October 14 – October 17, 1998

DOE Cooperative Agreement Number
DE-FC21-90MC25140

SOUTHERN COMPANY
Energy to Serve Your World™

POWER SYSTEMS DEVELOPMENT FACILITY

TECHNICAL PROGRESS REPORT
FOR KELLOGG BROWN & ROOT
TRANSPORT REACTOR TRAIN
WITH SIEMENS WESTINGHOUSE
PARTICULATE CONTROL DEVICE

TC04 REPORT: OCTOBER 14 – 17, 1998

DOE Cooperative Agreement Number
DE-FC21-90MC25140

Prepared by:
Southern Company Services, Inc.
Power Systems Development Facility
P.O. Box 1069
Wilsonville, AL 35186

June 2000

DISCLAIMER

This report was prepared as an account of work sponsored by an agency of the United States Government. Neither the United States Government nor any agency thereof, nor any of their employees, nor Southern Company Services, Inc., nor any of its employees, nor any of its subcontractors, makes any warranty, expressed or implied, or assumes any legal liability or responsibility for the accuracy, completeness, or usefulness of any information, apparatus, product, or process disclosed, or represents that its use would not infringe privately owned rights. Reference herein to any specific commercial product, process, or service by trade name, trademark, manufacturer or otherwise, does not necessarily constitute or imply its endorsement, recommendation, or favoring by the United States Government or any agency thereof. The views and opinions of authors expressed herein do not necessarily state or reflect those of the United States Government or any agency thereof.

Available to the public from the National Technical Information Service, U.S. Department of Commerce, 5285 Port Royal Road, Springfield, VA 22161. Phone orders accepted at (703) 487-4650.

CONTENTS

Section Page

Inside Cover
Disclaimer

Listing of Tables and Figures iii

1.0 EXECUTIVE SUMMARY 1.1-1

1.1 Introduction 1.1-1
1.2 TC04 Run 1.2-1
1.3 TC04 Inspection Report 1.3-1
1.4 Filter Element Materials Test Results 1.4-1
1.5 Thermal Stress Analysis 1.5-1

2.0 INTRODUCTION 2.1-1

2.1 The Power Systems Development Facility 2.1-1
2.2 Transport Reactor System Description 2.2-1
2.3 Siemens Westinghouse Particulate Control Device 2.3-1
2.4 Operation Status 2.4-1

3.0 PARTICLE FILTER SYSTEM 3.1-1

3.1 TC04 Overview 3.1-1

3.2 PCD Operation During Test Run TC04 ..... 3.2-1
3.2.1 Introduction 3.2-1
3.2.2 Test Objectives 3.2-1
3.2.3 Observations/Events - October 14 Through October 17, 1998 ..... 3.2-1
3.2.4 Run Summary 3.2-2

3.3 TC04 Inspection Report 3.3-1
3.3.1 Introduction 3.3-1
3.3.2 Manway Inspection 3.3-2

3.3.3 PCD Disassembly 3.3-2
3.3.3.1 Filter Elements 3.3-2
3.3.3.2 Ash Observations 3.3-3

3.3.4 Conclusions 3.3-3

3.4 Filter Element Materials Test Report 3.4-1

3.4.1 3M Oxide/Oxide 3.4-2
3.4.1.1 Tensile Results 3.4-2
3.4.1.2 Compressive Results 3.4-3
3.4.1.3 Summary 3.4-4

3.4.2 IF&P REECER™ 3.4-4
3.4.2.1 Density 3.4-4
3.4.2.2 Tensile Results 3.4-4
3.4.2.3 Summary 3.4-5

3.4.3 Pall 326 - Study of As-Manufactured Candle Weights 3.4-5
3.4.3.1 Density 3.4-5
3.4.3.2 Tensile Results 3.4-6
3.4.3.3 Summary 3.4-6

3.4.4 Pall 326 Exposed Elements 3.4-6
3.4.4.1 Density 3.4-6
3.4.4.2 Tensile Results 3.4-6
3.4.4.3 Summary 3.4-7

3.4.5 Pall Iron Aluminide 3.4-7
3.4.5.1 Density 3.4-7
3.4.5.2 Tensile Results 3.4-7
3.4.5.3 Flow Test Results 3.4-8
3.4.5.4 Summary 3.4-8

3.4.6 Schumacher TF20 and T10-20 Exposed Elements 3.4-9
3.4.6.1 Density 3.4-9
3.4.6.2 Tensile Results 3.4-9
3.4.6.3 Summary 3.4-10

3.4.7 Conclusions 3.4-10
3.4.8 References 3.4-11

3.5 Thermal Stress Analysis 3.5-1
3.5.1 Nomenclature 3.5-1
3.5.2 Temperature Distribution in Filter Element 3.5-2
3.5.3 Thermal Stresses and Strains 3.5-6
3.5.4 ANSYS Finite Element Model Results 3.5-8
3.5.5 Conclusion 3.5-11
3.5.6 References 3.5-11

TERMS TERMS-1

Listing of Tables

Table Page

2.2-1 Major Equipment in the Transport Reactor Train 2.2-3
2.2-2 Major Equipment in the Balance-of-Plant 2.2-4

3.2-1 TC04 Run Statistics - 10/14/98 Through 10/17/98 ..... 3.2-4
3.2-2 TC04 Major Events - 10/14/98 Through 10/17/98 ..... 3.2-4

3.4-1 Filter Elements Tested 3.4-12
3.4-2 Test Matrix 1 ..... 3.4-13
3.4-3 Test Matrix 2 ..... 3.4-13
3.4-4 Test Matrix 3 ..... 3.4-13
3.4-5 Test Matrix 4 ..... 3.4-14
3.4-6 Test Matrix 5 ..... 3.4-14
3.4-7 Tensile Results of 3M Oxide-Oxide 3.4-15
3.4-8 Compressive Results of 3M Oxide-Oxide 3.4-16
3.4-9 Density of IF&P REECER™ 3.4-17
3.4-10 Hoop Tensile Strength of IF&P REECER™ 3.4-18
3.4-11 Density of As-Manufactured Pall 326 ..... 3.4-19
3.4-12 Hoop Tensile Strength of As-Manufactured Pall 326 ..... 3.4-21
3.4-13 Density of Pall 326 After Operation 3.4-23
3.4-14 Hoop Tensile Strength of Pall 326 After Operation 3.4-24
3.4-15 Density of Pall FeAl 3.4-25
3.4-16 Axial Tensile Results for Pall FeAl 3.4-26
3.4-17 Hoop Tensile Results for Pall FeAl 3.4-27
3.4-18 Density of Schumacher TF20 ..... 3.4-28
3.4-19 Density of Schumacher T10-20 ..... 3.4-29
3.4-20 Hoop Tensile Strength of Schumacher TF20 ..... 3.4-30
3.4-21 Hoop Tensile Strength of Schumacher T10-20 ..... 3.4-31

3.5-1 Filter Element Properties Used in Thermal Model 3.5-13
3.5-2 Comparison of Tensile Strains Calculated by 1-D Model and ANSYS 3-D Model 3.5-13

Listing of Figures

Figure Page

2.2-1 Flow Diagram of the Transport Reactor Train in Combustion Mode of Operation 2.2-7

2.3-1 Siemens Westinghouse PCD 2.3-2

2.4-1 Operating Hours Summary for Transport Reactor Train Major Combustion Test Campaigns Through TC04 ..... 2.4-2

3.2-1 Filter Element Layout for TC04 ..... 3.2-5
3.2-2 TC04 Temperature and Pressure for October 14 Through October 18 ..... 3.2-6
3.2-3 TC04 Back-pulse Pressure and Face Velocity for October 14 Through October 18 ..... 3.2-7
3.2-4 TC04 Pressure Drop and Permeance for October 14 Through October 18 ..... 3.2-8
3.2-5 Temperature Transient on October 17, 1998 ..... 3.2-9

3.3-1 Broken Filters After TC04 ..... 3.3-5
3.3-2 Broken Pall 326 Filter Elements During Manway Inspection 3.3-6
3.3-3 Broken 1.5-Meter Pall 326 Supported by Thermocouples 3.3-6
3.3-4 Sintered Dust Cake Fragment Lodged Between Filters 3.3-7
3.3-5 Broken Filters After TC04 ..... 3.3-8
3.3-6 Broken Ensto Filter After TC04 ..... 3.3-9
3.3-7 Broken Pall 326 From Center of Lower Plenum 3.3-10
3.3-8 Damaged Membrane on PRD 66 Filter 3.3-11
3.3-9 Sintered Ash Layer on McDermott Filter Element 3.3-12
3.3-10 Appearance of Ash Cake on Top Plenum 3.3-13

3.4-1 Cutting Plan for 3M Oxide/Oxide Filter Elements 3.4-32
3.4-2 Cutting Plan for IF&P REECER™ Filter Elements 3.4-33
3.4-3 Cutting Plan for As-Manufactured Pall 326 Filter Elements 3.4-34
3.4-4 Cutting Plan for Exposed Pall 326 Filter Elements 3.4-35
3.4-5 Cutting Plan for Pall FeAl Filter Elements 3.4-36
3.4-6 Cutting Plan for Schumacher TF20 Filter Elements 3.4-37
3.4-7 Cutting Plan for Schumacher T10-20 Filter Elements 3.4-38
3.4-8 Hoop Tensile Strength of 1- and 2-Inch-Long Pall 326 Specimens 3.4-39
3.4-9 Pinhole in Element 8174 After 1,420 Hours in Operation 3.4-40
3.4-10 Hoop Tensile Stress-Strain Responses for As-Manufactured 3M Oxide-Oxide Filter Elements 3.4-41
3.4-11 Hoop Tensile Stress-Strain Responses for 3M Oxide-Oxide After 1,420 Hours in Operation 3.4-41
3.4-12 Hoop Tensile Stress-Strain Responses for 3M Oxide-Oxide After 1,982 Hours in Operation Including PCD Fire 3.4-42
3.4-13 Hoop Tensile Strength Versus Hours of Operation for 3M Oxide-Oxide 3.4-42

3.4-14 Axial Compressive Stress-Strain Responses for As-Manufactured 3M Oxide-Oxide 3.4-43
3.4-15 Hoop Tensile Strength Versus Hours of Operation for IF&P REECER™ 3.4-43
3.4-16 As-Manufactured Hoop Tensile Strength Versus Element Weight for Pall 326 ..... 3.4-44
3.4-17 Hoop Tensile Strength Versus Hours of Operation for Pall 326 ..... 3.4-44
3.4-18 Axial Tensile Stress-Strain Responses for Pall FeAl 3.4-45
3.4-19 Room-Temperature Hoop Tensile Stress-Strain Responses of As-Manufactured Pall FeAl 3.4-45
3.4-20 Room-Temperature Hoop Tensile Stress-Strain Responses of Pall FeAl After 1,356 Hours in Operation 3.4-46
3.4-21 Room-Temperature Hoop Tensile Stress-Strain Responses of Pall FeAl After 1,424 Hours in Operation 3.4-46
3.4-22 Room-Temperature Tensile Strength Versus Hours of Operation for Pall FeAl 3.4-47
3.4-23 Pressure Drop Versus Flow Rate for Pall Iron Aluminide Element 034H005 ..... 3.4-47
3.4-24 Tensile Strength Versus Hours of Operation for Schumacher TF20 and T10-20 ..... 3.4-48

3.5-1 Finite Difference Model for Thermal Transient Temperature and Stress Calculations 3.5-14
3.5-2 Temperature Distribution Calculated From Thermal Model for a Temperature Increase of 315°F/55 sec at the OD 3.5-15
3.5-3 Temperature Gradient During Thermal Transient and κ/l^2 for Ceramic Filter Elements 3.5-15
3.5-4 Strain Distribution Calculated From Thermal Model for a Temperature Increase of 315°F/55 sec at the OD 3.5-16
3.5-5 Tensile Strain During Thermal Transient and κ/l^2 for Ceramic Filter Elements 3.5-16
3.5-6 Tensile Strain During Thermal Transient/Strain-to-Failure and κ/l^2 for Ceramic Filter Elements 3.5-17
3.5-7 ANSYS Finite Model With Uniform Temperature Increase on Outside Surface 3.5-18
3.5-8 Temperature Distribution With a Uniform Temperature Increase on the Outside Surface 3.5-19
3.5-9 Strain Distribution With a Uniform Temperature Increase on the Outside Surface 3.5-19
3.5-10 ANSYS 3-D Model With Temperature Increase Over a 3-Inch Hot Spot on Outside Surface 3.5-20
3.5-11 Temperature Distribution With an Increase of 315°F/55 sec Applied to a 3-Inch-Diameter Hot Spot 3.5-21
3.5-12 Strain Distribution With a Temperature Increase of 315°F/55 sec Applied to a 3-Inch-Diameter Hot Spot 3.5-21

3.5-13 Loads Produced on Elements by Circumferential Temperature Gradients....3.5-22
3.5-14 Strain Distribution in IF&P REECER™ Element With 3-Inch-Diameter Hot Spot....3.5-23
3.5-15 Strain Distribution in Schumacher TF20 Element With 3-Inch-Diameter Hot Spot....3.5-24
3.5-16 Strain Distribution in Blasch 4-270 Element With 3-Inch-Diameter Hot Spot....3.5-25
3.5-17 Axial Temperature Distribution in Coors Element With Hot Spot, 1,300°F/55 sec Temperature Increase....3.5-26

1.0 EXECUTIVE SUMMARY

1.1 INTRODUCTION

This report discusses test campaign TC04 of the Kellogg Brown & Root (KBR) transport reactor train with a Siemens Westinghouse Power Corporation (Siemens Westinghouse) particle filter system at the Power Systems Development Facility (PSDF) located in Wilsonville, Alabama. The transport reactor is an advanced circulating fluidized-bed reactor designed to operate as either a combustor or a gasifier using one of two possible particulate control devices (PCD). The transport reactor was operated as a pressurized combustor during test campaign TC04.

Thermal events have occasionally lead to the failure of many filter elements at the PSDF ever since operations began on coal feed in August 1996. Essentially all of these failures since September 1997 have occurred during the transient operating conditions while changing from the propane-fired start-up burner to coal feed. If the coal is fed to the transport reactor at a temperature too low to fully combust the coal it will be carried into the PCD where it will be removed from the gas by the filter elements. This burning coal creates a temperature gradient on the wall of the filter element that can be large enough to cause the filter element to fail due to thermal stress.

On two occasions at the PSDF a second reason—using the coal feeder as a start-up bed feeder—has lead to the thermal failure of several filter elements. Due to the design of the feeder it is impossible to verify that all of the coal in the feeder has been removed prior to using it to add sand to the reactor. This sometimes causes "slugs" of coal to be fed to the reactor. If the coal cannot be fully combusted the burning coal can also enter the PCD. This type of event has happened on two occasions, in April 1997 and during TC04 in October 1998.

After having discussions with personnel from other test facilities it was determined that this problem was not unique to the PSDF. Therefore, thermal events such as what happened during TC04 have been analyzed at the PSDF for the past 2 years. These analyses have shown that the filter-element material of construction largely determines its ability to survive such an event. A secondary consideration is the microstructure of the filter element. Since TC04 was such a short test campaign this report will focus on modeling performed at the PSDF to understand what characteristics of a filter element make it more or less susceptible to this type of event. Thus, in addition to the brief run and inspection descriptions for TC04, this report contains results of filter element material testing and thermal transient modeling performed at the PSDF in 1999.

1.2 TC04 RUN

During the start-up, the transport reactor was empty as the refractory was heated and cured using the start-up burner. When the transport reactor temperature reached about 1,200°F sand was fed into the reactor to be used as a bed material for start-up. The sand addition was through the coal feeder and apparently there was a residual accumulation of coal inside the feeder that was carried into the reactor with the sand. When the sand began circulating the coal ignited, burning both in the transport reactor and the PCD. The run ended when fragments of several filter elements were found in the ash-removal system.

Upon inspection, six filter elements had failed: two 2-meter-long Pall 326 filters; two 1.5-meter-long Pall 326 filters; one Schumacher TF20; and one Ensto. From the inspection it was apparent that the fire was much more intense in the lower plenum/cone than in the upper plenum. The entire filter cake on the lower plenum had fused into a shell that could be peeled off of the filter elements.

As a result of this run the operating procedures were changed so that sand would not be fed through the coal feeder during subsequent runs in order to prevent this event from occurring again.

1.3 TC04 INSPECTION REPORT

Because of the severity of the transient and the number of filter elements broken, the filter system was shut down for disassembly. The initial inspection occurred on October 20, 1998, through the lower manway and on October 21 the plenum of the PCD was removed and placed in the maintenance bay for inspection and filter removal. In total, six filter elements were broken: the Ensto filter, both 2-meter Pall 326 filters, two 1.5-meter Pall 326, and one Schumacher TF20. All of the broken filters were located on the lower plenum.

The observations made during the inspection provided some very important insights as to the performance of various filter elements during thermal transients. These insights include:

1. As discussed in earlier reports, monolithic oxide filter elements (such as Coors, Blasch, and Ensto) are very sensitive to temperature gradients formed during thermal events due to their low-thermal conductivity.

2. Even though the monolithic "clay-bonded" silicon carbide filter elements sold by Pall and Schumacher are less sensitive to thermal events than the monolithic oxide elements they can still fail due to temperature gradients.

3. The Industrial Filter and Pump recrystallized silicon carbide (REECER) filter element is probably the most resistant of all the monolithic filter elements to thermal events due to its high-thermal conductivity.

4. The composite filter elements do not appear to be affected by thermal gradients. Aside from the one PRD-66 filter that was damaged (probably from being hit upon failure of a nearby element) no composite filter element appeared to be damaged by the thermal event.

5. The metal filter elements were not affected by the thermal event. This is expected due to the high-thermal conductivity and thin wall of the metal elements. It would be practically impossible in this system to have a thermal event in the PCD that would create a temperature gradient across a metal filter element that would cause it to fail.

1.4 FILTER ELEMENT MATERIALS TEST RESULTS

Property testing of filter elements continued in support of this test campaign. During this reporting period testing of exposed IF&P REECER™, Pall 326, and Schumacher TF20 and T10-20 filters was conducted and the results were compared to previous results obtained for these materials as-manufactured and after operation in the PCD. During previous testing the strength of exposed Pall 326 appeared to correlate more closely with virgin element weight (measured before the elements were first installed for operation) than to operation history. Five as-manufactured Pall 326 elements were tested to evaluate the effect of virgin weight on tensile strength.

Property tests have been conducted on 3M oxide/oxide composite and Pall iron aluminide (FeAl) elements for the first time during this reporting period. Baseline properties were obtained on as-manufactured elements and hoop tensile strength was measured after operation in the PCD.

In as-manufactured condition, 3M oxide/oxide composite offers some advantages over monolithic ceramic elements including survival during more severe thermal transients. After 1,420 hours in operation at 1,400°F the tensile strength was unchanged but the strain-to-failure decreased. After 1,982 hours of operation, including a thermal transient, the strain-to-failure decreased further. Additional operation would be required to determine if strain-to-failure continues to decrease and if this would lead to failures. The biggest obstacle to use of 3M elements is pinholes in the filtration mat as seen in one element after 1,420 hours of operation. The pinhole problem must be solved before more operational experience is achieved to address the other issues.

IF&P REECER™ has a relatively high-thermal diffusivity which leads to lower temperature gradients during thermal transients. This material has survived thermal transients in the PCD that caused clay-bonded SiC and monolithic oxide elements to fail; however, these results were obtained on fewer REECER™ elements with fewer hours of operation than on many other filter elements. Additional operational experience and material testing is needed to help predict long-term performance. Two specific areas should be addressed in future testing. First, the manufacturer has taken steps to control an inconsistent wall thickness and "bubbles." Measurements on future elements must confirm that these anomalies are indeed under control. Second, previous test results showed lower elevated temperature strain-to-failure for REECER™ than for other ceramic elements. Lower strain-to-failure would offset some of the advantage of high-thermal diffusivity and could lead to failure during thermal transients even with relatively low-temperature gradients. Future testing should better define the tensile strain-to-failure at elevated temperatures to allow an assessment of how much improvement this material may offer over the clay-bonded SiC materials during thermal transients.

Testing of five as-manufactured Pall 326 elements with varying weights showed no correlation between element weight and as-manufactured hoop tensile strength. No evidence of tensile strength degradation was seen after 2,830 hours of operation in combustion at 1,400°F. Results were inconclusive on whether strength decreased after exposure to a thermal transient.

Pall FeAl has a relatively high-tensile strength and with a high-thermal diffusivity and thin wall should perform well during thermal transients. Test results showed a decrease of ~15 percent in tensile strength and ~20 percent in strain-to-failure after 1,420 hours of operation at 1,400°F. Results were inconclusive on whether strength and strain-failure decreased further after exposure to a thermal transient. The tensile strength measured after operation is sufficient for operation at the PSDF. Testing after additional operation will determine if property degradation continues. Blinding is a major concern for FeAl elements. Flow testing after 2,780 hours in operation showed about a 45-percent decrease in permeability, still within acceptable limits. Again, testing after additional exposure would be required to determine whether permeability continued to decrease.

The hoop tensile strength of Schumacher TF20 and T10-20 decreased ~30 percent during the initial hours of operation and then remained unchanged for up to at least 1,800 hours of operation at 1,400°F. After operation during a thermal transient in the PCD no additional strength loss was seen. Based on the strength measurements so far the biggest concern for these elements operating at 1,400°F is material variability.

1.5 THERMAL STRESS ANALYSIS

Simple 1-dimensional (1-D) as well as 3-dimensional (3-D) ANSYS simulations were performed to calculate the temperature gradients, as well as the stress in the filter element due to temperature gradients, for a variety of filter elements.

The performance of several monolithic ceramic filter elements during thermal transients was studied in this effort. The filters evaluated were IF&P REECER™, Schumacher TF20, Pall 326, Coors P-100A-1, Blasch 4-270, and Ensto. A 1-D finite difference model was developed to calculate the temperature profiles in the elements under conditions measured during one thermal transient at the PSDF. A refinement to this 1-D model was developed using an ANSYS 3-D finite element model. The ANSYS considers the effects of axial and circumferential temperature gradients and more complex boundary conditions.

The results presented here show that elements with low ratios of thermal diffusivity/element wall thickness^2, κ/l^2, including monolithic aluminum oxide elements, will develop greater temperature gradients and thermal stresses and strains during thermal transients than elements with high κ/l^2. Thermal expansion will also have an effect, but for the filter elements considered here κ/l^2 is the most important factor in determining the thermal stress and strain level. Mechanical properties including tensile strain-to-failure and "toughness" will determine whether these strains lead to crack formation and whether cracks propagate and lead to element failure.

From the results obtained in this effort some areas to be addressed in future efforts have been identified. These include:

1. Development of a model that includes gas flow through the wall.

2. Modeling of the actual microstructure of the elements instead of the continuum assumed here.

3. More detailed temperature measurements to obtain better definition of the thermal loading and boundary conditions during thermal transients.

2.0 INTRODUCTION

This report provides an account of the TC04 test campaign with the Kellogg Brown & Root (KBR) transport reactor and the Siemens Westinghouse Power Corporation (Siemens Westinghouse) filter vessel at the Power Systems Development Facility (PSDF) located in Wilsonville, Alabama, 40 miles southeast of Birmingham. The PSDF is sponsored by the U. S. Department of Energy (DOE) and is an engineering-scale demonstration of two advanced coal-fired power systems. In addition to DOE, Southern Company Services, Inc., (SCS), Electric Power Research Institute (EPRI), and Peabody Holding Company are cofunders. Other cofunding participants supplying services or equipment include KBR, Foster Wheeler (FW), Siemens Westinghouse, and Combustion Power Company. SCS is responsible for constructing, commissioning, and operating the PSDF.

2.1 THE POWER SYSTEMS DEVELOPMENT FACILITY

SCS entered into an agreement with DOE/NETL for the design, construction, and operation of a hot-gas clean-up test facility for gasification and pressurized combustion. The purpose of the PSDF is to provide a flexible test facility that can be used to develop advanced power system components, evaluate advanced turbine system configurations, and assess the integration and control issues of these advanced power systems. The facility was designed as a resource for rigorous, long-term testing and performance assessment of hot-stream clean-up devices and other components in an integrated environment.

The PSDF will consist of five modules for systems and component testing. These modules include:

- An advanced-pressurized fluidized-bed combustion module (APFBC).
- A transport reactor module.
- A hot-gas clean-up module.
- A compressor/turbine module.
- A fuel cell module.

The APFBC module consists of FW technology for second-generation PFBC. This module relies on partial conversion of the coal to fuel gas in a carbonizer with the remaining char converted in a PFBC. Both the fuel-gas and PFBC-exhaust-gas streams are filtered to remove particulates and then combined to fire a combustion turbine. The transport reactor module includes KBR transport technology for pressurized combustion and gasification to provide either an oxidizing or reducing gas for parametric testing of hot-particulate-control devices. The filter systems that will be tested at PSDF include particulate control devices (PCD) supplied by Combustion Power Company and Siemens Westinghouse.

2.2 TRANSPORT REACTOR SYSTEM DESCRIPTION

The transport reactor is an advanced-circulating fluidized-bed reactor operated as either a combustor or as a gasifier using one of two possible hot-gas clean-up filter technologies (particulate control device or PCD) at a component size readily scaleable to commercial systems. The transport reactor train operating in the combustion mode is shown schematically in Figure 2.2-1. A taglist of all major equipment in the process train and associated balance-of-plant is provided in Tables 2.2-1 and -2. Two PCDs are shown in this flow diagram; however, only one PCD is tested with the transport reactor at a given time during operations. The intent is to be able to install, change out, or provide maintenance on a second PCD while one is being tested. This provides increased flexibility for the test facility and reduces downtime. The facility is sized to process nominally 2 ton/hour of coal. This size generates sufficient gas to test the PCDs at a nominal 1,000 ACFM of gas at the PCD inlet. Indirect cooling of the gas from the transport reactor allows testing of the PCD with inlet temperatures between 600 and 1,400°F and at pressures ranging from 150 to 305 psia. The PCD in this train receives particulate-laden gas from the transport reactor, which can operate in either gasification or combustion mode. In the gasification mode the gas exiting the PCD is oxidized, cooled, and filtered in a baghouse before being discharged to the atmosphere through a stack. The ash and char produced in the gasification mode are oxidized in a sulfator prior to disposal.

Coal is ground to a nominal-average-particle diameter between 250 and 350 μm mass mean diameter (MMD) when the transport reactor is operated in gasification mode and combustion mode, respectively. Sorbent is ground to a nominal-average-particle diameter of 20 μm MMD. Using feeders to control the rates, both coal and sorbent are pneumatically fed continuously into the transport gasifier/combustor.

Air is compressed to about 350 psia in the main air compressor and fed directly to the transport reactor. For start-up purposes a burner (BR0201) is provided at the reactor mixing zone. Liquefied propane gas (LPG) is used as start-up fuel. Fuel, sorbent, and gas feeds enter a mixing zone at the bottom of the reactor where they mix with recycled solids from the disengager cyclone. Coal conversion begins in this zone; the reaction mixture then flows upward into the narrower riser section at high velocity and then flows to the disengager.

The reactor typically operates at temperatures of 1,600 to 1,625°F in combustion mode. Provision is made to inject air at several different points along the riser to control the formation of NO_X. Limestone or dolomitic sorbents are fed into the reactor for sulfur capture, thus eliminating the need for downstream facilities to reduce plant sulfur emissions.

Solids and gases leaving the reactor flow into the disengager for bulk separation of the two phases. Most of the solids collected in the disengager are recycled to the reactor. Coal ash and spent sorbent are discharged from the transport reactor to maintain the solids inventory in the system. In the combustion mode heat removal from the reactor system is necessary to control the reactor temperature. This is accomplished by removing solids from the disengager, cooling the solids in the combustor heat exchanger (HX0203), and returning the solids to the reactor system.

The gas leaving the disengager, still containing a high loading of particulates, is then sent to a cyclone system for additional solids recovery prior to being fed to the PCDs. The cyclone is provided with spoiling gas to vary the solids loading into the effluent gas. The resulting conditioned gas next enters the PCD where essentially all of the remaining particulates in the gas are removed. The cleaned gas leaving the PCD is sent to a secondary gas cooler (HX0402) and ultimately cooled to about 600°F. All gas-stream cooling is accomplished by generating steam. A portion of the cooled gas is further cooled in the compressor feed cooler (HX0405) and sent to the recycle-gas-booster compressor (CO0401) where the pressure is increased to about 400 psia. This gas is used for aeration and fluidization in the combustor heat exchanger.

The main-gas stream from the secondary gas cooler is cooled further by dilution air and cleaned of any remaining particulates in a baghouse before being discharged to the atmosphere through a stack.

Table 2.2-1

Major Equipment in the Transport Reactor Train

TAG NAME	DESCRIPTION
BR0201	Reactor Start-Up Burner
BR0401	Thermal Oxidizer
BR0602	Sulfator Start-Up/PCD Preheat Burner
CO0201	Main Air Compressor
CO0401	Recycle Gas Booster Compressor
CO0601	Sulfator Air Compressor
CY0201	Primary Cyclone in the Reactor Loop
CY0207	Disengager in the Reactor Loop
CY0601	Sulfator Cyclone
DR0402	Steam Drum
DY0201	Feeder System Air Dryer
FD0206	Spent Solids Screw Cooler
FD0210	Coal Feeder System
FD0220	Sorbent Feeder System
FD0502	Fines Screw Cooler
FD0510	Spent Solids Transporter System
FD0520	Fines Transporter System
FD0530	Spent Solids Feeder System
FD0602	Sulfator Solids Screw Cooler
FD0610	Sulfator Sorbent Feeder System
FL0301	PCD — Siemens Westinghouse
FL0302	PCD — Combustion Power
FL0401	Compressor Intake Filter
HX0202	Primary Gas Cooler
HX0203	Combustor Heat Exchanger
HX0204	Transport Air Cooler
HX0402	Secondary Gas Cooler
HX0405	Compressor Feed Cooler
HX0601	Sulfator Heat Recovery Exchanger
ME0540	Heat Transfer Fluid System
RX0201	Transport Reactor
SI0602	Spent Solids Silo
SU0601	Sulfator

Table 2.2-2 (Page 1 of 3)

Major Equipment in the Balance-of-Plant

TAG NAME	DESCRIPTION
BO2920	Auxiliary Boiler
BO2921	Auxiliary Boiler – Superheater
CL2100	Cooling Tower
CO2201A-D	Service Air Compressor A-D
CO2202	Air-Cooled Service Air Compressor
CO2203	High-Pressure Air Compressor
CO2601A-C	Reciprocating N_2 Compressor A-C
CR0104	Coal and Sorbent Crusher
CV0100	Crushed Feed Conveyor
CV0101	Crushed Material Conveyor
DP2301	Baghouse Bypass Damper
DP2303	Inlet Damper on Dilution Air Blower
DP2304	Outlet Damper on Dilution Air Blower
DY2201A-D	Service Air Dryer A-D
DY2202	Air-Cooled Service Air Compressor Air Dryer
DY2203	High-Pressure Air Compressor Air Dryer
FD0104	MWK Coal Transport System
FD0111	MWK Coal Mill Feeder
FD0113	Sorbent Mill Feeder
FD0140	Coke Breeze and Bed Material Transport System
FD0154	MWK Limestone Transport System
FD0810	Ash Unloading System
FD0820	Baghouse Ash Transport System
FL0700	Baghouse
FN0700	Dilution Air Blower
HO0100	Reclaim Hopper
HO0105	Crushed Material Surge Hopper
HO0252	Coal Surge Hopper
HO0253	Sorbent Surge Hopper
HT2101	MWK Equipment Cooling Water Head Tank
HT2103	SCS Equipment Cooling Water Head Tank
HT0399	60-Ton Bridge Crane
HX2002	MWK Steam Condenser
HX2003	MWK Feed Water Heater

Table 2.2-2 (Page 2 of 3)

Major Equipment in the Balance-of-Plant

TAG NAME	DESCRIPTION
HX2004	MWK Subcooler
HX2103A	SCS Cooling Water Heat Exchanger
HX2103C	MWK Cooling Water Heat Exchanger
LF0300	Propane Vaporizer
MC3001-3017	MCCs for Various Equipment
ME0700	MWK Stack
ME0701	Flare
ME0814	Dry Ash Unloader for MWK Train
ML0111	Coal Mill for MWK Train
ML0113	Sorbent Mill for Both Trains
PG2600	Nitrogen Plant
PU2000A-B	MWK Feed Water Pump A-B
PU2100A-B	Raw Water Pump A-B
PU2101A-B	Service Water Pump A-B
PU2102A-B	Cooling Tower Make-Up Pump A-B
PU2103A-D	Circulating Water Pump A-D
PU2107	SCS Cooling Water Make-Up Pump
PU2109A-B	SCS Cooling Water Pump A-B
PU2111A-B	MWK Cooling Water Pump A-B
PU2300	Propane Pump
PU2301	Diesel Rolling Stock Pump
PU2302	Diesel Generator Transfer Pump
PU2303	Diesel Tank Sump Pump
PU2400	Fire Protection Jockey Pump
PU2401	Diesel Fire Water Pump #1
PU2402	Diesel Fire Water Pump #2
PU2504A-B	Waste Water Sump Pump A-B
PU2507	Coal and Limestone Storage Sump Pump
PU2700A-B	Demineralizer Forwarding Pump A-B

Table 2.2-2 (Page 3 of 3)

Major Equipment in the Balance-of-Plant

TAG NAME	DESCRIPTION
PU2920A-B	Auxiliary Boiler Feed Water Pump A-B
SB3001	125-V dc Station Battery
SB3002	UPS
SC0700	Baghouse Screw Conveyor
SG3000-3005	4,160-V, 480-V Switchgear Buses
SI0101	MWK Crushed Coal Storage Silo
SI0103	Crushed Sorbent Storage Silo
SI0111	MWK Pulverized Coal Storage Silo
SI0113	MWK Limestone Silo
SI0114	FW Limestone Silo
SI0810	Ash Silo
ST2601	N_2 Storage Tube Bank
TK2000	MWK Condensate Storage Tank
TK2001	FW Condensate Tank
TK2100	Raw Water Storage Tank
TK2300A-D	Propane Storage Tank A-D
TK2301	Diesel Storage Tank
TK2401	Fire Water Tank
XF3000A	230/4.16-kV Main Power Transformer
XF3001B-5B	4,160/480-V SS Transformer No. 1-5
XF3001G	480/120-V Miscellaneous Transformer
XF3010G	120/208 Distribution Transformer
XF3012G	UPS Isolation Transformer
VS2203	High-Pressure Air Receiver

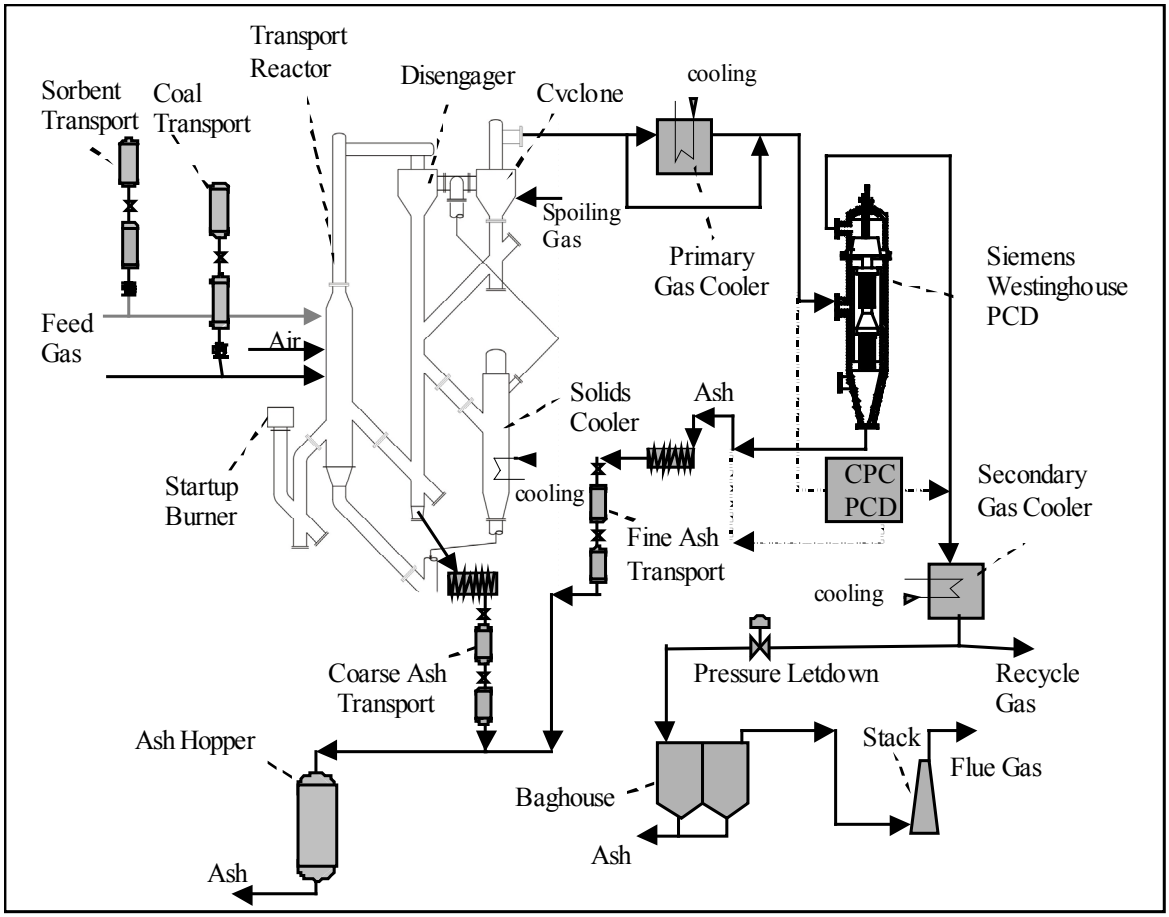

Figure 2.2-1 Flow Diagram of the Transport Reactor Train in Combustion Mode of Operation

2.3 SIEMENS WESTINGHOUSE PARTICULATE CONTROL DEVICE

Several different PCDs will be evaluated on the transport reactor train. The first PCD commissioned in 1996 and used in all of the testing to date was the filter system designed by Siemens Westinghouse. The dirty gas enters the PCD below the tubesheet, flows through the filter elements, and ash collects on the outside of the filter. The clean gas passes from the plenum/filter element assembly through the plenum pipe to the outlet pipe. As the ash collects on the outside surface of the filter elements the pressure drop across the filter system gradually increases. The filter cake is periodically dislodged by injecting a high-pressure gas pulse to the clean side of the candles. The cake then falls to the discharge hopper.

To date, the transport reactor has been operated only in the combustion mode. Initially, high-pressure air was used as the pulse gas for the PCD. However, the pulse gas was changed to nitrogen early in 1997. The pulse gas was routed individually to the two plenum/filter element assemblies via injection tubes mounted on the top head of the PCD vessel. The pulse duration was typically 0.1 to 0.5 seconds.

A sketch of the Siemens Westinghouse PCD is shown in Figure 2.3-1.

Siemens Westinghouse PCD FL0301

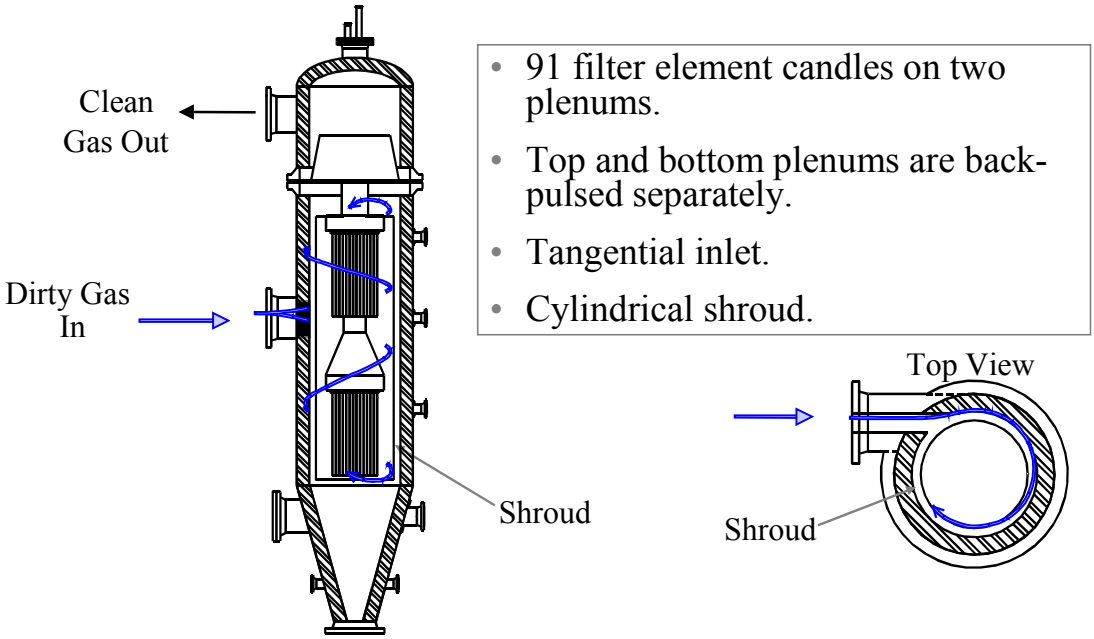

- 91 filter element candles on two plenums.
- Top and bottom plenums are back-pulsed separately.
- Tangential inlet.
- Cylindrical shroud.

Figure 2.3-1 Siemens Westinghouse PCD

2.4 OPERATION STATUS

Commissioning activities began in September 1995 and proceeded in parallel with construction activities. Design and construction of the transport reactor and associated equipment was completed in early summer of 1996. All separate components and subsystems were fully operational by midsummer and commissioning work was focused on integration issues for the entire transport reactor train. The first coal fire was achieved on August 18, 1996, in combustion mode. A series of combustion characterization tests was initiated to develop an understanding of reactor system operations. Test runs CCT1, CCT2, and CCT3 were completed by December 1996. Solids carryover from the reactor to the PCD was found to be excessive during these test runs. A number of start-up and design problems associated with various equipment were successfully addressed.

Three additional sets of characterization test runs (CCT4, CCT5, and CCT6) and one major test campaign (TC01) were undertaken during 1997. TC01 focused on exposing the PCD filter elements to process gas for 1,000 hours at temperatures from 1,350 to 1,400°F and achieving stable reactor operations. An Alabama bituminous coal from the Calumet Mine in the Mary Lee seam and Plum Run dolomite were used in these test runs.

Two test campaigns (TC02 and TC03) were successfully completed during 1998. TC02 was planned for reactor parametric testing to better quantify the effect of different variables on reactor and filter element operation. Test run TC02 was started on April 5, 1998, and completed on May 11, 1998. Based on TC02 observations, TC03 was planned for additional reactor parametric testing to better quantify the effect of different variables on reactor and PCD operation and to evaluate operation with an Eastern Kentucky bituminous coal and a Gregg Mine limestone from Florida. The third major test campaign, TC03, was performed from May 31 to August 10, 1998. Stable operations were demonstrated using the Eastern Kentucky coal and Plum Run dolomite, Bucyrus limestone, and Longview limestone during TC03. There were, however, circulation problems using the Eastern Kentucky coal and Florida Gregg Mine limestone because of deposits resulting from excessive fines (segregated) in the Eastern Kentucky feed. TC04 was started on October 14, 1998, but ended prematurely due to a temperature excursion in the PCD during the initial heat-up of the transport reactor system. Figure 2.4-1 provides a summary of operating hours for the major combustion test campaigns through TC04.

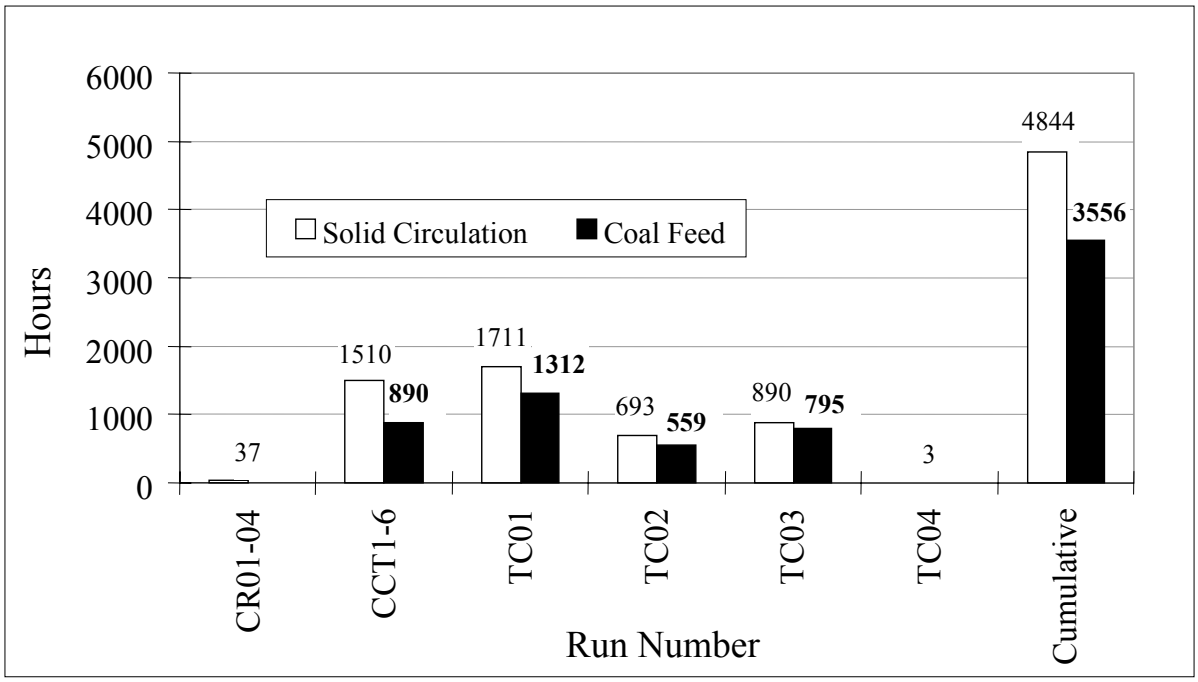

Figure 2.4-1 Operating Hours Summary for Transport Reactor Train Major Combustion Test Campaigns Through TC04

3.0 PARTICLE FILTER SYSTEM

3.1 TC04 OVERVIEW

Thermal events have occasionally lead to the failure of many filter elements at the PSDF ever since operations began on coal feed in August 1996. Essentially all of these failures since September 1997 have occurred during the transient operating conditions while changing from the propane-fired start-up burner to coal feed. If the coal is fed to the transport reactor at a temperature too low to fully combust the coal it will be carried into the PCD where it will be removed from the gas by the filter elements. This burning coal creates a temperature gradient on the wall of the filter element that can be large enough to cause the filter element to fail due to thermal stress.

On two occasions at the PSDF a second reason—using the coal feeder as a start-up bed feeder—has lead to the thermal failure of several filter elements. Due to the design of the feeder it is impossible to verify that all of the coal in the feeder has been removed prior to using it to add sand to the reactor. This sometimes causes "slugs" of coal to be fed to the reactor. If the coal cannot be fully combusted burning coal can also enter the PCD. This type of event happened in April 1997 and during test campaign TC04 in October 1998.

After having discussions with personnel from other test facilities it was determined that this problem was not unique to the PSDF. Therefore, thermal events such as what happened during TC04 have been analyzed at the PSDF for the past 2 years. These analyses have shown that the filter element construction material largely determines its ability to survive such an event. A secondary consideration is the microstructure of the filter element. Since TC04 was such a short test campaign this report will focus on modeling performed at the PSDF to understand what characteristics of a filter element make it more or less susceptible to this type of event.

This report contains four sections:

- TC04 Run Report – Briefly describes what events led up to the filter element failure.
- TC04 Inspection Report – Discusses the findings during the PCD disassembly and inspection. From a filter element standpoint the most interesting observation was that the Industrial Filter & Pump REECER filter element was the only monolithic filter element to survive the fire in the lower part of the PCD. Material testing confirms that the thermal conductivity of the REECER filter element is significantly higher than any other monolithic filter.
- Materials Test Report – Highlights material testing performed at the PSDF in 1999 and includes material testing on the 3M oxide and IF&P REECER as well as the Pall iron aluminide.
- Modeling of Thermal Transients – Simple 1-D as well as 3-D ANSYS simulations were performed to calculate the temperature gradients as well as the stress in the filter element due to temperature gradients for a variety of filter elements.

3.2 PCD OPERATION DURING TEST RUN TC04

3.2.1 Introduction

The TC04 test run ended before it had actually begun. During the start-up the transport reactor was empty as the refractory was heated and cured using the start-up burner. When the transport reactor temperature reached about 1,200°F sand was fed into the reactor to be used as a bed material for start-up. Sand addition was through the coal feeder, and apparently there was a residual accumulation of coal from the previous run inside the feeder that was carried into the reactor with the sand. When the sand began circulating the coal ignited, burning in both the transport reactor and the PCD. The run ended when fragments of several filter elements were found in the ash removal system.

Upon inspection, six filter elements had failed: two 2-meter-long Pall 326 filters; two 1.5-meter-long Pall 326 filters; one Schumacher TF20; and one Ensto. From the inspection it was apparent that the fire was much more intense in the lower plenum/cone than in the upper plenum. The entire filter cake on the lower plenum had fused into a shell that could be peeled off of the filter elements.

3.2.2 Test Objectives

The primary test objectives for the run included the following:

- Operate the PCD at Higher Face Velocities – To achieve this objective the total surface area of the PCD was reduced from the design value of 258 to 165 ft^2. Under normal operating flows the face velocity would be 7 to 8 ft/min.

- Test 2-Meter Filter Elements – Two-meter filter elements from Pall and 3M were installed for this test run. Pall required that the 2-meter filters be fixed to a support post at the bottom to eliminate any damage due to vibration. Two of these filters were installed and both of them failed during the fire. When the PCD was visually inspected through the manway the filter elements were still held at the bottom and were leaning against the inside of the shroud.

- Collect Element Temperature Data on Start-up – In April 1998 thermocouples were attached to the element surface to detect carryover of burning solids into the PCD during start-up. For this run thermocouples were also attached to several elements throughout the vessel. The thermocouples were wired to the high-speed data acquisition system which unfortunately was not operational during the fire. In subsequent runs, all thermocouples were wired to the plant DCS system.

3.2.3 Observations/Events – October 14, 1998, Through October 17, 1998

A. PCD Pulse System Started – October 14, 1998, at 21:40.

B. Main Air Compressor Started – October 15, 1998, at 02:30.

C. PCD Preheat Started – October 15, 1998, at 02:35.

D. Reactor Shut Down to Repair FD0520 – October 15, 1998, at 14:15. The system was temporarily shut down to repair a leak in the lock vessel spheri valve.

E. Restarted PCD Preheat – October 15, 1998, at 18:50.

F. Start-up Burner On – October 16, 1998, at 07:00.

G. Reactor Pressure Raised to 100 psig – October 16, 1998, at 15:00.

H. Reactor Pressure Raised to 120 psig – October 17, 1998, at 09:15.

I. Started Sand Addition – October 17, 1998, at 12:15. Sand was added to the transport reactor to build a solids inventory. The sand was fed into the system using the coal feeder.

J. Fire in PCD/Run Ended – October 17, 1998, at 17:50. There was a sharp, almost instantaneous, rise in the PCD plenum temperature from 825 to 990°F as recorded by plenum temperature TI3014. Shortly after the temperature spike the ash removal system plugged with fragments of broken filter elements and the run was terminated.

3.2.4 Run Summary

Sand addition to the transport reactor began at 09:30 on October 17, 1998. At that time the reactor temperature ranged from 1,200 to 1,400°F and the PCD temperature was over 800°F. Immediately after starting the coal feeder (FD0210) to feed the sand it was observed that the temperature in the reactor mixing zone increased. This was an indication that there was still some coal in the feeder and a coal/sand mixture was being fed to the reactor. Over the next 2 hours FD0210 was cycled on and off to gradually feed the sand and remove the coal from the feeder. During this 2 hours there was a slight increase in the temperature of the reactor as well as the PCD.

Starting at 11:30 there was no further increase in temperature when the feeder was turned on, so the assumption was made that most if not all of the coal had been removed from the feeder. Therefore, the feeder speed was increased to allow for the rapid accumulation of solids in the reactor so the J-legs and the cyclone dipleg could be sealed. By 13:30 there was indication that there was a solids level in the combustion heat exchanger and J-legs. However, there were some problems with the feeder line plugging. On one occasion during the sand addition there was a significant carryover of solids from the reactor to the PCD. This carryover caused a delay until the PCD cone could be emptied. The temperatures in the reactor as well as the PCD dropped as the cold sand entered the 1,200°F reactor.

By 16:30 there was a significant accumulation of solids in the reactor and a slow circulation of sand had begun. Sand addition was completed around 17:40 and a total of about 15,000 lb of sand had been added to the reactor. The temperature transient occurred at 17:50 (see Figure 3.2-5 for a graph showing the magnitude of the transient).

Within a few minutes of the temperature transient fragments of filter elements were found in the discharge of the ash removal system. Since the run was just beginning it was decided to shut down the PCD to remove the broken filters. During the inspection it was found that six filter elements had been broken: both of the 2-meter Pall 326 elements, two 1.5-meter Pall 326 elements, a Schumacher TF20 element, and the Ensto element. All of the broken filter elements were located on the bottom plenum. The intact filter elements on the bottom plenum included all of the composite filters as well as the IF&P REECER filters.

One interesting observation was that the fire seemed to be in the cone of the PCD. This conclusion comes from three separate observations:

- There is a 0.125-in.-diameter bare thermocouple located in both the top and bottom plenums. The temperature measured by these thermocouples is shown in Figure 3.2-5. The magnitude of the temperature as measured by these thermocouples is much greater for the lower plenum than for the top plenum.

- The entire filter cake on the elements in the lower plenum was fused and could be removed as a "shell." On the top plenum the surface of the ash was fused but the ash below the first ~1 mm was loose.

- Another indication that conditions were less severe in the top plenum was that almost all of the filter elements in the top plenum were monolithic silicon carbide filters from Pall and Schumacher, yet none of the top plenum elements were broken but all of the Pall and Schumacher filter elements on the lower plenum broke during the event. Details of the inspection can be found in section 3.3 of this report.

The root cause of this event is that during the sand addition coal was carried into the transport reactor with the sand. There are two theories as to why it took 8 hours from the beginning of sand addition for the event to occur:

1. The coal entered the transport reactor with the initial sand feed. This sand/coal mixture would fall to the lowest (and coldest) part of the reactor—the heat exchanger boot and J-leg. As more and more sand was added the entire reactor cooled; this area would then become covered and insulated from the start-up burner. The reactor did not begin to circulate until around 16:30, at which time the point circulation was slow. It may have taken the additional time for the coal to reach a temperature where it would ignite.

2. There may have been a large coal cake inside the feeder that broke loose after 17:00 and entered with the last of the sand feed. Due to the design of the coal feeder it is impossible to thoroughly inspect it before a run.

As a result of this run the operating procedures were changed so that sand would not be fed through the coal feeder during subsequent runs in order to prevent this event from occurring again.

Table 3.2-1

TC04 Run Statistics
10/14/1998 Through 10/17/1998

Start Time:	10/14/98 at 21:40
End Time:	10/18/98 at 19:00
Coal/Sorbent Type:	No Coals Fed to Reactor
Hours on Coal	N/A
Number of Filter Elements:	57
Filtration Area:	164.7 ft^2 (15.3 m^2)
Filter Element Layout Number:	10 (Figure 3.2-1)
Pulse Valve Open Time:	0.2 sec.
Pulse Time Trigger:	40 Minutes
Pulse Pressure:	265 to 365 psig (18 to 25 bar, g)
Pulse Logic:	Pulse on Timer

Table 3.2-2

TC04 Major Events
10/14/1998 Through 10/17/1998
(Refer To Figures 3.2-2 Through 3.2-4)

Event	Description	Date at Time
A	PCD Pulse System Started	10/14/98 at 21:40
B	Main Air Compressor Started	10/15/98 at 02:30
C	Started PCD Preheat	10/15/98 at 02:35
D	Reactor Shut Down to Repair FD0520	10/15/98 at 14:15
E	Restarted PCD Preheat	10/15/98 at 18:50
F	Start-up Burner On	10/16/98 at 07:00
G	Reactor Pressure Raised	10/16/98 at 15:00
H	Reactor Pressure Raised	10/17/98 at 09:15
I	Started Sand Addition	10/17/98 at 12:15
J	Fire in PCD – Run Ended	10/17/98 at 17:50

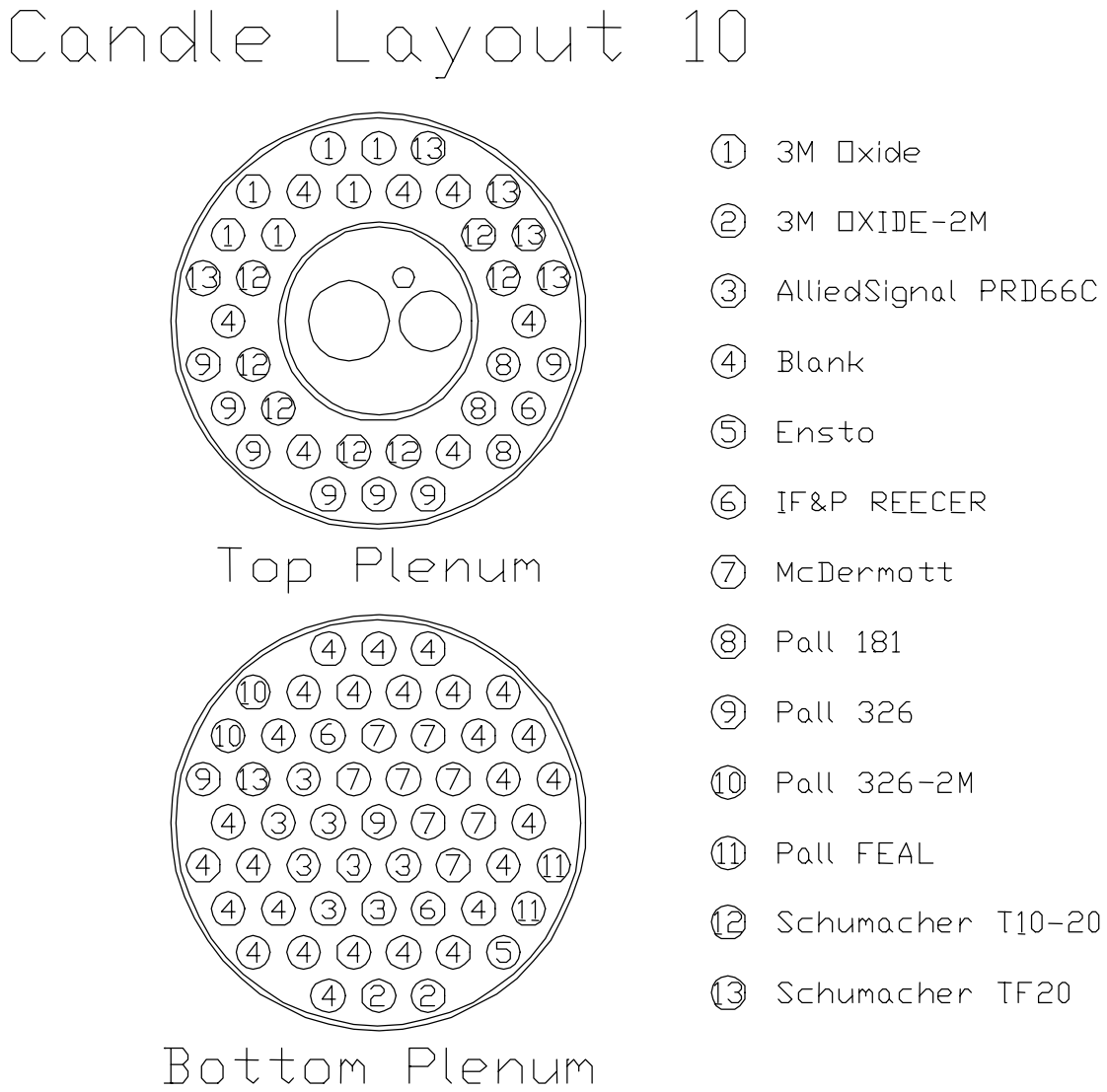

Figure 3.2-1 Filter Element Layout for TC04

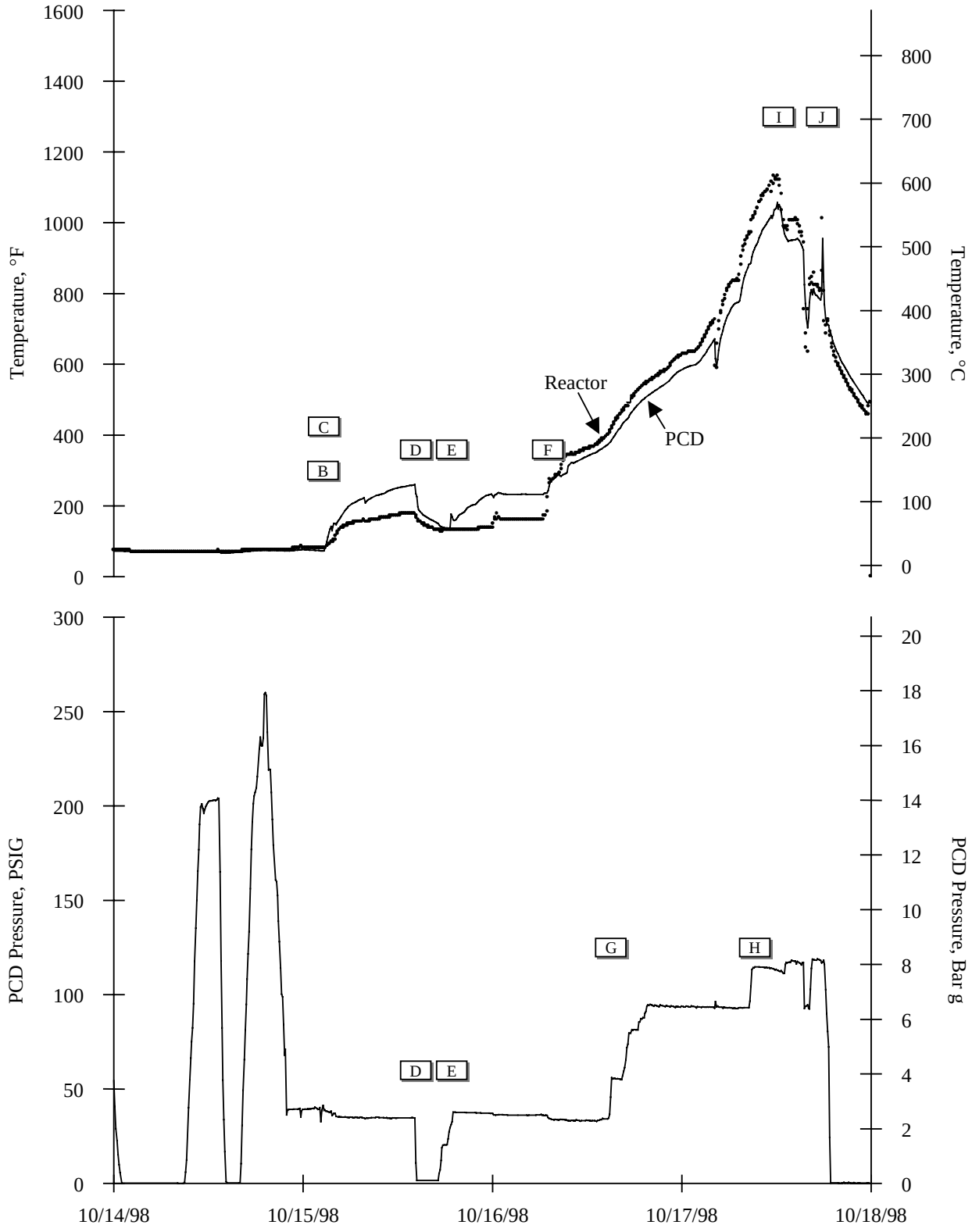

Figure 3.2-2 TC04 Temperature and Pressure for October 14 Through October 18

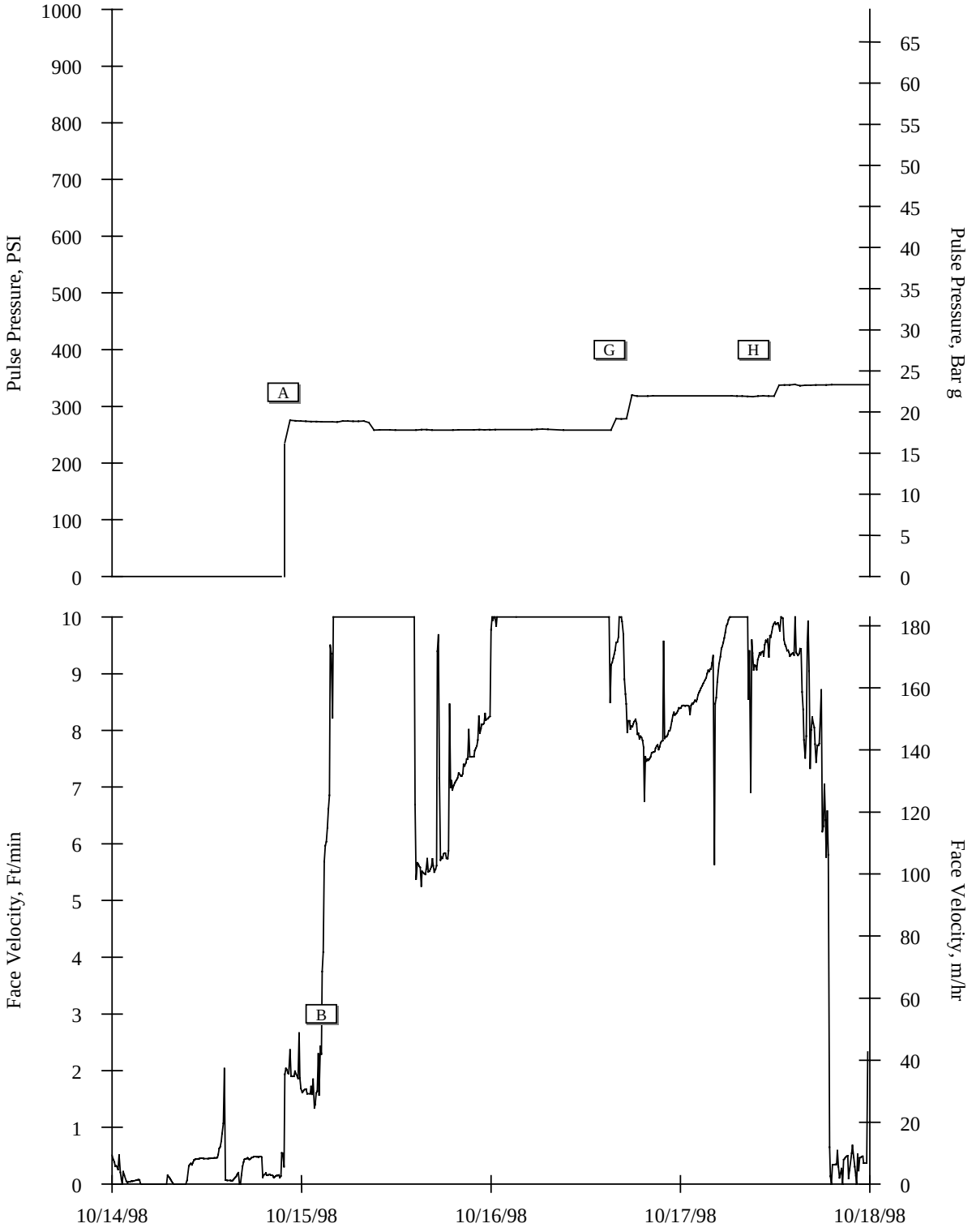

Figure 3.2-3 TC04 Back-Pulse Pressure and Face Velocity for October 14 Through October 18

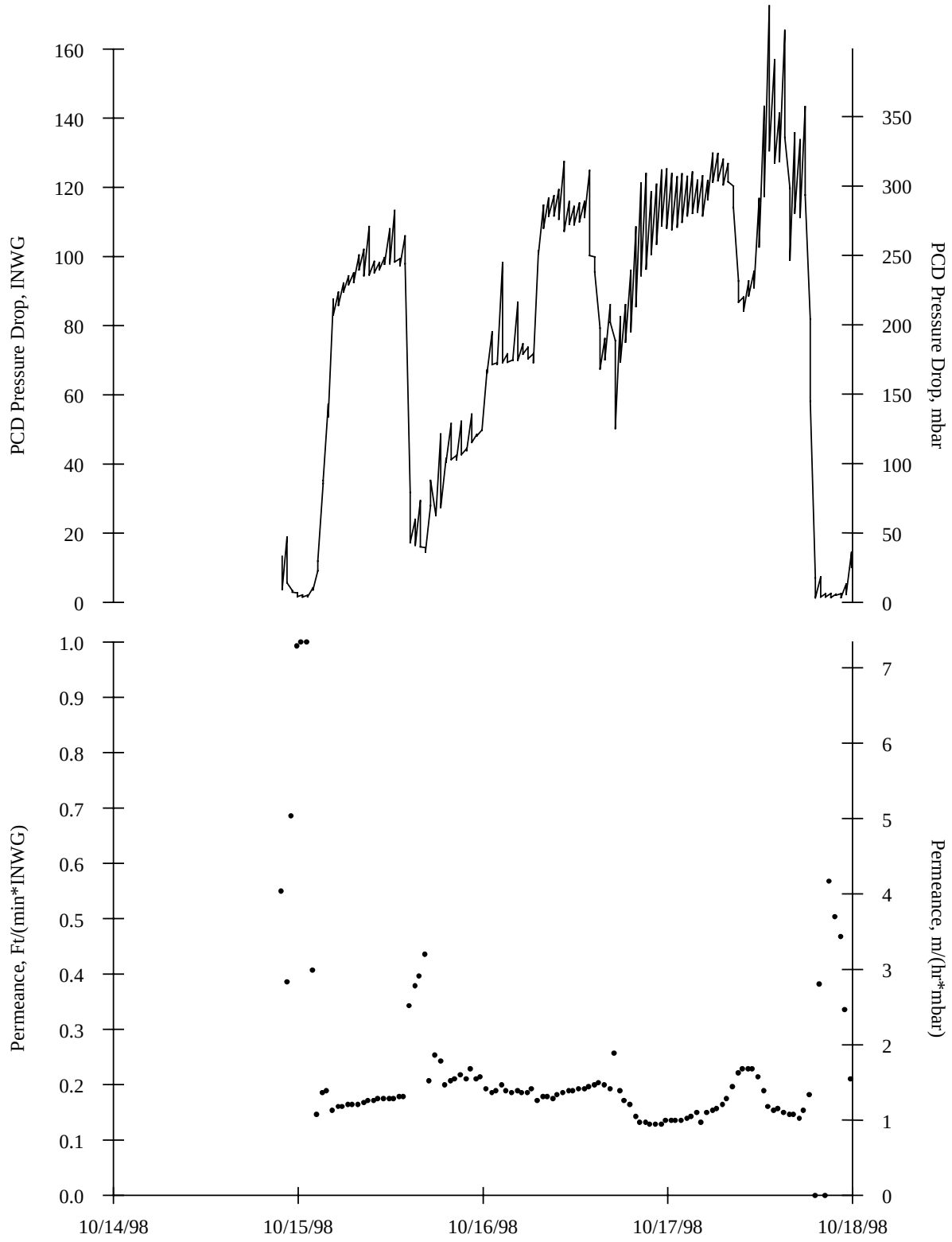

Figure 3.2-4 TC04 Pressure Drop and Permeance for October 14 Through October 18

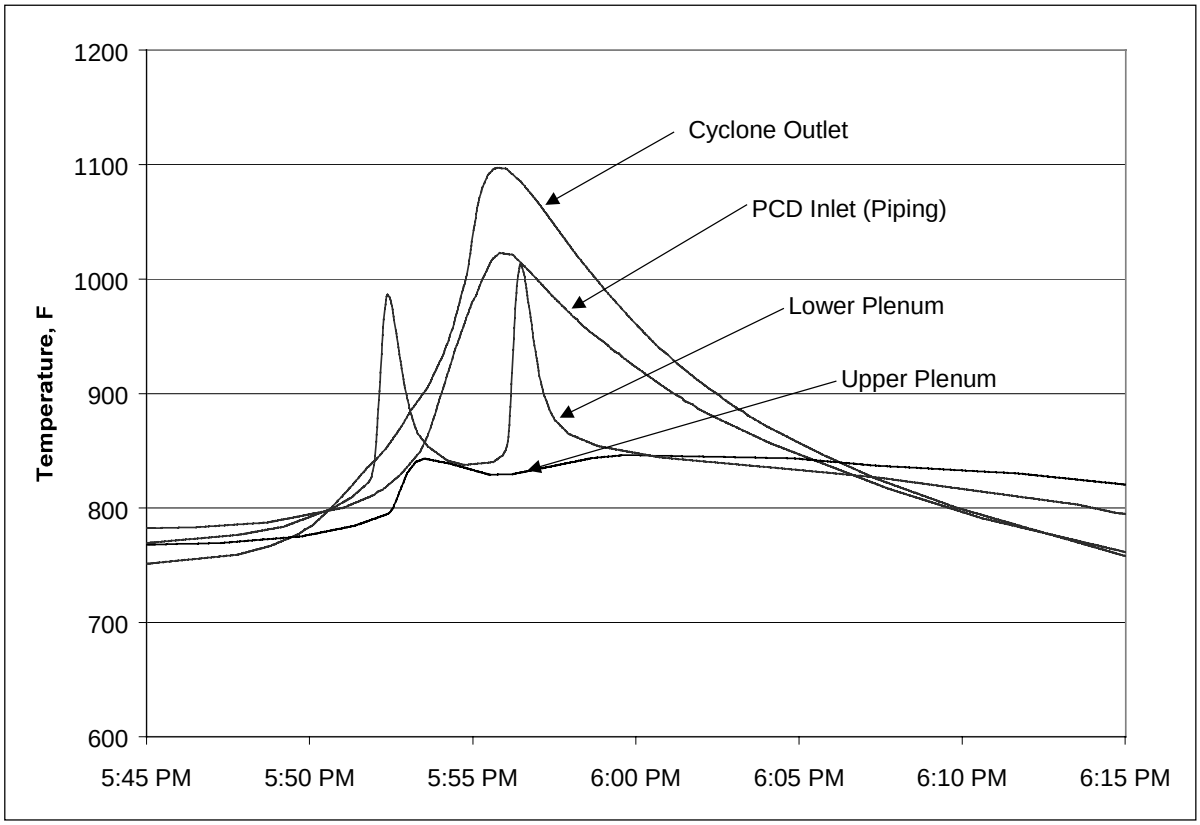

Figure 3.2-5 Temperature Transient on October 17, 1998

3.3 TC04 INSPECTION REPORT

3.3.1 Introduction

TC04 ended abruptly on October 17, 1998, when the thermal transient in the PCD was observed and the ash removal system plugged with fragments of ceramic filter elements. When the maintenance group disassembled the discharge of the dispense vessel fragments of both monolithic oxide and monolithic silicon carbide filter elements were found. Ensto Ceramics Oy in Finland manufactured the only monolithic oxide filter in the system. From the color of the membrane of the silicon carbide elements it appeared that there were fragments of both Pall and Schumacher filters. (The membrane of the Schumacher filter is a lighter shade of gray than the membrane of the Pall filters.)

Based on the severity of the transient and the number of filter elements broken it was decided to shut down the filter system for disassembly. The initial inspection occurred on October 20 through the lower manway, and on October 21 the plenum of the PCD was removed and placed in the maintenance bay for inspection and filter removal. In total, six filter elements were broken: the Ensto filter, both 2-meter Pall 326 filters, two 1.5-meter Pall 326, and one Schumacher TF20. All of the broken filters were located on the lower plenum. The location of the broken filters can be seen in Figure 3.3-1.

During the inspection there were several interesting observations:

- The filter cake on the lower plenum elements had sintered into a thin shell that could be removed from the element in large pieces. The strength of the cake was such that it could be circumferentially "peeled" off of the element in one piece. The filter cake on the upper plenum appeared "cracked" (similar to the glaze found on some pottery). However, the thickness of this layer was roughly 1 mm thick. Below the "cracked" layer the ash was loose and could be easily brushed off the filter. This seemed to indicate that severity of the fire inside the PCD was located in the lower part of the vessel.

- The majority of the filter elements in the lower plenum were composite filters. Only 8 of the 28 filters installed were monolithic ceramics. With the exception that the ash was fused onto the surface of most of the composite filter elements, all of these appeared to have no external damage. In general, the ash fused to the surface of the McDermott filters tended to remove some of the surface fibers as it was peeled from the surface. One PRD-66 filter did have damage to its surface that appeared to be due to the failure of the adjacent Pall 326.

- Of the eight monolithic filters installed on the lower plenum, six failed. The only two monolithic filters that survived the transient were Industrial Filter & Pump recrystallized silicon carbide (REECER™). These elements probably survived due to the high-thermal conductivity of this material. This is discussed in depth in section 3.5 of this report.

3.3.2 Manway Inspection

Once the manway was opened all of the broken elements could be seen. However, at the time it was not known if there were additional filter elements broken in the top plenum. The most obvious filter elements broken were the 2-meter Pall 326 elements. Due to vibration concerns, Pall had manufactured these elements with a ceramic pin at the bottom. This pin was used to fix the element at the bottom to alleviate concerns about vibration. The fixing hardware was attached to a metal support post in the adjacent holder. When the PCD was inspected it was found that these elements were still held at the bottom but leaning against the shroud as shown in Figure 3.3-2.

The broken Ensto filter as well as one of the 1.5-meter Pall 326 filters could be "seen" since they were missing from the filter assembly. It was difficult to see how much of the filter element remained attached to the tubesheet. However, the 1.5-meter Pall 326 located in the center of the lower plenum had been instrumented with thermocouples. It had broken and was hanging by the thermocouples much lower than the rest of the filter elements as shown in Figure 3.3-3.

One other interesting observation was the "fragment" that was lodged between the filter elements shown in Figure 3.3-4. Initially, this was thought to be a fragment of one of the broken filter elements. However, when the PCD was disassembled it was discovered that this was actually a section of the sintered filter cake approximately 1 mm thick.

3.3.3 PCD Disassembly

3.3.3.1 Filter Elements

The PCD was disassembled on October 21, 1998. The most obvious damage was on the northwest side of the lower plenum where the Schumacher TF20, 1.5-meter Pall 326, and the 2-meter Pall 326 elements were located. All four elements were located adjacent to each other and approximately 6 to 12 inches of the filter elements were still attached to the tubesheet (see Figure 3.3-5). The 1.5-meter Pall 326 had been instrumented with thermocouples to detect any thermal transients; unfortunately, as mentioned already in the run report, these thermocouples were not monitored during the transient. To the right of the Schumacher and 1.5-meter Pall elements shown in Figure 3.3-5 is a Buffalo Conax fitting used to provide a pressure seal around the thermocouple wires.

The Ensto element failed very close to the filter flange, as shown in Figure 3.3-6. Only about 3 inches of the filter element remained below the flange.

The damaged 1.5-meter Pall 326 element located in the center of the lower plenum was very interesting. This element was also instrumented, and the instrumentation wiring supported many of the filter fragments. As shown in Figure 3.3-7, the filter element cracked in both the circumferential and axial directions similar to the cracking seen in the Coors filter elements when they failed due to thermal gradients.

One of the eight PRD-66 filter elements was damaged during the event but it was not broken. As seen in Figure 3.3-8, pieces of the membrane were missing from the filter element. Membrane "spalling" of PRD-66 elements had occurred in the Westinghouse filter system at the Tidd Facility in Brilliant, Ohio, but it is believed that the damage to this filter was not caused by the same mechanism. This filter element was located adjacent to the 1.5-meter Pall 326 in the center of the lower plenum that shattered during the thermal transient. All of the damage to the PRD-66 filter occurred on the side of the element facing the broken Pall filter. It is possible that as the Pall 326 filter shattered pieces of the broken filter hit the PRD-66 filter, causing the membrane to be damaged.

One very important observation is that of the eight monolithic filter elements on the lower plenum the only two that were not broken were the Industrial Filter and Pump recrystallized silicon carbide filter elements. Materials testing of these elements indicate that the thermal conductivity of the elements is substantially higher than any other monolithic filter. Because of higher conductivity it is difficult for temperature gradients to form across the filter element wall during a thermal event such as the one experienced in TC04. This makes the filter element much more likely to survive such a transient. A more detailed description of the filter element properties can be found in section 3.4 of this report; thermal transients are discussed in section 3.5.

3.3.3.2 Ash Observations

In addition to the observations regarding the broken filters there was a substantial difference between the filter cake on the upper and lower plenum. On the lower plenum the filter cake was very thin and had formed a 1- to 2-mm thick "shell" over the surface of the filter elements. This shell was sintered ash and it could be peeled off of the filter element in large (6- to 12-inch) fragments. The sintered ash cake attached to a McDermott filter element on the lower plenum is shown in Figure 3.3-9.

On the top plenum the appearance of the filter cake was completely different (see Figure 3.3-10). Initially, it was believed that the cracked appearance of the filter cake was due to cracks in the filter elements that were showing through the filter cake. However, when the filter cake was touched the cake fell off the element in fragments. It appeared that the surface of the filter cake had sintered and then cracked due to thermal expansion as the elements cooled. However, the sintering of the ash on the top plenum was much less extensive than the sintering on the lower plenum.

It was concluded that the magnitude of the thermal event during TC04 was much more severe in the lower section of the PCD because of (1) the severity of the ash sintering and (2) no breakage of monolithic SiC filters in the top plenum.

3.3.4 Conclusions

The observations made during the inspection provided some very important insights as to the performance of various filter elements during thermal transients. These insights include:

- Monolithic oxide filter elements are very sensitive to temperature gradients formed during thermal events due to their low-thermal conductivity.

- Even though the monolithic "clay-bonded" silicon carbide filter elements sold by Pall and Schumacher are less sensitive to thermal events than the monolithic oxide elements (such as Coors, Blasch, and Ensto) they can still fail due to temperature gradients.

- The Industrial Filter and Pump recrystallized silicon carbide (REECER) filter element is probably the most resistant of all the monolithic filter elements to thermal events due to its high-thermal conductivity.

- The composite filter elements do not appear to be affected by thermal gradients. Aside from the one PRD-66 filter that was damaged (probably from being hit upon failure of a nearby element) no composite filter appeared to be damaged by the thermal event.

- The metal filter elements were not affected by the thermal event. This is expected due to the high-thermal conductivity and thin wall of the metal elements. It would be practically impossible in this system to have a thermal event in the PCD that would create a temperature gradient across a metal filter element that would cause it to fail.

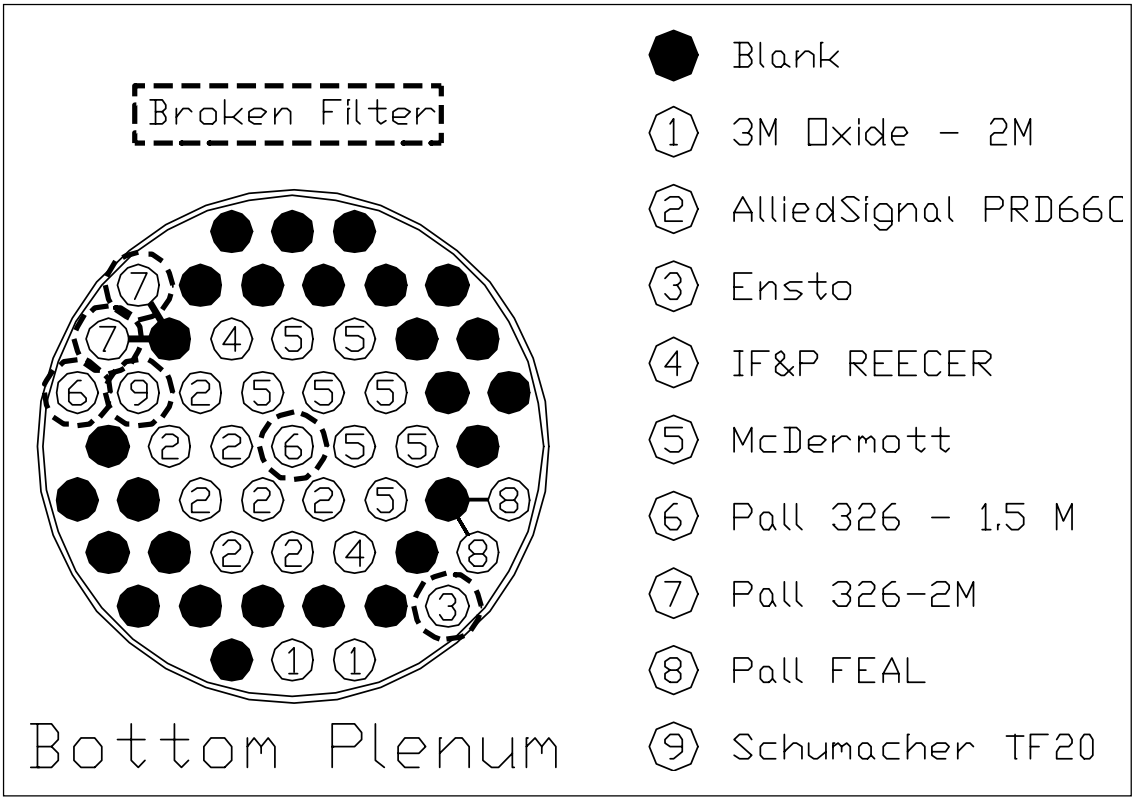

Figure 3.3-1 Broken Filters After TC04

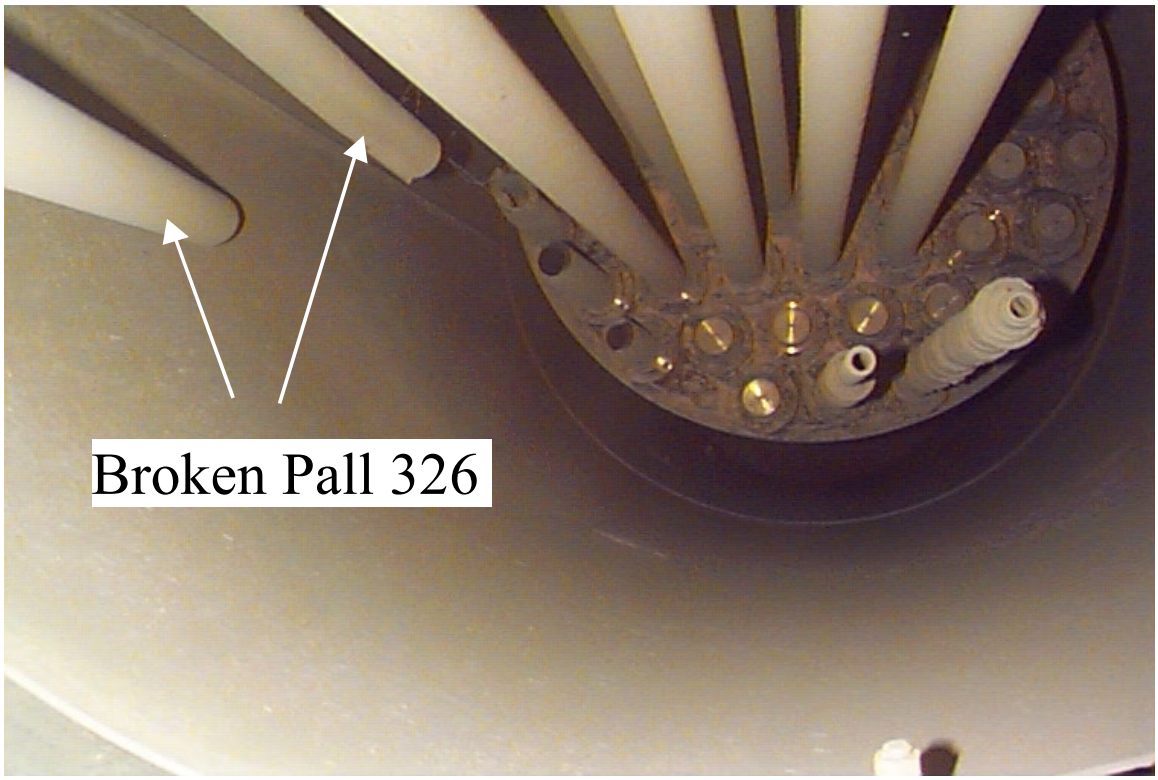

Figure 3.3-2 Broken Pall 326 Filter Elements During Manway Inspection

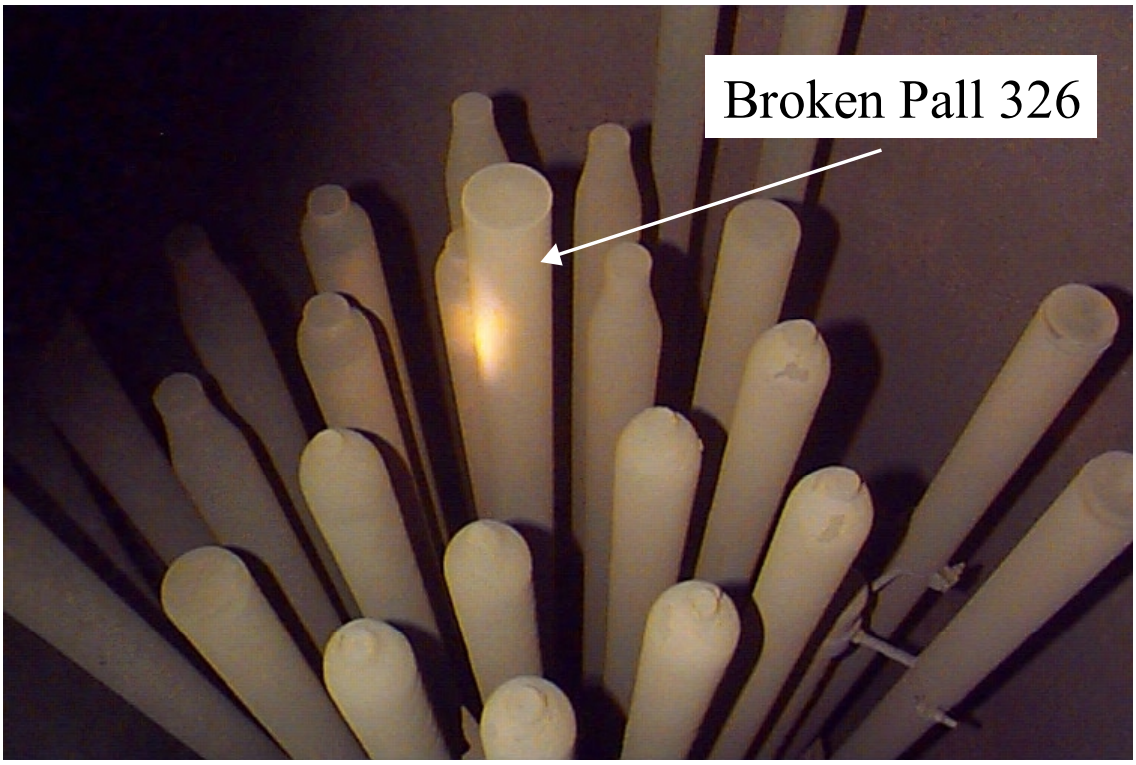

Figure 3.3-3 Broken 1.5-Meter Pall 326 Supported by Thermocouples

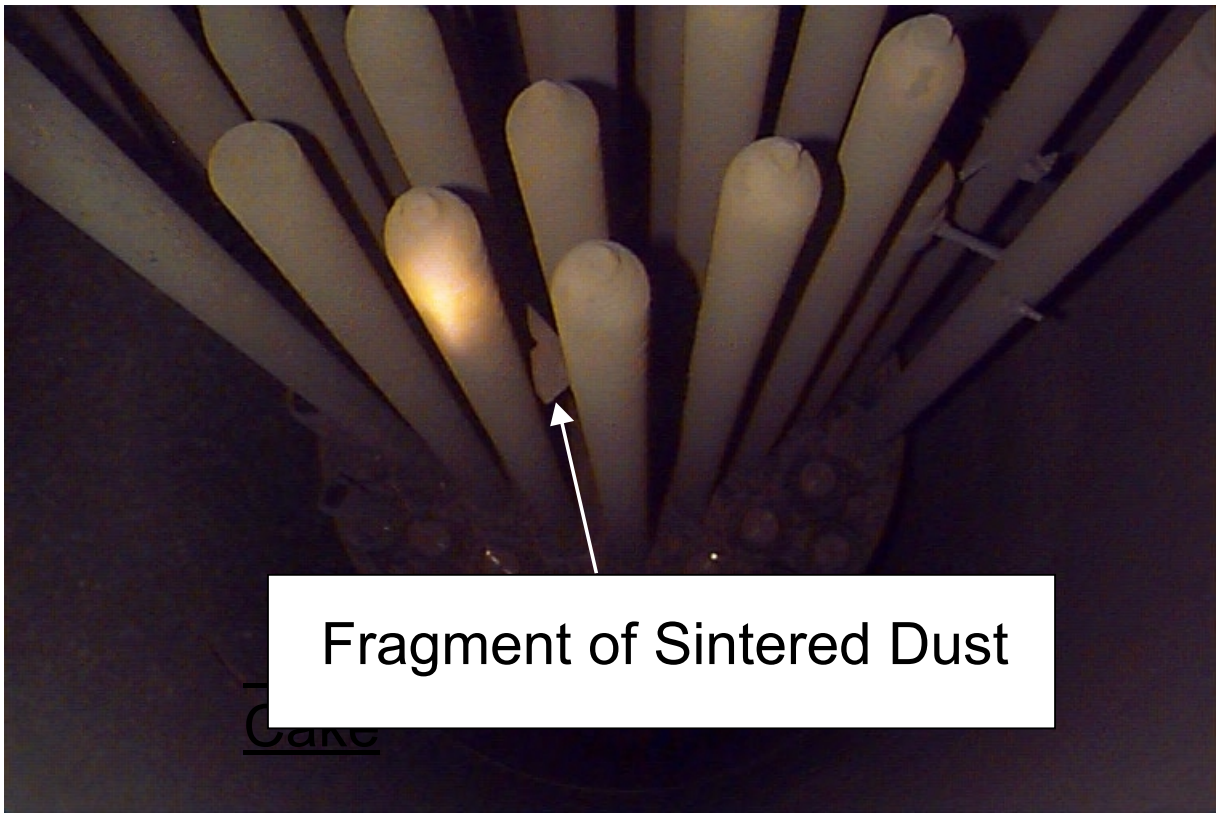

Figure 3.3-4 Sintered Dust Cake Fragment Lodged Between Filters

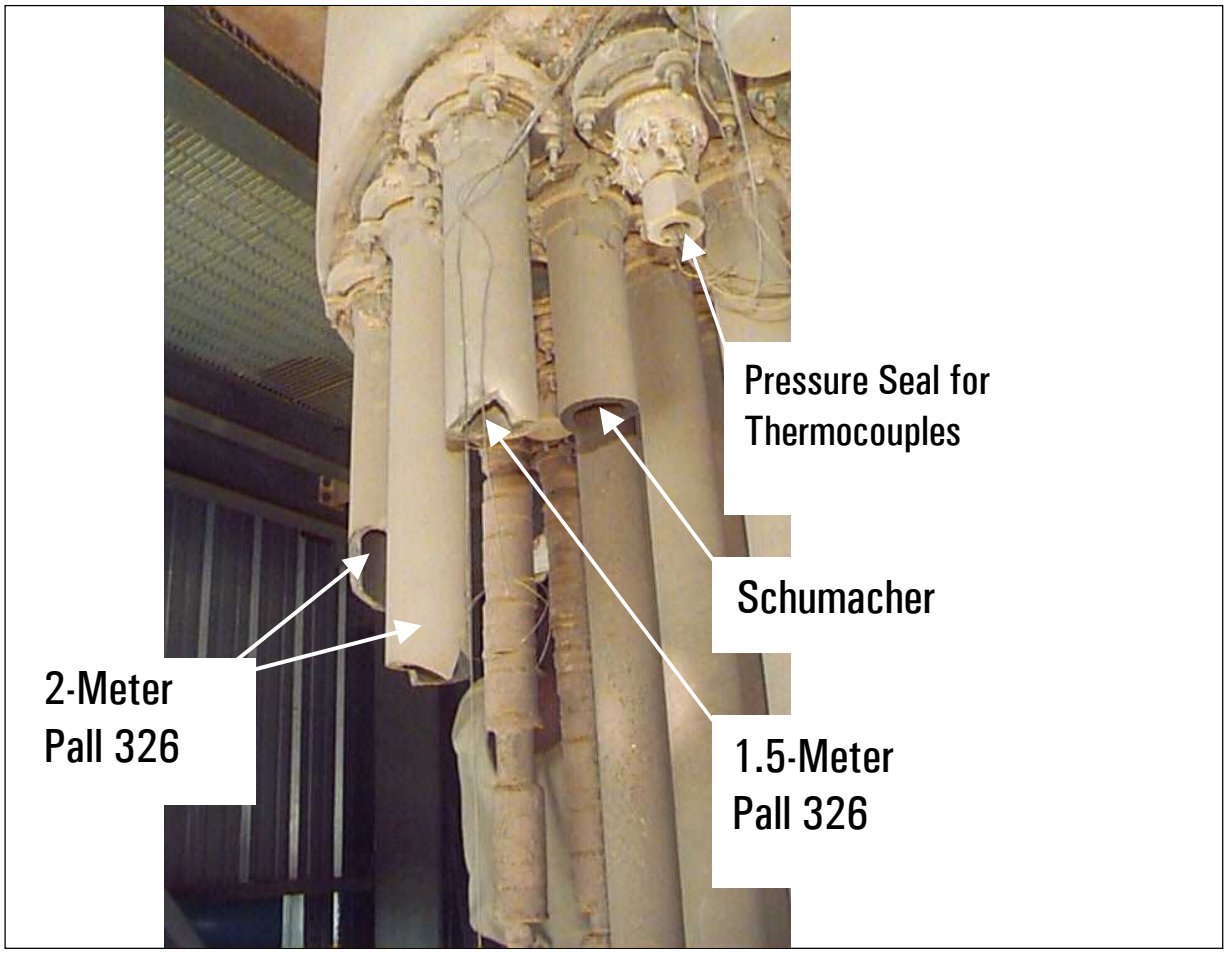

Figure 3.3-5 Broken Filters After TC04

Figure 3.3-6 Broken Ensto Filter After TC04

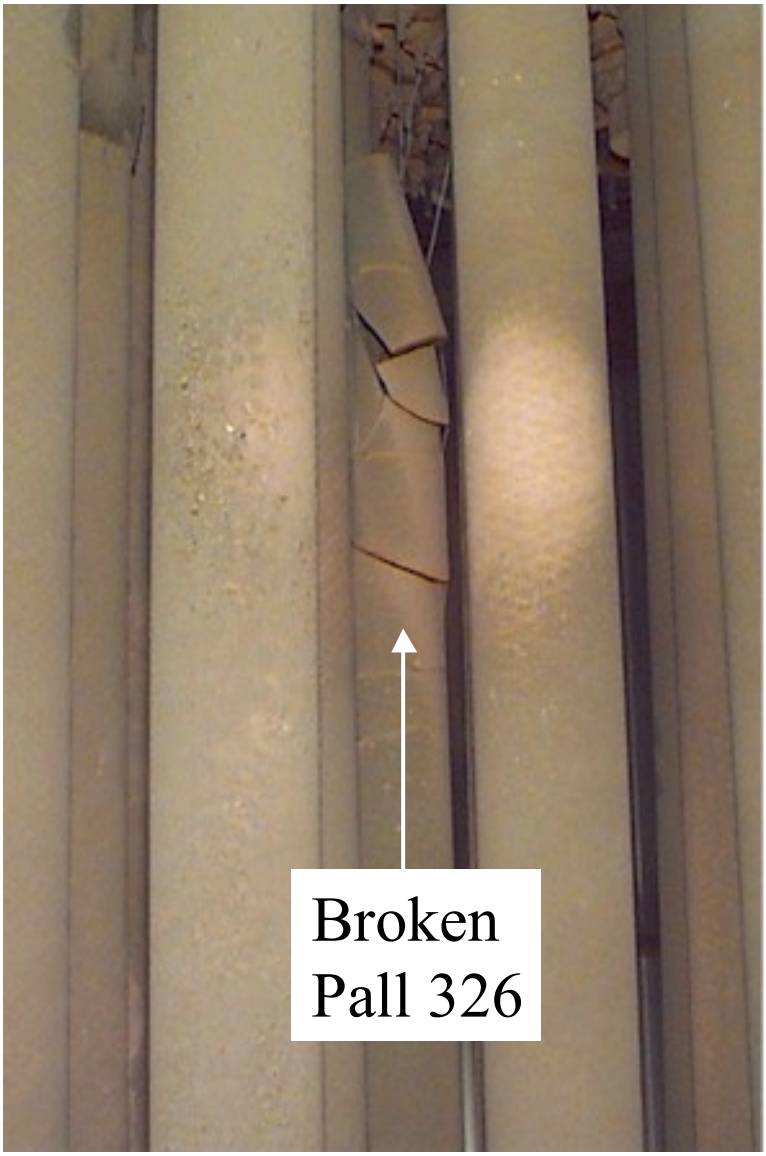

Figure 3.3-7 Broken Pall 326 From Center of Lower Plenum

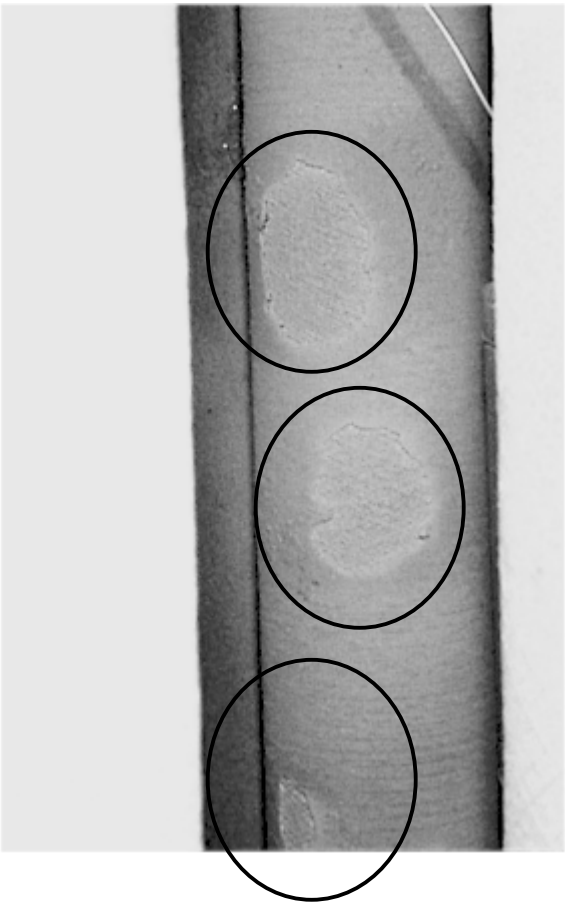

Figure 3.3-8 Damaged Membrane on PRD-66 Filter

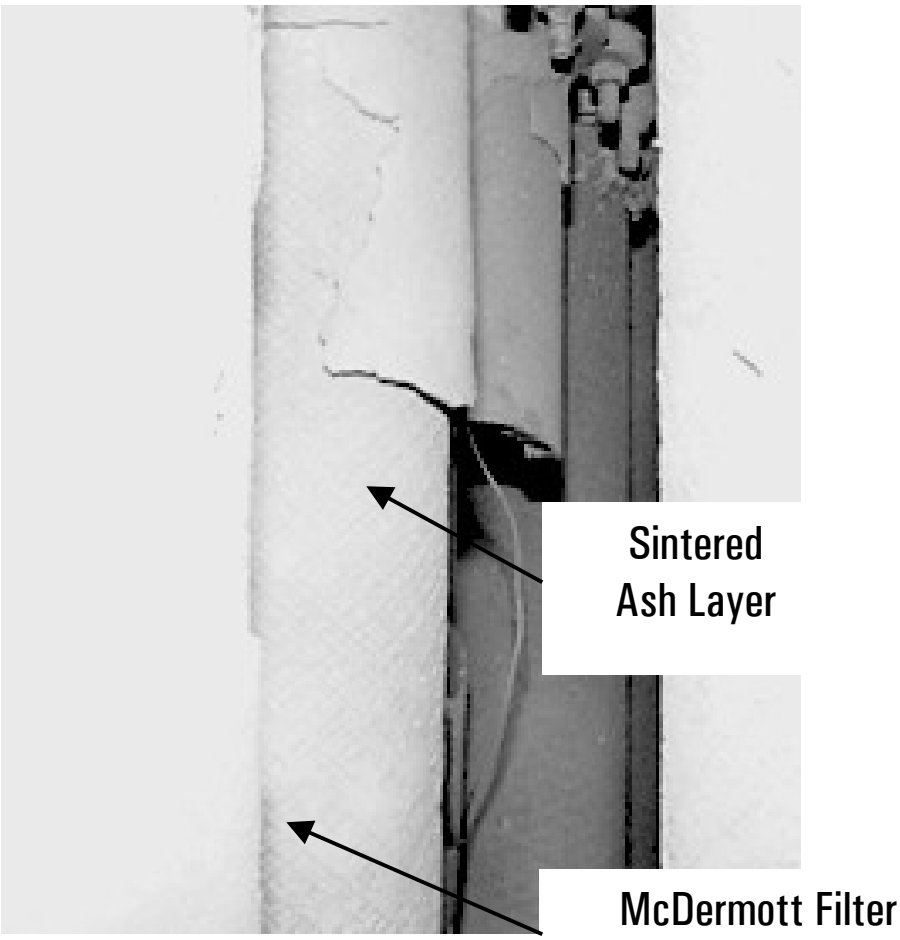

Figure 3.3-9 Sintered Ash Layer on McDermott Filter Element

Figure 3.3-10 Appearance of Ash Cake on Top Plenum

3.4 FILTER ELEMENT MATERIALS TEST REPORT

Property testing of filter elements continued in support of this test campaign. During this reporting period testing of exposed IF&P REECER™, Pall 326, and Schumacher TF20 and T10-20 filters was conducted and the results were compared to previous results obtained for these materials as-manufactured and after operation in the PCD. Descriptions of these materials were given in previous reports (references 1 and 2) and are not repeated here. During previous testing the strength of exposed Pall 326 appeared to correlate more closely with virgin element weight (measured before the elements were first installed for operation) than to operation history. Five as-manufactured Pall 326 elements were tested to evaluate the effect of virgin weight on tensile strength.

Property tests have been conducted on 3M oxide/oxide composite and Pall iron aluminide (FeAl) for the first time during this reporting period. Baseline properties were obtained on as-manufactured elements and hoop tensile strength was measured after operation in the PCD. Material descriptions are as follows.

- 3M oxide/oxide is a three-layer composite filter with nominal overall dimensions of 1.95-in. inside diameter (I.D.) x 2.375-in. outside diameter (O.D.) x 60 in. The inside and outside layers provide structural support for the filter mat in between. The inside and outside support layers are both Nextel 610 fiber (composition >99 percent Al_2O_3) in an alumino-silicate matrix. The filter mat is chopped alumina fiber.

- Pall iron aluminide is a sintered powder metal filter with nominal overall dimensions of 2.22-in. I.D. x 2.35-in. O.D. x 60 in. The filters are in three sections connected by welded joints. The flange is welded to one end and an end cap to the other.

The elements tested and the test matrices are summarized in Tables 3.4-1 through -6. Cutting plans for all elements tested in this test campaign are shown in Figures 3.4-1 through -7. Test results obtained for each type of filter element are presented in sections 3.4.1 through 3.4.6. The specimen length used for all ceramic and metal hoop tensile elements was 2 inches. The 2-inch specimen length represents a change from the 1-inch specimens used in most previous efforts. This change was made in response to concerns about the effect of edge conditions on measured strength. If there is any such effect it may be less with a 2-inch specimen than a 1-inch specimen. When comparing the strengths measured on specimens of different volumes the possible effect of volume on tensile strength must be considered; however, the effect of using 2-inch instead of 1-inch specimens should be minimal for these materials. For a material whose strength is controlled by the presence of flaws, the Weibull Volume Theory gives the relationship between strength and volume as:

$$(\sigma_1/\sigma_2) = (V_2/V_1)^{1/m}$$

where:

V1, V2 = two different specimen volumes,
σ_1,σ_2 = strength of specimens having volumes V_1 and V_2, and
m = Weibull modulus ($m \cong 1.2$/Coefficient of Variation).

For a material with a coefficient of variation (COV) in strength of 10 percent, the effect of doubling the specimen volume (for example, increasing length from 1 to 2 inches) is less than 6 percent. All of the ceramic materials tested in this effort have a COV of less than 10 percent (at least within a particular element) except one REECER™ element that had a COV of 14 percent. As-manufactured Pall 326 clay-bonded SiC specimens have been tested with both 1- and 2-inch lengths. The results for 1-inch specimens were previously reported in reference 1 (see page 3.4-11). All strength values obtained for 1- and 2-inch as-manufactured Pall 326 specimens are plotted in Figure 3.4-8 and no volume effect was seen. Based on the results for Pall 326 showing no effect on strength and the Weibull analysis showing a maximum effect of less than 6 percent, the change in specimen length to help alleviate concerns over the effect of end conditions appears justified.

3.4.1 3M Oxide/Oxide

Hoop tensile and axial compressive test results obtained on 3M oxide/oxide composite elements, as-manufactured and after operation in the PCD, are presented in this section. The candles were operated in combustion mode at a nominal temperature of 1,400°F. A potentially major issue not addressed in these test results is pinholes in the filtration mat layer. A pinhole was discovered in element number 8174 approximately 10.3 inches from the flanged end after 1,420 hours in operation. A photograph is shown in Figure 3.4-9. This type of pinhole is unlikely to cause an element to fracture but is potentially more damaging than a fractured element because of the fail-safes currently in use. These fail-safes require more ash to trigger their operation than a pinhole leak will produce; however, the leak will be large enough to damage a turbine.

3.4.1.1 Tensile Results

Hoop tensile testing was conducted on 1-, 2-, and 3-inch-long specimens. The failure mode of the 1- and 2-inch specimens was fiber pullout and not the proper failure mode—tensile failure of the fibers. Proper failures were obtained for the 3-inch specimens and all results reported were obtained from 3-inch specimens. The 3-inch specimen length and a high-Poisson ratio (Poisson ratio was not measured—the behavior observed during testing indicates that it was relatively high) caused the specimen length to decrease during hydrostatic tensile loading more for 3M than for any other filter elements tested. The decrease in specimen length opened the 0.005-in. clearance between the test specimen and the test fixture, allowing the rubber bladder to extrude. This led to failures at the ends of the specimens. Metal bands (hose clamps) approximately 5/16-in. wide were used to constrain the ends and prevent this type of failure. All results shown were obtained on specimens with ends constrained by metal bands.

Stress calculations for the 3M specimens were difficult because of their multi-layer construction. Stresses were calculated assuming the inner layer carries all load imposed by the hydrostatic pressure. Dimensions used for calculating material stresses from measured hydrostatic pressures were the measured specimen I.D. and the nominal thickness of the inside layer of 0.055 inch. Maximum hydrostatic pressure is also reported for each specimen, which may be more appropriate for comparison of different filter elements with different wall thicknesses.

Hoop tensile stress-strain responses for as-manufactured material are shown in Figure 3.4-10 and the results are summarized in Table 3.4-7. These responses showed a "yield" point at a stress level that ranged from ~1,730 to ~2,120 psi (hydrostatic pressure ranged from 90 to 130 psig). Above this stress level, there was significant strain with little increase in stress. Tensile failure of the fibers was not obtained, but there was permanent deformation as the specimens remained barrel-shaped after unloading. The maximum-tensile stress ranged from 2,210 to 2,840 psi (hydrostatic pressure ranged from 120 to 150 psig). Young's modulus calculated from the stress-strain curves ranged from 2.1 to 4.0 msi with an average of 3.1 msi. Because these Young's modulus values were calculated based on a nominal wall thickness and the assumption that all load is carried in the inner composite layer, these values should be considered only for comparison of elements (element-to-element variability, as-manufactured vs. used, etc.).

Responses measured after 1,420 hr in operation are presented in Figure 3.4-11 and the results are summarized in Table 3.4-7. The results do not indicate a decrease in tensile strength after operation; however, the curves show a change in response from the as-manufactured specimens. A yield point can still be identified in five of six specimens tested at stress levels of 2,300 to 3,580 psi (hydrostatic pressures of 120 to 200 psig) but the amount of deformation after yielding was much less than for the as-manufactured specimens. The failure mode changed as tensile failure of the fibers was obtained in all of the specimens after 1,420 hr of operation. Ultimate strengths ranged from 2,440 to 4,060 psi (hydrostatic pressures of 130 psig to 230 psig). Young's modulus ranged from 2.2 to 4.9 msi with an average of 3.2 msi.

Responses measured after 1,982 hr of operation, including an incident of coal burn inside the PCD, are presented in Figure 3.4-12 and the results are summarized in Table 3.4-7. Further changes were seen although the ultimate strength was still unchanged. Tensile failure of the fibers was obtained in all specimens as the curves began to roll over; no yielding was seen. Ultimate strengths ranged from 2,480 to 3,270 psi (hydrostatic pressures ranged from 130 to 190 psig). Young's modulus ranged from 2.9 to 3.4 msi with an average of 3.1 msi.

Tensile strength is plotted versus hours of operation in Figure 3.4-13. The results show no strength loss during ~2,000 hours of operation at a nominal temperature of 1,400°F in the PCD; however, there were material changes evident in the stress-strain curves. After operation, the strain capacity was decreased significantly and after the thermal transient the strain capacity was further reduced. More experience in operation would be required to assess whether the strain capacity continues to decrease with operation and whether this would lead to candle failures.

3.4.1.2 Compressive Results

Axial compressive stress-strain responses of as-manufactured material are shown in Figure 3.4-14 and the results are summarized in Table 3.4-8. These curves showed yield-stress values of 1,730 to 2,900 psi and ultimate strengths of 2,870 to 3,660 psi. At the ultimate-strength level, strain continued to increase with decreasing load; loading was stopped. No visible failures were seen on unloading. Young's modulus ranged from 2.4 to 4.0 msi with an average of 3.4 msi, approximately the same as in the hoop direction.

3.4.1.3 Summary

Hoop tensile results indicate that the strength did not decrease during ~2,000 hours of combustion operation at a nominal temperature of 1,400°F; however, the strain capability did decrease. The maximum-axial load these elements can withstand was calculated to be 670 lb, assuming an axial-yield strength of 1,970 psi (the same as the hoop-yield strength) and a 1.90-in. I.D. x 0.055-in.-thick wall. The tensile loads on the elements during operation have not been determined; however, based on experience to date the load capacity of these elements appears sufficient.

The biggest obstacle to use of 3M elements in the PCD is the pinholes developing in the filtration mat. More experience in operation is needed to assess such issues as the decrease in strain capacity during operation, the effect of vibration, sealing at the flanged end, etc., but the pinhole problem must be addressed before any more operational experience is achieved.

3.4.2 IF&P REECER™

Hoop tensile testing was conducted on two REECER™ filter elements after operation in the PCD in combustion mode at a nominal temperature of 1,400°F and the results were compared to results previously reported for as-manufactured material (see reference 2). The two elements tested in this effort were from the same manufacturing "batch" as the two elements previously tested. Some manufacturing anomalies were seen in the elements tested during the earlier effort and the same anomalies were seen in the elements tested in this effort. Wall thickness varied along the length of the elements by ~0.05 to 0.10 inch. Also, "bubbles" up to ~1/8 in. in diameter were seen in the element walls. Some of these bubbles were internal and some extended to the inside surface. None extended to the outside surface. There was no evidence that these manufacturing anomalies have affected performance during operation; however, IF&P is working to prevent them in the future.

3.4.2.1 Density

Density was measured on the tensile specimens before testing and the results are summarized in Table 3.4-9. The average density was 2.39 gr/cm^3. The filter elements were water washed before testing but some ash remained in the pores. These densities were calculated based on weights measured with ash in the pores and, therefore, do not represent a material property. The values are for comparisons only.

3.4.2.2 Tensile Results

Hoop tensile results are summarized in Table 3.4-10 and strength is plotted versus hours in operation in Figure 3.4-15. The two used elements were in operation during the same period, except that element number FE98073102 experienced a fire in the PCD during the October 1998 test campaign. Strengths measured after 1,420 hours in operation were higher than strengths measured on as-manufactured elements. This could represent either an increase in strength during operation or candle-to-candle variability. No work was done to determine the reasons for higher strength in the elements tested after operation. The results also indicated that

the strength was unaffected by the fire. Examination of the failed specimens showed that 13 of the 18 failed at one of the "bubbles"; however, the strengths were not significantly different for the specimens that failed at the bubbles versus those with no visible bubbles.

3.4.2.3 Summary

IF&P REECER™ has a higher thermal diffusivity than any ceramic filter material tested so far; thus lower temperature gradients during thermal transients (see reference 2). During operation these elements have survived thermal transients that led to failure of monolithic oxide and clay-bonded SiC elements. Hoop tensile testing showed that the as-manufactured strength is comparable to the Pall and Schumacher clay-bonded SiC elements. After 1,420 hours of operation in combustion mode the average tensile strength measured was higher than the as-manufactured strength. The measured strength was unaffected by exposure to a thermal transient.

The relatively high-thermal conductivity and results in operation so far have generated strong interest in this material; however, the results have been obtained on fewer elements with fewer hours of operation than many other filter elements. Additional operational experience and material testing is needed to help predict long-term performance. Several specific areas that should be addressed in future testing have been identified; two of these areas are discussed below. First, the manufacturer has taken steps to control the anomalies discussed above — inconsistent wall thickness and "bubbles." Measurements on future elements must confirm that these anomalies are indeed under control. Second, previous test results (see reference 2) showed a lower elevated-temperature strain-to-failure for REECER™ than for other ceramic elements. Lower strain-to-failure would offset some of the advantage gained by high-thermal diffusivity and could lead to failure during thermal transients even with relatively low-temperature gradients. Future testing should better define the tensile strain-to-failure at elevated temperatures to allow an assessment of how much improvement this material may offer over the clay-bonded SiC materials during thermal transients.

3.4.3 Pall 326 – Study of As-Manufactured Candle Weights

Previous test results for Pall 326 and 442T suggested a possible correlation between hoop tensile strength and as-manufactured element weight (see reference 2). This correlation appeared stronger than the correlation between strength and operational history. For this effort the hoop tensile strength was measured on five as-manufactured elements of varying weights. The elements were selected to include the lowest weight (4,305 grams) and the highest weight (4,615 grams) elements available at the PSDF. The as-manufactured weights reported here were supplied by Pall and were measured before the elements were shipped to the PSDF.

3.4.3.1 Density

Individual specimen densities and as-manufactured element weights are summarized in Table 3.4-11. The specimen densities did not correlate with the as-manufactured weights of the elements from which they were removed due to dimensional variations. Specimen densities ranged from 1.78 gr/cm^3 to 1.86 gr/cm^3 and the average value was 1.81 gr/cm^3.

3.4.3.2 Tensile Results

Hoop tensile results are summarized in Table 3.4-12 and the strength is plotted versus as-manufactured element weight in Figure 3.4-16. These results do not show a correlation between as-manufactured weight and strength for Pall 326. While a small variation from element to element was seen, all of these strength measurements taken together indicate a relatively consistent strength. If all 45 tensile strength measurements are grouped together an average strength of 2,050 psi with a coefficient of variation of 5 percent is obtained. The individual variations in strength did not correlate with individual specimen densities.

3.4.3.3 Summary

Over the range of element weights tested in this effort, as-manufactured element weight does not control tensile strength.

3.4.4 Pall 326 Exposed Elements

Two Pall 326 elements were tested after PCD operation in combustion mode at a nominal operating temperature of 1,400°F. Element 1075-3 was in operation for 2,830 hours; element 1069-3 for the same 2,830 hours and also experienced a thermal transient due to a fire in the PCD in October 1998. Results obtained in this effort were compared to previously reported results for Pall 326.

3.4.4.1 Density

Density was measured on the tensile specimens before testing and the results are summarized in Table 3.4-13. The average density of element 1075-3 was 1.96 gr/cm^3 and the average density of element 1069-3 was 1.86 gr/cm^3. The filter elements were water washed before testing but some ash remained in the pores. These densities were calculated based on weights measured with ash in the pores and, therefore, do not represent a material property. The values are for comparisons only.

3.4.4.2 Tensile Results

Hoop tensile results are summarized in Table 3.4-14. All hoop tensile strengths measured thus far in this effort or previous efforts are plotted versus hours in operation in Figure 3.4-17. These results show evidence of variability from element to element—especially element 3-24A, tested after 429 hours of operation at the PSDF (see reference 2); however, there is no evidence of strength degradation in 2,830 hours of operation at 1,400°F. Comparison of elements 1075-3 and 1069-3 would indicate a strength loss due to exposure to the thermal transient; however, the strength difference between these two elements may be due to material variability as seen between the two elements tested after 429 hours of operation. The strengths measured after operation at Karhula indicate that an operating temperature of 1,550°F may lead to strength degradation not seen during operation at 1,400°F.

3.4.4.3 Summary

No evidence of tensile strength degradation is seen for up to 2,830 hours of operation in combustion mode at 1,400°F. Due to variability from element to element, results are inconclusive on whether strength decreased after exposure to the thermal transient.

3.4.5 Pall Iron Aluminide

3.4.5.1 Density

Density was measured on the hoop tensile specimens before testing and the results are summarized in Table 3.4-15. The density of as-manufactured specimens ranged from 3.89 to 4.00 gr/cm^3 and the average density was 3.92 gr/cm^3. The exposed elements were water washed before testing but some ash remained in the pores. The average density of the exposed specimens was 4.00 gr/cm^3. These density values were calculated based on weights measured with ash in the pores and, therefore, do not represent a material property. The values are for comparisons only.

3.4.5.2 Tensile Results

Axial tensile results obtained from as-manufactured material are summarized in Table 3.4-16 and the stress-strain responses are shown in Figure 3.4-18. At room temperature, the virgin material had an average ultimate tensile strength of 19,000 psi; Young's modulus of 5.2 msi; and strain-to-failure of 9.5 mils/inch. The stress-strain responses showed a gradual yielding before ultimate strength was reached. The yield strength based on a 0.05-percent offset (a line was drawn parallel to the initial slope of the stress-strain curve but offset by 0.0005 and the intersection of this line with the stress-strain curve is the 0.05-percent-offset yield strength) calculated at 12,800 psi. At 1,400°F, the ultimate strength decreased to 6,200 psi and the yield strength to 4,200 psi. Young's modulus decreased to 3.5 msi and strain-to-failure increased to 15 mils/inch at 1,400°F. Based on the room-temperature yield strength of 12,800 psi and the average dimensions of the elements the maximum axial load these candles can withstand is 6,900 lb, sufficient to withstand the anticipated loads during operation. From the average Young's modulus of 5.2 msi and the average dimensions of the elements the first fundamental natural frequency was calculated to be 16 Hz. After 1,356 hours of operation at 1,400°F the ultimate strength and yield strength decreased ~15 percent to 16,000 and 11,100 psi and strain-to-failure decreased ~20 percent to 7.3 mils/inch. Young's modulus was unchanged.

Hoop tensile results are summarized in Table 3.4-17 and the stress-strain responses are shown in Figures 3.4-19 through -21. The ultimate strength of the as-manufactured element ranged from ~16,600 to ~18,000 psi (maximum hydrostatic pressure ranged from 1,060 to 1,170 psig) and the average value was 17,300 psi (hydrostatic pressure of 1,130 psig). The 0.05-percent-yield stress was ~13,000 psi. Young's modulus in the initial linear portion of the curve ranged from 5.8 to 7.3 msi and the average value was 6.1 msi. Strain-to-failure ranged from 4.7 to 5.7 mils/inch and the average value was 5.1 mils/inch.

After 1,356 hours of operation at 1,400°F the ultimate hoop tensile strength ranged from ~11,800 to ~15,200 psi (maximum hydrostatic pressure ranged from 790 to 1,060 psig) and the average value was 14,200 psi (hydrostatic pressure of 930 psig). Again, yielding was seen; average 0.05-percent-yield strength was ~10,800 psi. Young's modulus in the initial linear portion of the curve ranged from 5.4 to 7.5 msi; average value was 6.1 msi. Strain-to-failure ranged from 2.5 to 4.9 mils/inch; average value was 4.0 mils/inch. These properties indicate a strength decrease of ~15 percent and a decrease in strain-to-failure of ~20 percent. Young's modulus was unchanged.

After 1,424 hours of operation at 1,400°F, including a thermal transient, the ultimate hoop tensile strength ranged from ~11,300 to ~15,100 psi (maximum hydrostatic pressure ranged from 720 to 1070 psig); average value was 13,100 psi (hydrostatic pressure of 870 psig). Young's modulus in the initial linear portion of the curve ranged from 6.1 to 6.3 msi; average value was 6.2 msi. Strain-to-failure ranged from 1.9 to 3.6 mils/inch; average value was 2.6 mils/inch. These average properties would indicate a decrease in strength and strain capability after the thermal transient; however, the individual values showed that three specimens appeared lower and three appeared unchanged. The variation in strengths could be due to material variability, with no effect due to the thermal transient, or the variation could be the result of more severe thermal transient conditions in some regions than others with strength loss in the region where the conditions were most severe.

Figure 3.4-22 shows axial and hoop tensile strengths plotted versus hours of operation.

3.4.5.3 Flow Test Results

Element 034H005 was flow tested in as-manufactured condition. After 2,780 hours of operation at 1,400°F in combustion it was water washed, dried with warm air, and retested. The resulting pressure drop versus face velocity curves are shown in Figure 3.4-23. Permeability was calculated from ΔP versus velocity curves. Before operation, the permeability was 9 nanoperms (nPm) and after operation the permeability was 5 nPm. This permeability of 5 nPm allows the pressure drop across the element to remain acceptable. Additional elements will be flow tested to determine whether permeability continues to decrease with a resulting increase in pressure drop or remains steady with additional operation.

3.4.5.4 Summary

Room temperature tensile strength decreased ~15 percent after 1,356 hours of operation at 1,400°F. The stress-strain curves retained the nonlinear behavior after operation, indicating that ductility was retained. Testing after additional exposure would be required to determine whether further degradation occurs. Strengths measured after operation during a thermal transient were inconclusive to determine whether the element was damaged by the transient. Blinding is a major concern for FeAl elements. Flow testing after 2,780 hr in operation showed a decrease in permeability from 9 to 5 nPm, still within acceptable limits. Again, testing after additional exposure would be required to determine whether permeability continued to decrease.

3.4.6 Schumacher TF20 and T10-20 Exposed Elements

Test results for Schumacher TF20 and T10-20 elements are presented together in this section. The structural wall is the same for these two materials. Only the membrane layer is different. Since the membrane layer is only ~100 µm thick compared to ~10 mm for the structural wall the difference in membrane layer should have little or no effect on material properties. Previously reported virgin tensile strengths were actually ~20 percent lower for TF20 than T10-20; however, only one T10-20 element was tested. Based on data scatter seen and the similar composition of these two materials this difference is likely due to element-to-element variability. This should be confirmed by additional testing of virgin T10-20. For this report, the two materials will be treated as though the mechanical properties are the same.

3.4.6.1 Density

Density was measured on the specimens before testing and the results are summarized in Table 3.4-18 for TF20 and 3.4-19 for T10-20. The density of TF20 ranged from 1.93 to1.96 gr/cm^3 and the average density was 1.94 gr/cm^3. The density of T10-20 ranged from 1.97 to1.99 gr/cm^3 and the average density was 1.98 gr/cm^3. The elements were water washed before testing but some ash remained in the pores. These density values were calculated based on weights measured with ash in the pores and, therefore, do not represent a material property. The values are for comparisons only.

3.4.6.2 Tensile Results

Hoop tensile strength was measured on three TF20 elements and two T10-20 elements after PCD operation in combustion mode at a nominal operating temperature of 1,400°F. All of the TF20 elements and one of the two T10-20 elements were in operation during a thermal transient due to a fire in the PCD. The results are summarized in Table 3.4-20 for TF20 and -21 for T10-20. All hoop tensile strengths measured thus far in this effort or previous efforts are plotted versus hours in operation in Figure 3.4-24. These results show a strength decrease of ~30 percent during the first 491 hours of operation. The strength decrease may occur much earlier than 491 hours but no elements have been tested with fewer hours in operation. No further strength decrease is seen for up to 1,800 hours of operation. The average retained strength of nearly 1,300 psi is sufficient for operation at the PSDF. The four elements in operation during the thermal transient had the same nominal strengths as elements not exposed to the thermal transient. These results indicate no damage due to the thermal transient.

Evidence of material variability is seen in some specimens with much lower strengths than other specimens from the same element. Three of the elements tested, two in this current effort and one tested earlier, had individual specimens with tensile strengths 25 to 50 percent lower than the average strength of the other specimens from the same element. Densities of the low-strength specimens were the same as the densities of the average-strength specimens from the same element. None of the Schumacher elements have failed in operation so far due to low-tensile strength; however, the material variability is of concern.

3.4.6.3 Summary

The hoop tensile strength of Schumacher TF20 and T10-20 decreases ~30 percent from ~1,900 to ~1,300 psi during the initial hours of operation. For up to at least 1,800 hours of operation at 1,400°F the strength remains unchanged at ~1,300 psi. Elements tested after operation during a thermal transient in the PCD showed no additional strength loss due to this transient. Based on the strength measurements so far the biggest concern for these elements operating at 1,400°F is material variability.

3.4.7 Conclusions

In as-manufactured condition, 3M oxide/oxide composite offers some advantages over monolithic ceramic elements, including survival during more severe thermal transients. After 1,420 hours in operation at 1,400°F the tensile strength was unchanged but the strain-to-failure decreased. After 1,982 hours of operation including a thermal transient the strain-to-failure decreased further. Additional operation would be required to determine if strain-to-failure continues to decrease and if this would lead to failures. The biggest obstacle to use of 3M elements is pinholes in the filtration mat as seen in element 8174 after 1,420 hours of operation. The pinhole problem must be solved before more operational experience is achieved to address the other issues.

IF&P REECER™ has a relatively high-thermal diffusivity which leads to lower temperature gradients during thermal transients. This material has survived thermal transients in the PCD that caused clay-bonded SiC and monolithic oxide elements to fail; however, these results were obtained on fewer REECER™ elements with fewer hours of operation than many other filter elements. Additional operational experience and material testing is needed to help predict long-term performance. Two specific areas that should be addressed in future testing are discussed below. First, the manufacturer has taken steps to control an inconsistent wall thickness and "bubbles." Measurements on future elements must confirm that these anomalies are indeed under control. Second, previous test results showed lower elevated temperature strain-to-failure for REECER™ than for other ceramic elements. Lower strain-to-failure would offset some of the advantage of high-thermal diffusivity and could lead to failure during thermal transients even with relatively low-temperature gradients. Future testing should better define the tensile strain-to-failure at elevated temperatures to allow an assessment of how much improvement this material may offer over the clay-bonded SiC materials during thermal transients.

Testing of five as-manufactured Pall 326 elements with varying weights showed no correlation between element weight and as-manufactured hoop-tensile strength. No evidence of tensile-strength degradation was seen after 2,830 hours of operation in combustion at 1,400°F. Results were inconclusive on whether strength decreased after exposure to a thermal transient.

Pall FeAl has a relatively high-tensile strength and with a high-thermal diffusivity and thin wall should perform well during thermal transients. Test results showed a decrease of ~15 percent in tensile strength and ~20 percent in strain-to-failure after 1,420 hours of operation at 1,400°F. Results were inconclusive on whether strength and strain-failure decreased further after exposure to a thermal transient. The tensile strength measured after operation is sufficient for

operation at the PSDF. Testing after additional operation will determine if property degradation continues. Blinding is a major concern for FeAl elements. Flow testing after 2,780 hrs in operation showed a decrease in permeability from 9 to 5 nPm, still within acceptable limits. Again, testing after additional exposure would be required to determine whether permeability continued to decrease.

The hoop-tensile strength of Schumacher TF20 and T10-20 decreased ~30 percent during the initial hours of operation and then remained unchanged for up to at least 1,800 hours of operation at 1,400°F. After operation during a thermal transient in the PCD no additional strength loss was seen. Based on the strength measurements so far the biggest concern for these elements operating at 1,400°F is material variability.

3.4.8 References

1. Spain, J. D., and Starrett, H. S., "Physical, Mechanical, and Thermal Properties of Several Candidate Candle Filter Materials," Report Number SRI-ENG-99-016-8484.2.4-I-F, Prepared for U.S. Department of Energy Federal Energy Technology Center, Contract No. DE-AC21-94MC31160 (publication in production process).

2. Spain, J. D., and Starrett, H. S., "Mechanical and Thermal Evaluation of Several Candle Filter Materials," SRI-ENG-99-019-9386-I-F, Report to Southern Company Services, Purchase Order C-97-001785, May 1999.

Table 3.4-1

Filter Elements Tested

Material	Manufacturer's Candle ID	Operation Hours	Test Matrix
Pall FeAl	Log 034H-002	Virgin	1
Pall FeAl	Log 034H-001	1,356	2
Pall FeAl	Log 504J	1,424 (PCD Fire)	2
Pall 326	1291-3	Virgin	3
Pall 326	1324-7	Virgin	3
Pall 326	1333-4	Virgin	3
Pall 326	1366-5	Virgin	3
Pall 326	1324-4	Virgin	3
Pall 326	1075-3	2,830	4
Pall 326	1069-3	2,834 (PCD Fire)	4
Schumacher TF20	324H21	491 (PCD Fire)	4
Schumacher TF20	324H01	994 (PCD Fire)	4
Schumacher TF20	324H04	1,234 (PCD Fire)	4
Schumacher T10-20	324H02	1,788	4
Schumacher T10-20	324H01	1,792 (PCD Fire)	4
IF&P REECER™	FE98073105	1,420	4
IF&P REECER™	FE98073102	1,424 (PCD Fire)	4
3M Oxide/Oxide	8011	Virgin	5
3M Oxide/Oxide	8174	1,420	4
3M Oxide/Oxide	8003	1,982 (PCD Fire)	4

Table 3.4-2

Test Matrix 1

Test	Direction	Room Temp	Elevated Temp
Tension	Hoop	6	
Tension	Axial	3	2
Thermal Expansion	Axial	2---------->	
Microstructure – Microscopy, SEM, EDX, As Requested		Yes	
Strength of Weld		Yes	

Table 3.4-3

Test Matrix 2

Test	Direction	Room Temp	Elevated Temp
Tension	Hoop	6	
Tension	Axial	4 (Element 034H-001 only)	
Microstructure – Microscopy, SEM, EDX, As Requested		Yes	
Strength of Weld		Yes	

Table 3.4-4

Test Matrix 3

Test	Direction	Room Temp
Tension	Hoop	45 (9 Specimens From 5 Different Candles of Different Virgin Weight)

Table 3.4-5

Test Matrix 4

Test	**Direction**	**Room Temp**
Tension	Hoop	9
Microstructure – Microscopy, SEM, EDX, As Requested		Yes

Table 3.4-6

Test Matrix 5

Test	**Direction**	**Room Temp**
Tension	Hoop	9
Compression	Axial	2
Microstructure – Microscopy, SEM, EDX, As Requested		Yes

Table 3.4-7

Tensile Results of 3M Oxide-Oxide

Filter Identification	Specimen Number	Hours in Operation	Specimen I.D.[1] (in.)	Hydrostatic Pressure at Yield (psig)	Tensile Yield Strength (psi)	Maximum Hydrostatic Pressure (psig)	Tensile Strength (psi)	Young's Modulus[5] (msi)	Notes
8011	Tn-Hoop-145	As-manuf.	1.87	120	2120	140	2520	4.0	See Note 2
8011	Tn-Hoop-146	As-manuf.	1.89	130	2270	140	2570		See Note 3
8011	Te-ax-5	As-manuf.	1.91	100	1730	120	2210	2.1	See Note 2
8011	Te-ax-6	As-manuf.	2.00	90	1750	150	2840	3.3	See Note 2
		Average		110	1968	138	2535	3.1	
		Standard Deviation		16	234	11	224		
		Coefficient of Variation (COV)		14%	12%	8%	9%		
8174	Tn-Hoop-330	1420	1.87	200	3550	230	4060	4.9	See Note 2
8174	Tn-Hoop-331	1420	1.89	200	3580	210	3720	2.7	See Note 2
8174	Tn-Hoop-332	1420	1.96	130	2400	150	2670	2.9	See Note 2
8174	Tn-Hoop-333	1420	1.95	130	2380	140	2480	2.6	See Note 2
8174	Tn-Hoop-334	1420	1.98	120	2300	130	2440	2.2	See Note 2
8174	Tn-Hoop-335	1420	1.99	130	2380	130	2470	4.1	See Note 2
		Average		152	2765	165	2973	3.2	
		Standard Deviation		34	567	40	660	0.9	
		COV		23%	20%	24%	22%	29%	
8003	Tn-Hoop-324	1982	1.86			170	2870	3.2	See Note 4
8003	Tn-Hoop-325	1982	1.88			190	3270	3.0	See Note 4
8003	Tn-Hoop-326	1982	1.96			180	3220	3.4	See Note 4
8003	Tn-Hoop-327	1982	1.96			140	2490	2.9	See Note 4
8003	Tn-Hoop-328	1982	2.00			130	2480	3.3	See Note 4
8003	Tn-Hoop-329	1982	2.00			140	2600	3.0	See Note 4
		Average				158	2822	3.1	
		Standard Deviation				23	326	0.2	
		COV				14%	12%	6%	

Notes:

1. The rough outside surface made accurate O.D. measurements impossible. All stress calculations were based on the measured I.D. and a nominal wall thickness of 0.055 in.
2. These stress-strain responses showed a definite "yield point" where large strains were seen with little increase in stress. No yield point was seen for the specimens in operation during the PCD fire.
3. Strain was not measured on this specimen. Yield strength was taken to be the point where a drop in internal pressure was seen on the load-time response.
4. In operation during PCD fire.
5. Young's modulus was obtained in the initial linear portion of the stress-strain curve. The values were calculated based on the same assumptions as the strength values and are intended for use only in comparison of elements (element-to-element variability, as-manufactured vs. used, etc.)
6. All specimens were 3" long. The ends were constrained with 5/16" hose clamps to prevent the bladder from extruding.

Table 3.4-8

Compressive Results of 3M Oxide-Oxide

Filter Identification	Specimen Number	Test Temperature (°F)	Specimen I.D.[1] (in.)	Compressive Yield Strength (psi)	Ultimate Compressive Strength (psi)	Young's Modulus (msi)
8011	Cm-ax-1	RT[2]	1.92	2,550	3,230	3.5
8011	Cm-ax-3	RT	1.93	2,550	3,660	4.0
8011	Cm-ax-4	RT	1.94	2,900	2,950	3.7
8011	Cm-ax-5	RT	See Note 3	1,730	2,870	2.4

1. The rough outside surface made accurate O.D. measurements impossible. All stress calculations were based on a nominal wall thickness of 0.055 in.
2. RT = room temperature
3. The specimen I.D. was not measured on this specimen. The average value of the other specimens was used for the stress calculation.

Table 3.4-9

Density of IF&P REECER™

Candle	Specimen Number	Hours in Operation	ID (in.)	OD (in.)	Density (gr/cm³)
FE98073105	Tn-Hoop-353	1420	1.574	2.395	2.46
FE98073105	Tn-Hoop-354	1420	1.617	2.397	2.53
FE98073105	Tn-Hoop-355	1420	1.574	2.394	2.42
FE98073105	Tn-Hoop-356	1420	1.620	2.400	2.39
FE98073105	Tn-Hoop-357	1420	1.623	2.398	2.38
FE98073105	Tn-Hoop-358	1420	1.627	2.403	2.37
FE98073105	Tn-Hoop-359	1420	1.663	2.399	2.38
FE98073105	Tn-Hoop-360	1420	1.679	2.400	2.39
FE98073105	Tn-Hoop-361	1420	1.679	2.397	2.39
		Average			2.41
		Standard Deviation			0.05
		Coefficient of Variation (COV)			2.0%
FE98073102	Tn-Hoop-362	1424	1.602	2.407	2.38
FE98073102	Tn-Hoop-363	1424	1.612	2.401	2.37
FE98073102	Tn-Hoop-364	1424	1.645	2.409	2.38
FE98073102	Tn-Hoop-365	1424	1.694	2.402	2.38
FE98073102	Tn-Hoop-366	1424	1.707	2.401	2.40
FE98073102	Tn-Hoop-367	1424	1.688	2.405	2.35
FE98073102	Tn-Hoop-368	1424	1.743	2.400	2.36
FE98073102	Tn-Hoop-369	1424	1.746	2.401	2.37
FE98073102	Tn-Hoop-370	1424	1.738	2.400	2.36
			Average		2.37
			Standard Deviation		0.02
			COV		0.6%

Table 3.4-10

Hoop Tensile Strength of IF&P REECER™

Candle	Specimen Number	Hours in Operation	I.D. (in.)	O.D. (in.)	Max. Hydrostatic Pressure (psig)	Ultimate Strength (psi)	Remarks
FE98073109	Tn-Hoop-118	As-Manuf.	1.72	2.41	493	1530	See Note 1
FE98073109	Tn-Hoop-119	As-Manuf.	1.72	2.40	587	1810	See Note 1
FE98073109	Tn-Hoop-120	As-Manuf.	1.73	2.40	628	1980	See Note 1
FE98073109	Tn-Hoop-121	As-Manuf.	1.78	2.40	657	2260	
FE98073109	Tn-Hoop-122	As-Manuf.	1.78	2.41	711	2450	See Note 1
FE98073109	Tn-Hoop-123	As-Manuf.	1.80	2.40	645	2300	See Note 1
FE98073109	Tn-Hoop-124	As-Manuf.	1.82	2.39	564	2120	
FE98073109	Tn-Hoop-125	As-Manuf.	1.83	2.40	626	2380	
FE98073109	Tn-Hoop-126	As-Manuf.	1.82	2.39	519	1930	See Note 1
		Average			603	2084	
		Standard Deviation			65	282	
		Coeffecient of Variation (COV)			11%	14%	
FE98073110	Tn-Hoop-127	As-Manuf.	1.59	2.40	882	2260	
FE98073110	Tn-Hoop-128	As-Manuf.	1.60	2.41	819	2130	
FE98073110	Tn-Hoop-129	As-Manuf.	1.62	2.43	824	2130	
FE98073110	Tn-Hoop-130	As-Manuf.	1.68	2.40	570	1660	See Note 1
FE98073110	Tn-Hoop-131	As-Manuf.	1.70	2.40	605	1830	
FE98073110	Tn-Hoop-132	As-Manuf.	1.71	2.41	671	2040	See Note 2
FE98073110	Tn-Hoop-133	As-Manuf.	1.76	2.40	548	1800	
FE98073110	Tn-Hoop-134	As-Manuf.	1.75	2.39	626	2070	
FE98073110	Tn-Hoop-135	As-Manuf.	1.78	2.39	595	2060	
		Average			682	1998	
		Standard Deviation			118	181	
		COV			17%	9%	
FE98073105	Tn-Hoop-353	1420	1.57	2.40	1044	2633	See Note 1
FE98073105	Tn-Hoop-354	1420	1.62	2.40	1305	3487	See Note 1
FE98073105	Tn-Hoop-355	1420	1.57	2.39	964	2435	See Note 1
FE98073105	Tn-Hoop-356	1420	1.62	2.40	935	2501	See Note 1
FE98073105	Tn-Hoop-357	1420	1.62	2.40	972	2614	See Note 1
FE98073105	Tn-Hoop-358	1420	1.63	2.40	1225	3300	
FE98073105	Tn-Hoop-359	1420	1.66	2.40	1189	3391	See Note 1
FE98073105	Tn-Hoop-360	1420	1.68	2.40	1008	2941	See Note 1
FE98073105	Tn-Hoop-361	1420	1.68	2.40	1030	3014	
		Average			1075	2924	
		Standard Deviation			124	378	
		COV			12%	13%	
FE98073102	Tn-Hoop-362	1424	1.60	2.41	1225	3174	See Notes 1,3
FE98073102	Tn-Hoop-363	1424	1.61	2.40	1109	2930	See Notes 1,3
FE98073102	Tn-Hoop-364	1424	1.64	2.41	1160	3187	See Note 3
FE98073102	Tn-Hoop-365	1424	1.69	2.40	1001	2982	See Notes 1,3
FE98073102	Tn-Hoop-366	1424	1.71	2.40	1073	3267	See Note 3
FE98073102	Tn-Hoop-367	1424	1.69	2.41	986	2901	See Notes 1,3
FE98073102	Tn-Hoop-368	1424	1.74	2.40	1001	3236	See Notes 1,3
FE98073102	Tn-Hoop-369	1424	1.75	2.40	841	2730	See Notes 1,3
FE98073102	Tn-Hoop-370	1424	1.74	2.40	1037	3325	See Note 3
		Average			1048	3081	
		Standard Deviation			105	190	
		COV			10%	6%	

Notes:
1. Failed at "bubble".
2. Specimen had "bubbles" but did not fail at one.
3. In operation during PCD fire.

Table 3.4-11 (Page 1 of 2)

Density of As-Manufactured Pall 326

Candle	Specimen Number	Element Weight (gr)	I.D. (in.)	O.D. (in.)	Density (gr/cm³)
1366-5	Tn-Hoop-201	4305	1.549	2.355	1.82
1366-5	Tn-Hoop-202	4305	1.550	2.357	1.81
1366-5	Tn-Hoop-203	4305	1.555	2.359	1.82
1366-5	Tn-Hoop-204	4305	1.575	2.350	1.80
1366-5	Tn-Hoop-205	4305	1.575	2.362	1.80
1366-5	Tn-Hoop-206	4305	1.579	2.364	1.81
1366-5	Tn-Hoop-207	4305	1.596	2.356	1.80
1366-5	Tn-Hoop-208	4305	1.597	2.357	1.80
1366-5	Tn-Hoop-209	4305	1.599	2.352	1.81
		Average			1.81
		Standard Deviation			0.007
		Coefficient of Variation (COV)			0.38%
1333-4	Tn-Hoop-210	4380	1.562	2.355	1.83
1333-4	Tn-Hoop-211	4380	1.550	2.359	1.81
1333-4	Tn-Hoop-212	4380	1.553	2.362	1.80
1333-4	Tn-Hoop-213	4380	1.573	2.362	1.82
1333-4	Tn-Hoop-214	4380	1.573	2.360	1.81
1333-4	Tn-Hoop-215	4380	1.575	2.367	1.81
1333-4	Tn-Hoop-216	4380	1.591	2.365	1.80
1333-4	Tn-Hoop-217	4380	1.592	2.359	1.81
1333-4	Tn-Hoop-218	4380	1.598	2.361	1.81
		Average			1.81
		Standard Deviation			0.009
		COV			0.47%
1324-7	Tn-Hoop-219	4389	1.552	2.364	1.82
1324-7	Tn-Hoop-220	4389	1.551	2.366	1.82
1324-7	Tn-Hoop-221	4389	1.555	2.370	1.82
1324-7	Tn-Hoop-222	4389	1.571	2.378	1.81
1324-7	Tn-Hoop-223	4389	1.574	2.383	1.80
1324-7	Tn-Hoop-224	4389	1.576	2.382	1.81
1324-7	Tn-Hoop-225	4389	1.596	2.372	1.81
1324-7	Tn-Hoop-226	4389	1.596	2.368	1.81
1324-7	Tn-Hoop-227	4389	1.599	2.362	1.81
		Average			1.81
		Standard Deviation			0.005
		COV			0.27%

Table 3.4-11 (Page 2 of 2)

Density of As-Manufactured Pall 326

Candle	Specimen Number	Element Weight (gr)	I.D. (in.)	O.D. (in.)	Density (gr/cm³)
1324-4	Tn-Hoop-228	4525	1.574	2.386	1.79
1324-4	Tn-Hoop-229	4525	1.577	2.391	1.78
1324-4	Tn-Hoop-230	4525	1.578	2.394	1.78
1324-4	Tn-Hoop-231	4525	1.575	2.379	1.81
1324-4	Tn-Hoop-232	4525	1.576	2.378	1.81
1324-4	Tn-Hoop-233	4525	1.580	2.379	1.80
1324-4	Tn-Hoop-234	4525	1.622	2.397	1.78
1324-4	Tn-Hoop-235	4525	1.625	2.395	1.78
1324-4	Tn-Hoop-236	4525	1.627	2.393	1.78
		Average			1.79
		Standard Deviation			0.011
		COV			0.63%
1291-3	Tn-Hoop-237	4615	1.546	2.377	1.85
1291-3	Tn-Hoop-238	4615	1.550	2.377	1.85
1291-3	Tn-Hoop-239	4615	1.552	2.379	1.84
1291-3	Tn-Hoop-240	4615	1.571	2.389	1.85
1291-3	Tn-Hoop-241	4615	1.570	2.387	1.84
1291-3	Tn-Hoop-242	4615	1.571	2.387	1.85
1291-3	Tn-Hoop-243	4615	1.587	2.372	1.85
1291-3	Tn-Hoop-244	4615	1.590	2.372	1.86
1291-3	Tn-Hoop-245	4615	1.617	2.397	1.84
		Average			1.85
		Standard Deviation			0.006
		COV			0.32%

Table 3.4-12 (Page 1 of 2)

Hoop Tensile Strength of As-Manufactured Pall 326

Candle	Specimen Number	Element Weight (gr)	I.D. (in.)	O.D. (in.)	Specimen Density (gr/cm^3)	Ultimate Strength (psi)	Remarks
1366-5	Tn-Hoop-201	4305	1.55	2.35	1.82	2109	
1366-5	Tn-Hoop-202	4305	1.55	2.36	1.81	2192	
1366-5	Tn-Hoop-203	4305	1.56	2.36	1.82	2069	
1366-5	Tn-Hoop-204	4305	1.57	2.35	1.80	2183	
1366-5	Tn-Hoop-205	4305	1.58	2.36	1.80	2119	
1366-5	Tn-Hoop-206	4305	1.58	2.36	1.81	2162	
1366-5	Tn-Hoop-207	4305	1.60	2.36	1.80	2099	
1366-5	Tn-Hoop-208	4305	1.60	2.36	1.80	2083	
1366-5	Tn-Hoop-209	4305	1.60	2.35	1.81	2206	
		Average			1.81	2136	
		Standard Deviation			0.01	48	
		Coefficient of Variation (COV)			0.4%	2.2%	
1333-4	Tn-Hoop-210	4380	1.56	2.36	1.83	1932	
1333-4	Tn-Hoop-211	4380	1.55	2.36	1.81	1986	
1333-4	Tn-Hoop-212	4380	1.55	2.36	1.80	1992	
1333-4	Tn-Hoop-213	4380	1.57	2.36	1.82	2017	
1333-4	Tn-Hoop-214	4380	1.57	2.36	1.81	2015	
1333-4	Tn-Hoop-215	4380	1.58	2.37	1.81	2082	
1333-4	Tn-Hoop-216	4380	1.59	2.36	1.80	2095	
1333-4	Tn-Hoop-217	4380	1.59	2.36	1.81	2116	
1333-4	Tn-Hoop-218	4380	1.60	2.36	1.81	1904	
		Average			1.81	2015	
		Standard Deviation			0.01	68	
		COV			0.5%	3.4%	
1324-7	Tn-Hoop-219	4389	1.55	2.36	1.82	1981	
1324-7	Tn-Hoop-220	4389	1.55	2.37	1.82	1807	
1324-7	Tn-Hoop-221	4389	1.56	2.37	1.82	1905	
1324-7	Tn-Hoop-222	4389	1.57	2.38	1.81	1957	
1324-7	Tn-Hoop-223	4389	1.57	2.38	1.80	2048	
1324-7	Tn-Hoop-224	4389	1.58	2.38	1.81	1991	
1324-7	Tn-Hoop-225	4389	1.60	2.37	1.81	1986	
1324-7	Tn-Hoop-226	4389	1.60	2.37	1.81	2028	
1324-7	Tn-Hoop-227	4389	1.60	2.36	1.81	1955	
		Average			1.81	1962	
		Standard Deviation			0.01	67	
		COV			0.3%	3.4%	

Table 3.4-12 (Page 2 of 2)

Hoop Tensile Strength of As-Manufactured Pall 326

Candle	Specimen Number	Element Weight (gr)	I.D. (in.)	O.D. (in.)	Specimen Density (gr/cm^3)	Ultimate Strength (psi)	Remarks
1324-4	Tn-Hoop-228	4525	1.57	2.39	1.79	2159	
1324-4	Tn-Hoop-229	4525	1.58	2.39	1.78	2205	
1324-4	Tn-Hoop-230	4525	1.58	2.39	1.78	2055	
1324-4	Tn-Hoop-231	4525	1.57	2.38	1.81	2034	
1324-4	Tn-Hoop-232	4525	1.58	2.38	1.81	2051	
1324-4	Tn-Hoop-233	4525	1.58	2.38	1.80	2077	
1324-4	Tn-Hoop-234	4525	1.62	2.40	1.78	1884	
1324-4	Tn-Hoop-235	4525	1.62	2.40	1.78	1776	
1324-4	Tn-Hoop-236	4525	1.63	2.39	1.78	1785	
			Average		1.79	2003	
			Standard Deviation		0.01	145	
			COV		0.6%	7.3%	
1291-3	Tn-Hoop-237	4615	1.55	2.38	1.85	2156	
1291-3	Tn-Hoop-238	4615	1.55	2.38	1.85	2202	
1291-3	Tn-Hoop-239	4615	1.55	2.38	1.84	2112	
1291-3	Tn-Hoop-240	4615	1.57	2.39	1.85	2093	
1291-3	Tn-Hoop-241	4615	1.57	2.39	1.84	2145	
1291-3	Tn-Hoop-242	4615	1.57	2.39	1.85	2120	
1291-3	Tn-Hoop-243	4615	1.59	2.37	1.85	2170	
1291-3	Tn-Hoop-244	4615	1.59	2.37	1.86	2162	
1291-3	Tn-Hoop-245	4615	1.62	2.40	1.84	2171	
			Average		1.85	2148	
			Standard Deviation		0.01	32	
			COV		0.3%	1.5%	

Table 3.4-13

Density of Pall 326 After Operation

Candle	Specimen Number	Hours in Operation	I.D. (in.)	O.D. (in.)	Density (gr/cm³)
1075-3	Tn-Hoop-246	2830	1.572	2.398	1.94
1075-3	Tn-Hoop-247	2830	1.551	2.375	1.99
1075-3	Tn-Hoop-248	2830	1.555	2.376	1.99
1075-3	Tn-Hoop-249	2830	1.574	2.390	1.95
1075-3	Tn-Hoop-250	2830	1.574	2.389	1.94
1075-3	Tn-Hoop-251	2830	1.577	2.386	1.94
1075-3	Tn-Hoop-252	2830	1.597	2.378	1.94
1075-3	Tn-Hoop-253	2830	1.599	2.371	1.95
1075-3	Tn-Hoop-254	2830	1.598	2.367	1.95
		Average			1.96
		Standard Deviation			0.019
		Coefficient of Variation (COV)			0.96%
1069-3	Tn-Hoop-255	2834	1.553	2.377	1.87
1069-3	Tn-Hoop-256	2834	1.556	2.380	1.87
1069-3	Tn-Hoop-257	2834	1.558	2.384	1.86
1069-3	Tn-Hoop-258	2834	1.575	2.392	1.85
1069-3	Tn-Hoop-259	2834	1.576	2.393	1.85
1069-3	Tn-Hoop-260	2834	1.576	2.388	1.86
1069-3	Tn-Hoop-261	2834	1.597	2.380	1.85
1069-3	Tn-Hoop-262	2834	1.598	2.378	1.85
1069-3	Tn-Hoop-263	2834	1.600	2.374	1.86
		Average			1.86
		Standard Deviation			0.007
		COV			0.39%

Table 3.4-14

Hoop Tensile Strength of Pall 326 After Operation

Candle	Specimen Number	Hours in Operation	I.D. (in.)	O.D. (in.)	Ultimate Strength (psi)	Remarks
1075-3	TN-Hoop-246	2830				
1075-3	TN-Hoop-247	2830	1.55	2.37	2479	
1075-3	TN-Hoop-248	2830	1.55	2.38	2369	
1075-3	TN-Hoop-249	2830	1.57	2.39	2102	
1075-3	TN-Hoop-250	2830	1.57	2.39	2054	
1075-3	TN-Hoop-251	2830	1.58	2.39	2066	
1075-3	TN-Hoop-252	2830	1.60	2.38	1848	
1075-3	TN-Hoop-253	2830	1.60	2.37	1911	
1075-3	TN-Hoop-254	2830	1.60	2.37	1983	
		Average			2102	
		Standard Deviation			204	
		Coefficient of Variation (COV)			9.7%	
1069-3	TN-Hoop-255	2834	1.55	2.38	1794	See Note 1
1069-3	TN-Hoop-256	2834	1.56	2.38	1784	See Note 1
1069-3	TN-Hoop-257	2834	1.56	2.38	1658	See Note 1
1069-3	TN-Hoop-258	2834	1.58	2.39	1749	See Note 1
1069-3	TN-Hoop-259	2834	1.58	2.39	1729	See Note 1
1069-3	TN-Hoop-260	2834	1.58	2.39	1689	See Note 1
1069-3	TN-Hoop-261	2834	1.60	2.38	1702	See Note 1
1069-3	TN-Hoop-262	2834	1.60	2.38	1658	See Note 1
1069-3	TN-Hoop-263	2834	1.60	2.37	1816	See Note 1
		Average			1731	
		Standard Deviation			55	
		COV			3.2%	

Notes: 1. In operation during PCD fire.

Table 3.4-15

Density of Pall FeAl

Candle	Specimen Number	Hours in Operation	I.D. (in.)	O.D. (in.)	Density (gr/cm^3)
034H-002	Tn-Hoop-309	virgin	2.220	2.369	3.91
034H-002	Tn-Hoop-310	virgin	2.219	2.369	3.89
034H-002	Tn-Hoop-311	virgin	2.217	2.369	3.90
034H-002	Tn-Hoop-312	virgin	2.219	2.369	3.90
034H-002	Tn-Hoop-313	virgin	2.221	2.371	3.93
034H-002	Tn-Hoop-314	virgin	2.204	2.350	4.00
034H-002	Tn-Hoop-315	virgin	2.226	2.374	3.92
		Average			3.92
		Standard Deviation			0.03
		Coefficient of Variation (COV)			0.89%
034H-001	Tn-Hoop-316	1356	2.214	2.367	3.97
034H-001	Tn-Hoop-317	1356	2.218	2.372	3.96
034H-001	Tn-Hoop-318	1356	2.214	2.367	4.01
034H-001	Tn-Hoop-320	1356	2.199	2.358	3.92
034H-001	Tn-Hoop-321	1356	2.204	2.360	3.97
034H-001	Tn-Hoop-322	1356	2.218	2.356	4.00
034H-001	Tn-Hoop-323	1356	2.230	2.368	3.99
		Average			3.97
		Standard Deviation			0.03
		COV			0.74%
504J	Tn-Hoop-336	1424	2.187	2.331	4.05
504J	Tn-Hoop-337	1424	2.180	2.325	4.05
504J	Tn-Hoop-338	1424	2.169	2.314	4.11
504J	Tn-Hoop-339	1424	2.185	2.329	4.02
504J	Tn-Hoop-340	1424	2.178	2.337	4.00
504J	Tn-Hoop-341	1424	2.172	2.331	4.01
		Average			4.04
		Standard Deviation			0.04
		COV			0.95%

Table 3.4-16

Axial Tensile Results for Pall FeAl

Candle	Specimen Number	Hours in Operation	Test Temperature (°F)	0.05% Yield Strength (psi)	Ultimate Strength (psi)	Young's Modulus (msi)	Strain-to-Failure (mils/in.)	Remarks
034H-002	Tn-Ax-1	virgin	RT	13400	20200	5.26	10.1	
034H-002	Tn-Ax-3	virgin	RT	12770	18670	4.94	9.56	
034H-002	Tn-Ax-4	virgin	RT	12160	18400	5.38	8.95	
			Average	12777	19090	5.19	9.54	
034H-002	Tn-Ax-2	virgin	1400	4140	6440	3.83	14.0	
034H-002	Tn-Ax-5	virgin	1400	4340	6110	3.29	15.6	
			Average	4240	6275	3.56	14.8	
034H-001	Tn-Ax-6	1356	RT	10820	15680	5.36	6.71	
034H-001	Tn-Ax-7	1356	RT	10920	15100	5.36	5.76	
034H-001	Tn-Ax-8	1356	RT	11040	16440	5.28	8.32	
034H-001	Tn-Ax-9	1356	RT	11570	16950	4.89	8.45	
			Average	11088	16043	5.22	7.31	

Note: RT = room temperature

Table 3.4-17

Hoop Tensile Results for Pall FeAl

Candle	Specimen Number	Hours in Operation	I.D. (in.)	O.D. (in.)	Maximum Hydrostatic Pressure (psig)	Ultimate Strength (psi)	Young's Modulus (msi)	Maximum Strain at O.D. (mils/in.)	Remarks
034H-002	Tn-Hoop-309	virgin	2.22	2.37	1170	18000	6.09	5.63	
034H-002	Tn-Hoop-310	virgin	2.22	2.37	1150	17590	7.29	4.93	
034H-002	Tn-Hoop-311	virgin	2.22	2.37	1160	17460	5.84	5.18	
034H-002	Tn-Hoop-312	virgin	2.22	2.37	1110	17100	5.96	4.90	
034H-002	Tn-Hoop-313	virgin	2.22	2.37	1150	17720	5.64	5.69	
034H-002	Tn-Hoop-314	virgin	2.20	2.35	1060	16580	5.78	4.70	
034H-002	Tn-Hoop-315	virgin	2.23	2.37	1080	16750	5.84	4.82	
		Average			1126	17314	6.06	5.12	
		Standard Deviation			40	483	0.52	0.37	
		Coefficient of Variation (COV)			4%	3%	9%	7%	
034H-001	Tn-Hoop-316	1356	2.21	2.37	790	11840	5.69	2.51	
034H-001	Tn-Hoop-317	1356	2.22	2.37	970	14470	5.83	4.24	
034H-001	Tn-Hoop-318	1356	2.21	2.37	900	13490	7.47	3.20	
034H-001	Tn-Hoop-320	1356	2.20	2.36	1060	15220	5.78	4.79	
034H-001	Tn-Hoop-321	1356	2.20	2.36	1030	15020	5.89	4.25	
034H-001	Tn-Hoop-322	1356	2.22	2.36	910	15110	5.39	4.86	
034H-001	Tn-Hoop-323	1356	2.23	2.37	870	14460	6.41	4.08	
		Average			933	14230	6.07	3.99	
		Standard Deviation			87	1118	0.64	0.79	
		COV			9%	8%	11%	20%	
504J	Tn-Hoop-336	1424	2.19	2.33	721	11257	6.10	1.86	See Note 1
504J	Tn-Hoop-337	1424	2.18	2.32	755	11720	6.20	1.97	See Note 1
504J	Tn-Hoop-338	1424	2.17	2.31	728	11259	6.30	1.88	See Note 1
504J	Tn-Hoop-339	1424	2.19	2.33	891	13978	6.06	2.82	See Note 1
504J	Tn-Hoop-340	1424	2.18	2.34	1068	15119	6.13	3.61	See Note 1
504J	Tn-Hoop-341	1424	2.17	2.33	1061	15079	6.28	3.47	See Note 1
		Average			870	13069	6.18	2.60	
		Standard Deviation			148	1705	0.09	0.74	
		COV			17%	13%	1%	28%	

Notes: 1. In operation during PCD fire.

Table 3.4-18

Density of Schumacher TF20

Candle	Specimen Number	Hours in Operation	I.D. (in.)	O.D. (in.)	Density (gr/cm³)
324H21	Tn-Hoop-264	491	1.561	2.386	1.94
324H21	Tn-Hoop-265	491	1.568	2.384	1.94
324H21	Tn-Hoop-266	491	1.572	2.379	1.95
324H21	Tn-Hoop-267	491	1.587	2.387	1.94
324H21	Tn-Hoop-268	491	1.585	2.381	1.94
324H21	Tn-Hoop-269	491	1.591	2.387	1.94
324H21	Tn-Hoop-270	491	1.605	2.389	1.93
324H21	Tn-Hoop-271	491	1.601	2.384	1.93
324H21	Tn-Hoop-272	491	1.607	2.385	1.93
		Average			1.94
		Standard Deviation			0.008
		Coefficient of Variation (COV)			0.40%
324H01	Tn-Hoop-273	994	1.558	2.384	1.95
324H01	Tn-Hoop-274	994	1.567	2.381	1.94
324H01	Tn-Hoop-275	994	1.574	2.379	1.96
324H01	Tn-Hoop-276	994	1.586	2.381	1.95
324H01	Tn-Hoop-277	994	1.584	2.383	1.94
324H01	Tn-Hoop-278	994	1.586	2.386	1.94
324H01	Tn-Hoop-279	994	1.615	2.393	1.93
324H01	Tn-Hoop-280	994	1.609	2.382	1.94
324H01	Tn-Hoop-281	994	1.591	2.362	1.96
		Average			1.94
		Standard Deviation			0.008
		COV			0.41%
324H04	Tn-Hoop-282	1234	1.556	2.381	1.93
324H04	Tn-Hoop-283	1234	1.545	2.379	1.93
324H04	Tn-Hoop-284	1234	1.584	2.389	1.94
324H04	Tn-Hoop-285	1234	1.585	2.380	1.94
324H04	Tn-Hoop-286	1234	1.587	2.384	1.94
324H04	Tn-Hoop-287	1234	1.587	2.387	1.94
324H04	Tn-Hoop-288	1234	1.603	2.381	1.95
324H04	Tn-Hoop-289	1234	1.606	2.381	1.96
324H04	Tn-Hoop-290	1234	1.606	2.379	1.94
		Average			1.94
		Standard Deviation			0.007
		COV			0.34%

Table 3.4-19

Density of Schumacher T10-20

Candle	Specimen Number	Hours in Operation	I.D. (in.)	O.D. (in.)	Density (gr/cm³)
324H02	Tn-Hoop-291	1788	1.564	2.378	1.98
324H02	Tn-Hoop-292	1788	1.566	2.370	1.98
324H02	Tn-Hoop-293	1788	1.570	2.368	1.98
324H02	Tn-Hoop-294	1788	1.588	2.380	1.98
324H02	Tn-Hoop-295	1788	1.590	2.379	1.98
324H02	Tn-Hoop-296	1788	1.585	2.376	1.99
324H02	Tn-Hoop-297	1788	1.600	2.376	1.99
324H02	Tn-Hoop-298	1788	1.606	2.382	1.98
324H02	Tn-Hoop-299	1788	1.602	2.375	1.98
		Average			1.98
		Standard Deviation			0.004
		Coefficient of Variation (COV)			0.19%
324H01	Tn-Hoop-300	1792	1.562	2.381	1.97
324H01	Tn-Hoop-301	1792	1.569	2.380	1.97
324H01	Tn-Hoop-302	1792	1.571	2.381	1.97
324H01	Tn-Hoop-303	1792	1.588	2.383	1.98
324H01	Tn-Hoop-304	1792	1.589	2.385	1.97
324H01	Tn-Hoop-305	1792	1.592	2.386	1.98
324H01	Tn-Hoop-306	1792	1.604	2.391	1.99
324H01	Tn-Hoop-307	1792	1.605	2.390	1.99
324H01	Tn-Hoop-308	1792	1.608	2.389	1.98
		Average			1.98
		Standard Deviation			0.007
		COV			0.35%

Table 3.4-20

Hoop Tensile Strength of Schumacher TF20

Candle	Specimen Number	Hours in Operation	I.D. (in.)	O.D. (in.)	Ultimate Strength (psi)	Remarks
324H21	Tn-Hoop-264	491	1.56	2.39	1419	See Note
324H21	Tn-Hoop-265	491	1.57	2.38	1426	See Note
324H21	Tn-Hoop-266	491	1.57	2.38	1136	See Note
324H21	Tn-Hoop-267	491	1.59	2.39	1384	See Note
324H21	Tn-Hoop-268	491	1.58	2.38	1391	See Note
324H21	Tn-Hoop-269	491	1.59	2.39	1358	See Note
324H21	Tn-Hoop-270	491	1.60	2.39	1362	See Note
324H21	Tn-Hoop-271	491	1.60	2.38	1307	See Note
324H21	Tn-Hoop-272	491	1.61	2.39	1233	See Note
		Average			1335	
		Standard Deviation			90	
		Coefficient of Variation (COV)			7%	
324H01	Tn-Hoop-273	994	1.56	2.38	1361	See Note
324H01	Tn-Hoop-274	994	1.57	2.38	1306	See Note
324H01	Tn-Hoop-275	994	1.57	2.38	1374	See Note
324H01	Tn-Hoop-276	994	1.59	2.38	1259	See Note
324H01	Tn-Hoop-277	994	1.58	2.38	1252	See Note
324H01	Tn-Hoop-278	994	1.59	2.39	1314	See Note
324H01	Tn-Hoop-279	994	1.62	2.39	1356	See Note
324H01	Tn-Hoop-280	994	1.61	2.38	1312	See Note
324H01	Tn-Hoop-281	994	1.59	2.36	1296	See Note
		Average			1314	
		Standard Deviation			41	
		COV			3%	
324H04	Tn-Hoop-282	1234	1.56	2.38	1296	See Note
324H04	Tn-Hoop-283	1234	1.55	2.38	1231	See Note
324H04	Tn-Hoop-284	1234	1.58	2.39	1268	See Note
324H04	Tn-Hoop-285	1234	1.59	2.38	1231	See Note
324H04	Tn-Hoop-286	1234	1.59	2.38	622	See Note
324H04	Tn-Hoop-287	1234	1.59	2.39	1234	See Note
324H04	Tn-Hoop-288	1234	1.60	2.38	1244	See Note
324H04	Tn-Hoop-289	1234	1.61	2.38	1320	See Note
324H04	Tn-Hoop-290	1234	1.61	2.38	1252	See Note
		Average			1189	
		Standard Deviation			202	
		COV			17%	

Note: In operation during PCD fire

Table 3.4-21

Hoop Tensile Strength of Schumacher T10 – 20

Candle	Specimen Number	Hours in Operation	I.D. (in.)	O.D. (in.)	Ultimate Strength (psi)	Remarks
324H02	Tn-Hoop-291	1788	1.56	2.38	1157	
324H02	Tn-Hoop-292	1788	1.57	2.37	1237	
324H02	Tn-Hoop-293	1788	1.57	2.37	1489	
324H02	Tn-Hoop-294	1788	1.59	2.38	1357	
324H02	Tn-Hoop-295	1788	1.59	2.38	1404	
324H02	Tn-Hoop-296	1788	1.59	2.38	867	
324H02	Tn-Hoop-297	1788	1.60	2.38	1318	
324H02	Tn-Hoop-298	1788	1.61	2.38	1499	
324H02	Tn-Hoop-299	1788	1.60	2.38	1479	
	Average				1312	
	Standard Deviation				192	
	Coefficient of Variation (COV)				15%	
324H01	Tn-Hoop-300	1792	1.56	2.38	1456	See Note
324H01	Tn-Hoop-301	1792	1.57	2.38	1441	See Note
324H01	Tn-Hoop-302	1792	1.57	2.38	1429	See Note
324H01	Tn-Hoop-303	1792	1.59	2.38	1313	See Note
324H01	Tn-Hoop-304	1792	1.59	2.39	1255	See Note
324H01	Tn-Hoop-305	1792	1.59	2.39	1313	See Note
324H01	Tn-Hoop-306	1792	1.60	2.39	1308	See Note
324H01	Tn-Hoop-307	1792	1.61	2.39	1341	See Note
324H01	Tn-Hoop-308	1792	1.61	2.39	1372	See Note
	Average				1359	
	Standard Deviation				66	
	COV				5%	

Note: In operation during PCD fire

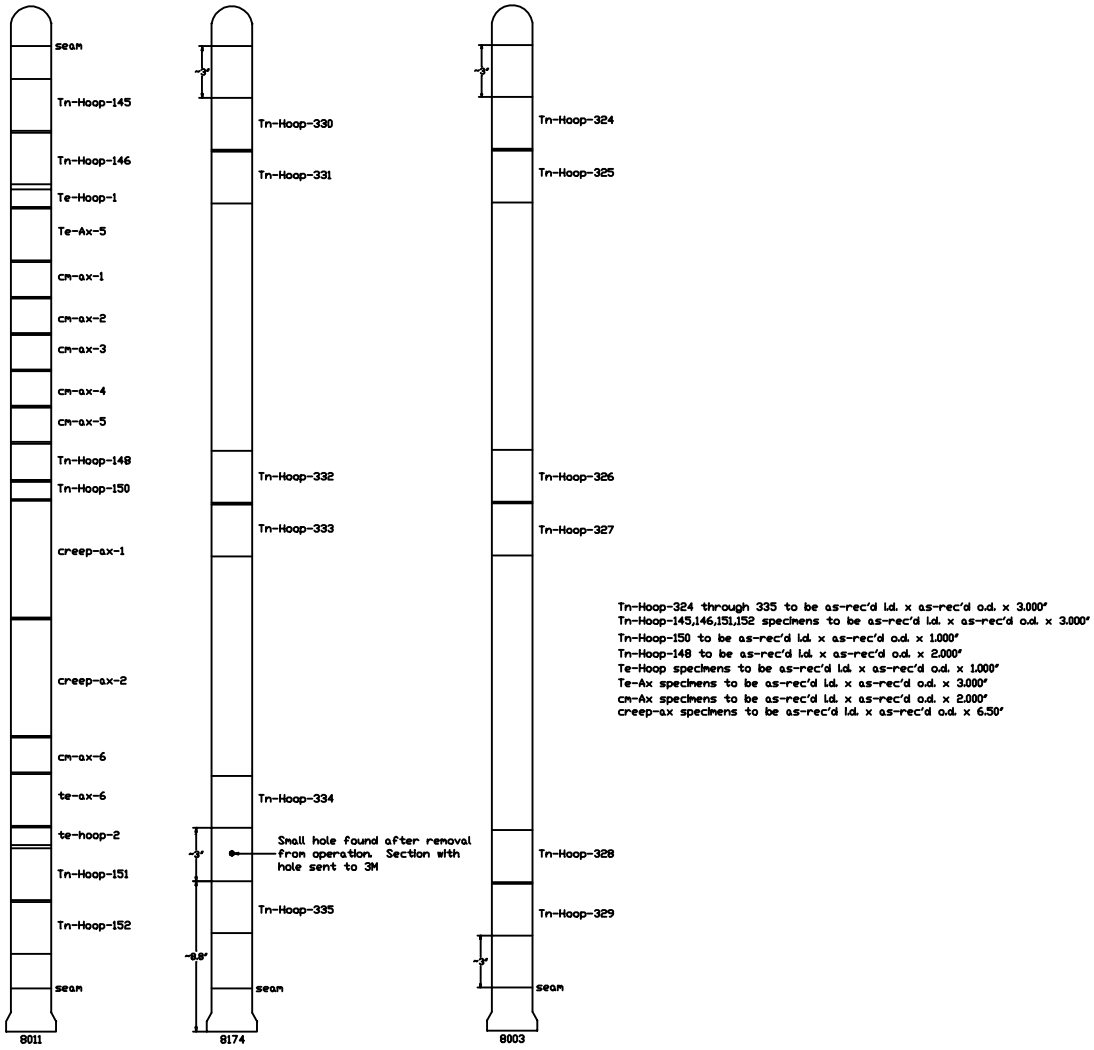

Figure 3.4-1 Cutting Plan for 3M Oxide/Oxide Filter Elements

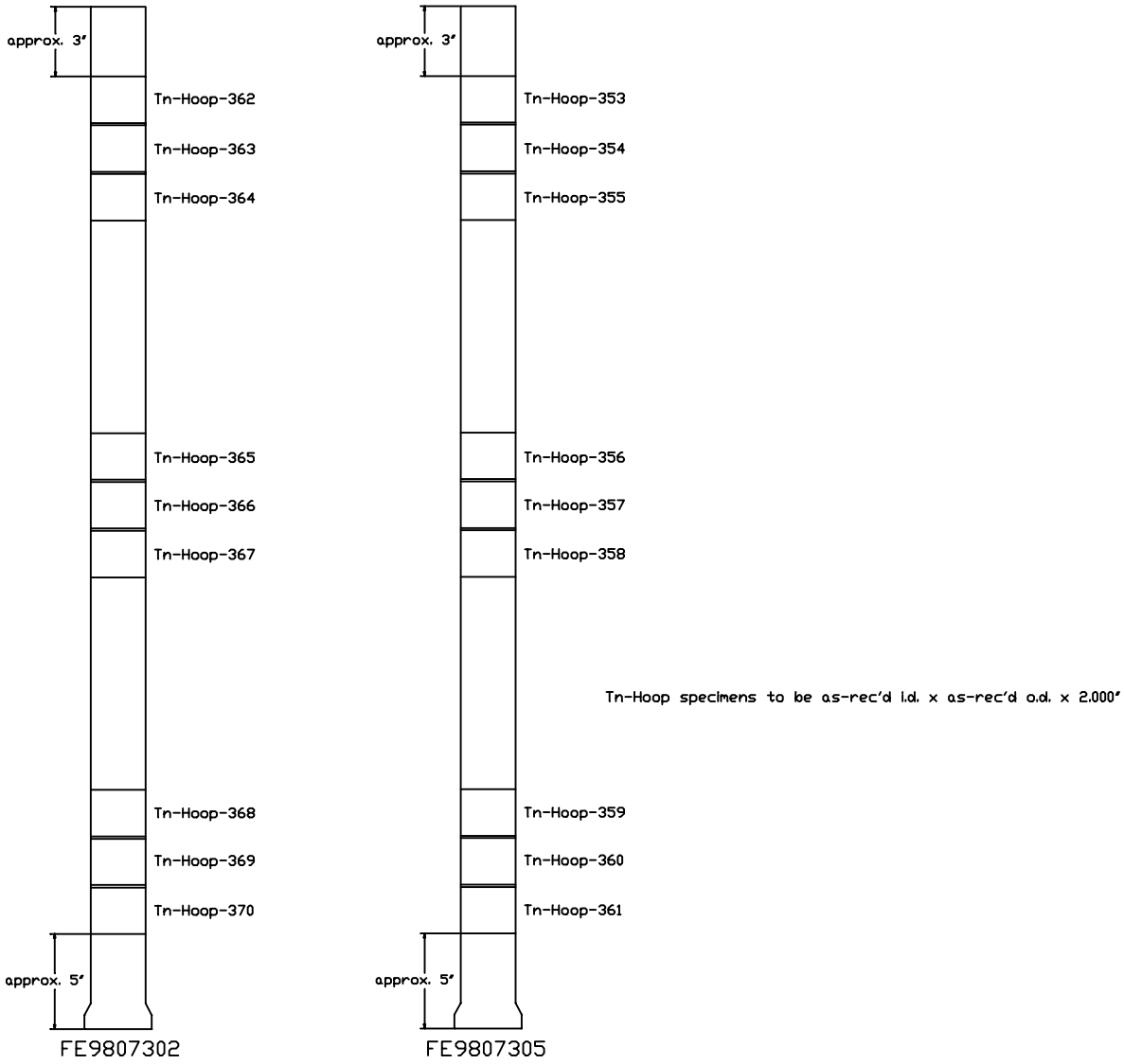

Figure 3.4-2 Cutting Plan for IF&P REECER™ Filter Elements

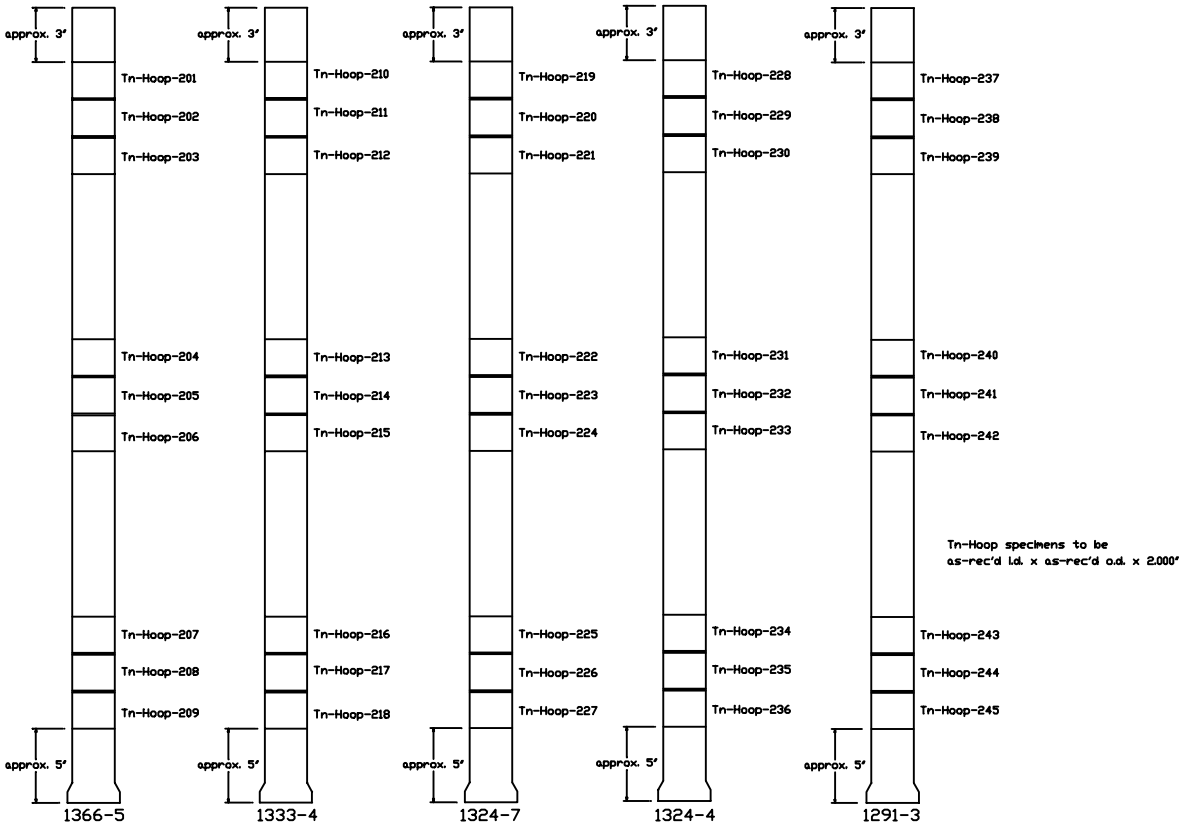

Figure 3.4-3 Cutting Plan for As-Manufactured Pall 326 Filter Elements

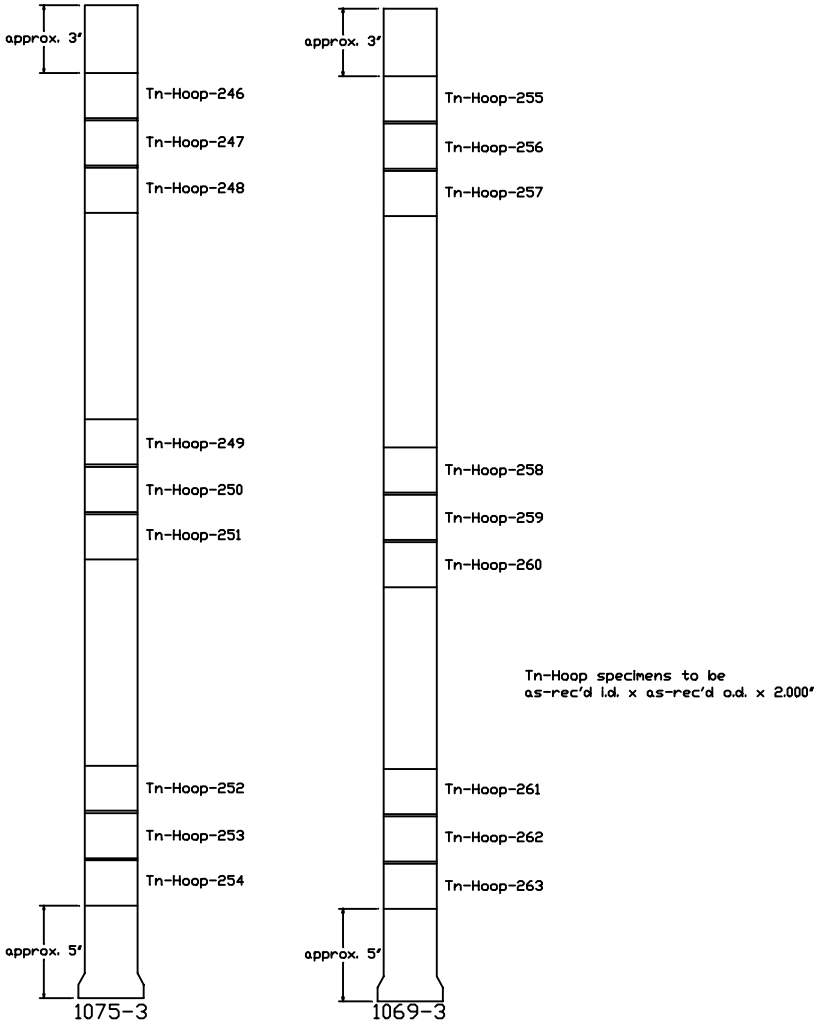

Figure 3.4-4 Cutting Plan for Exposed Pall 326 Filter Elements

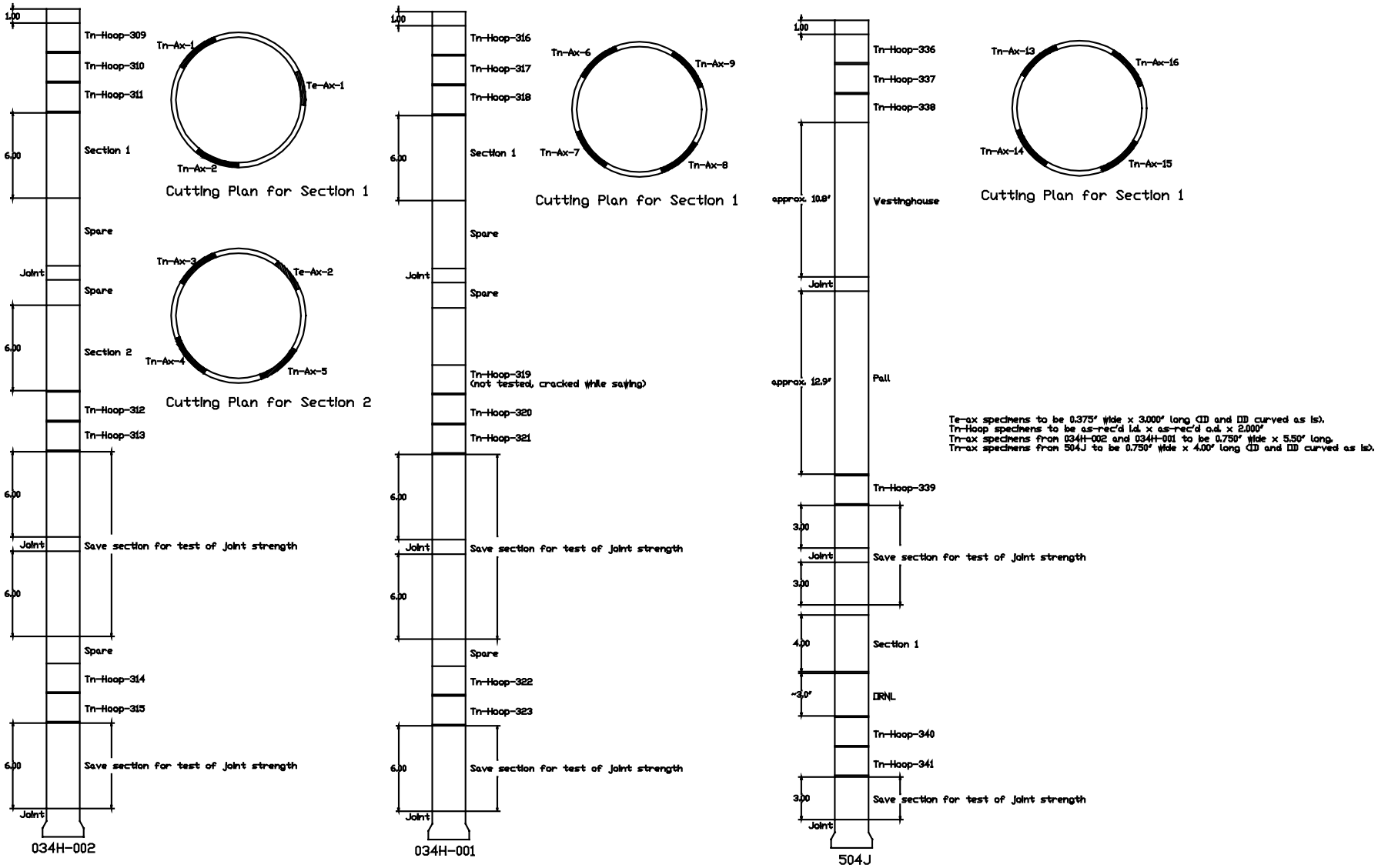

Figure 3.4-5 Cutting Plan for Pall FeAl Filter Elements

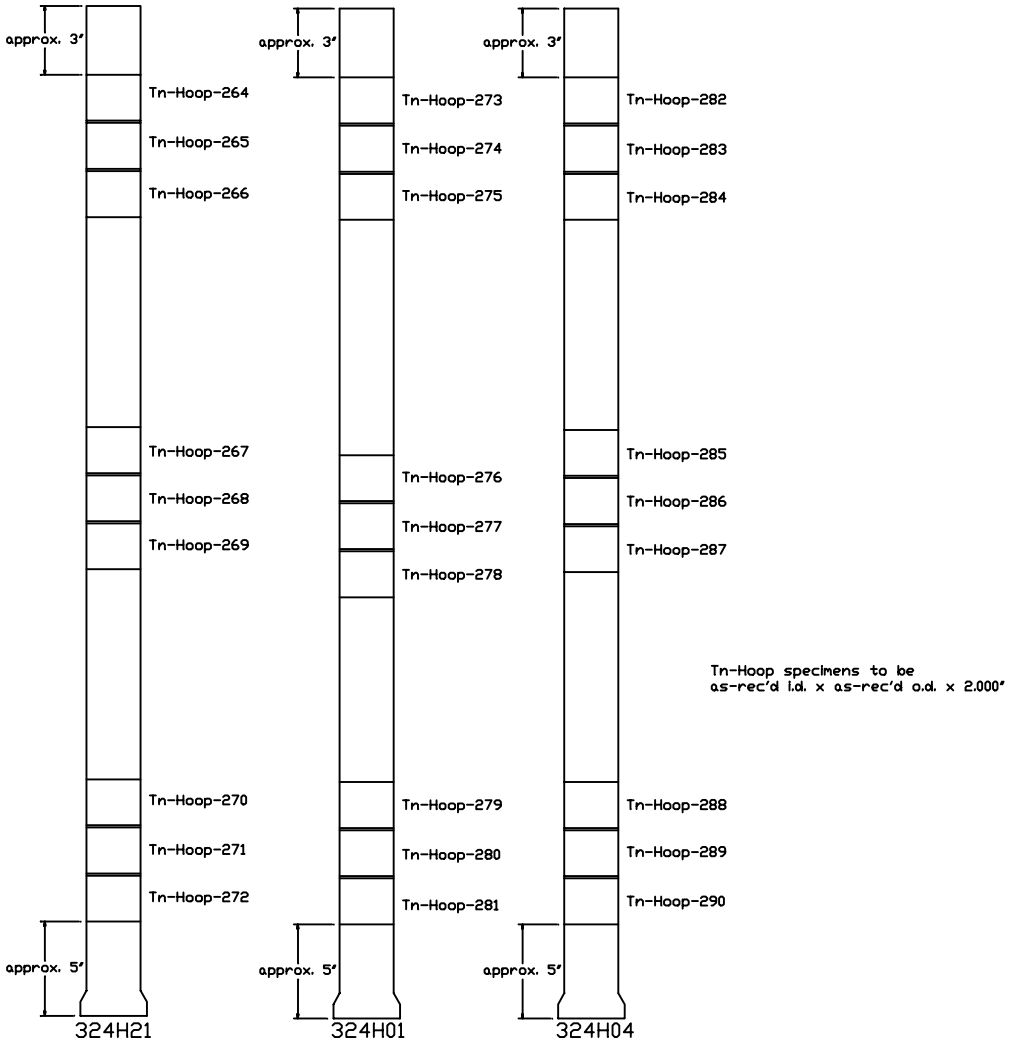

Figure 3.4-6 Cutting Plan for Schumacher TF20 Filter Elements

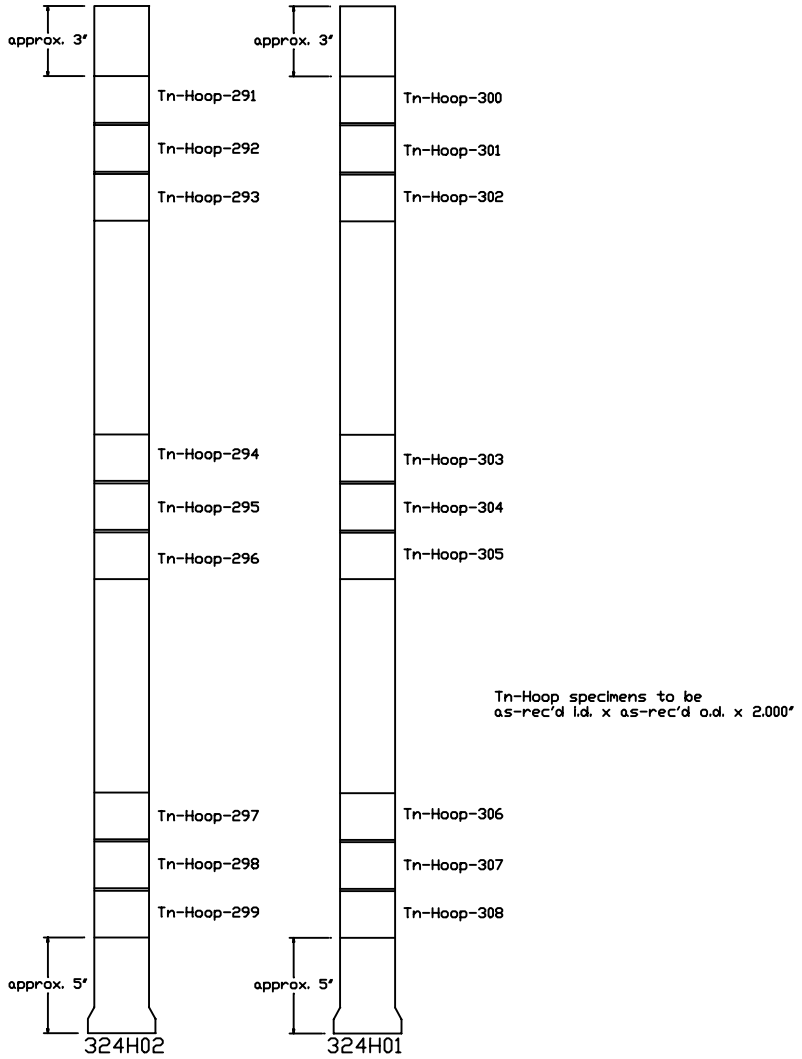

Figure 3.4-7 Cutting Plan for Schumacher T10-20 Filter Elements

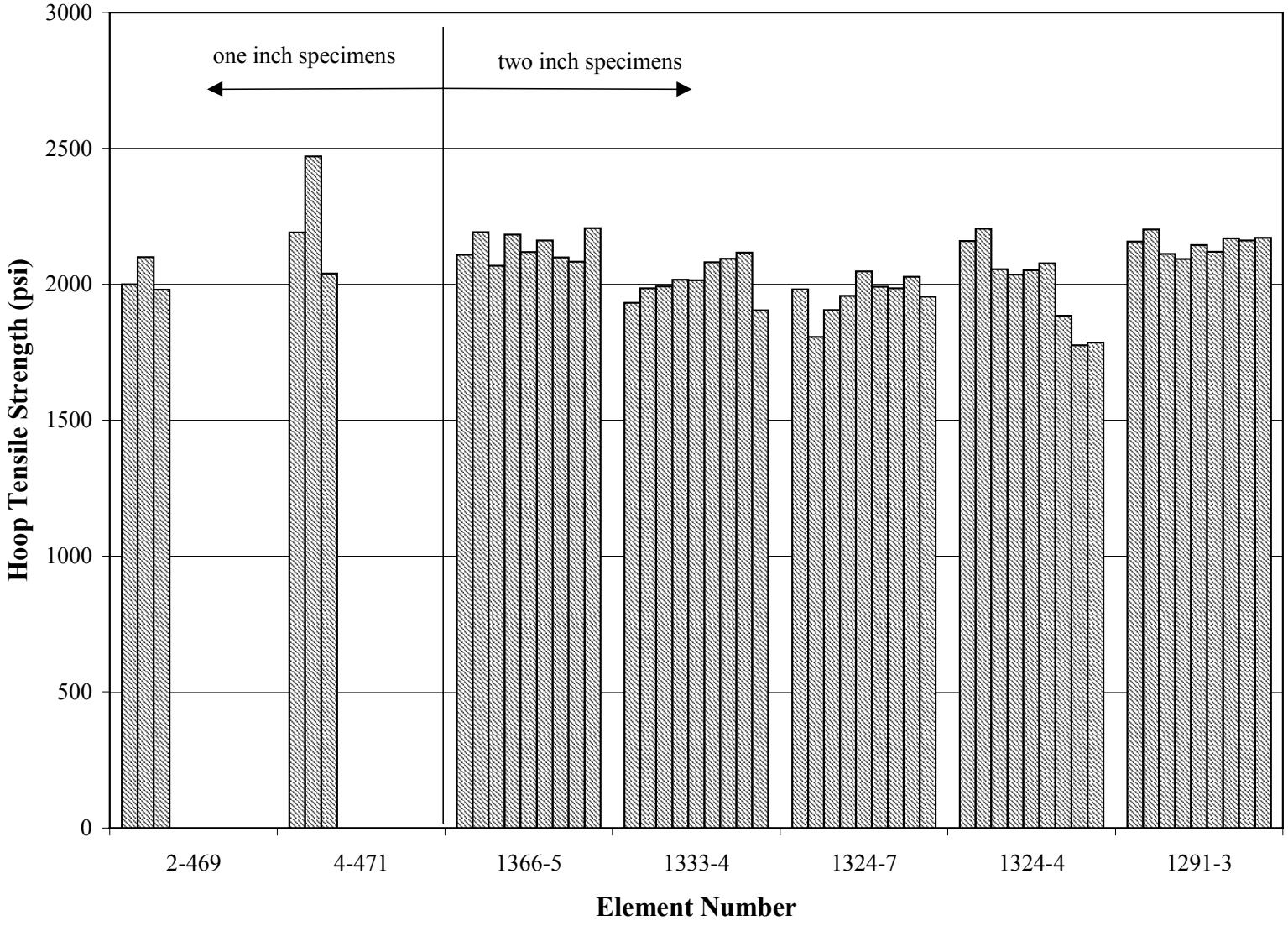

Figure 3.4-8 Hoop Tensile Strength of 1- and 2-Inch-Long Pall 326 Specimens

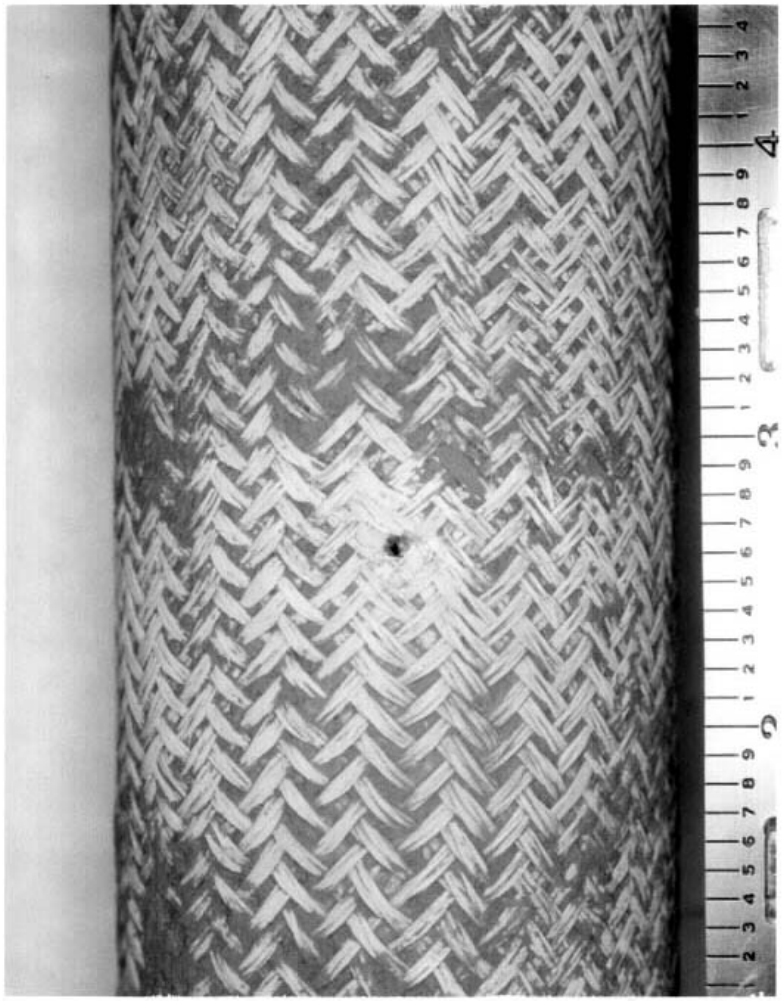

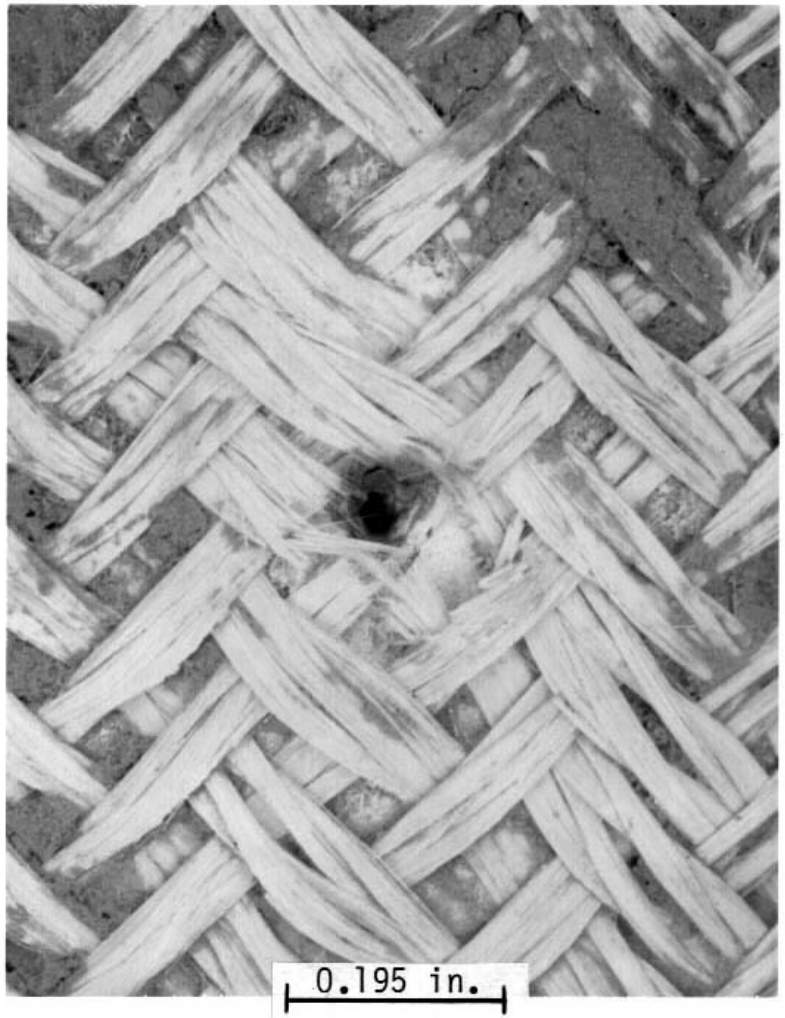

Figure 3.4-9 Pinhole in Element 8174 After 1,420 Hours in Operation

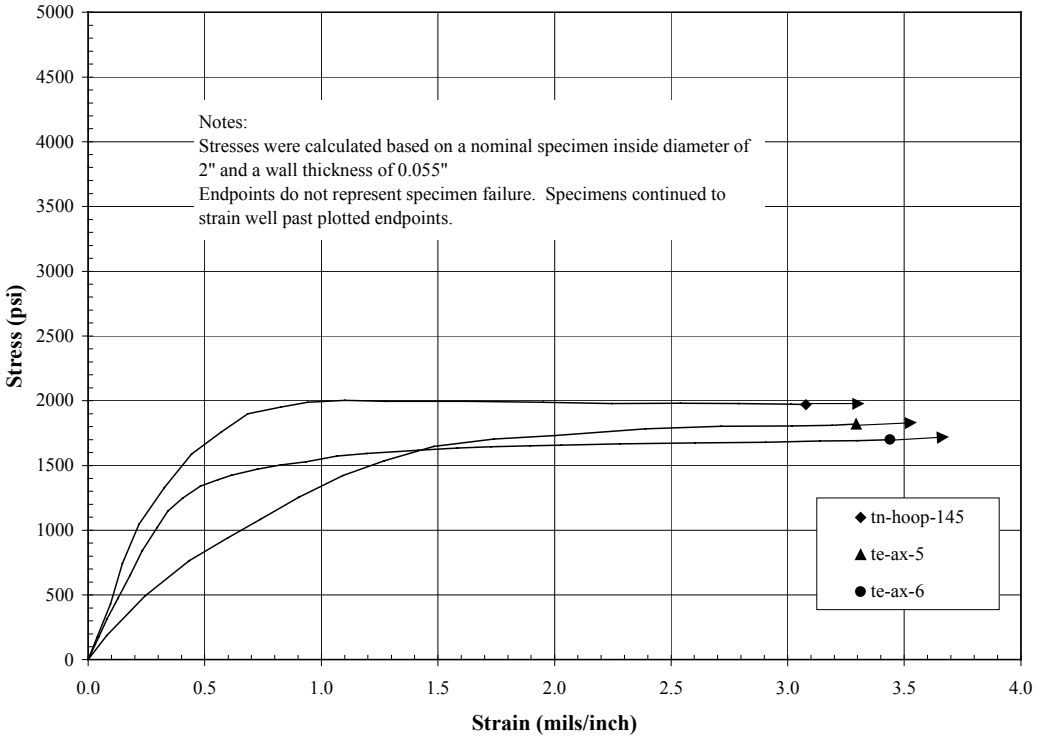

Figure 3.4-10 Hoop Tensile Stress-Strain Responses for As-Manufactured 3M Oxide-Oxide Filter Elements

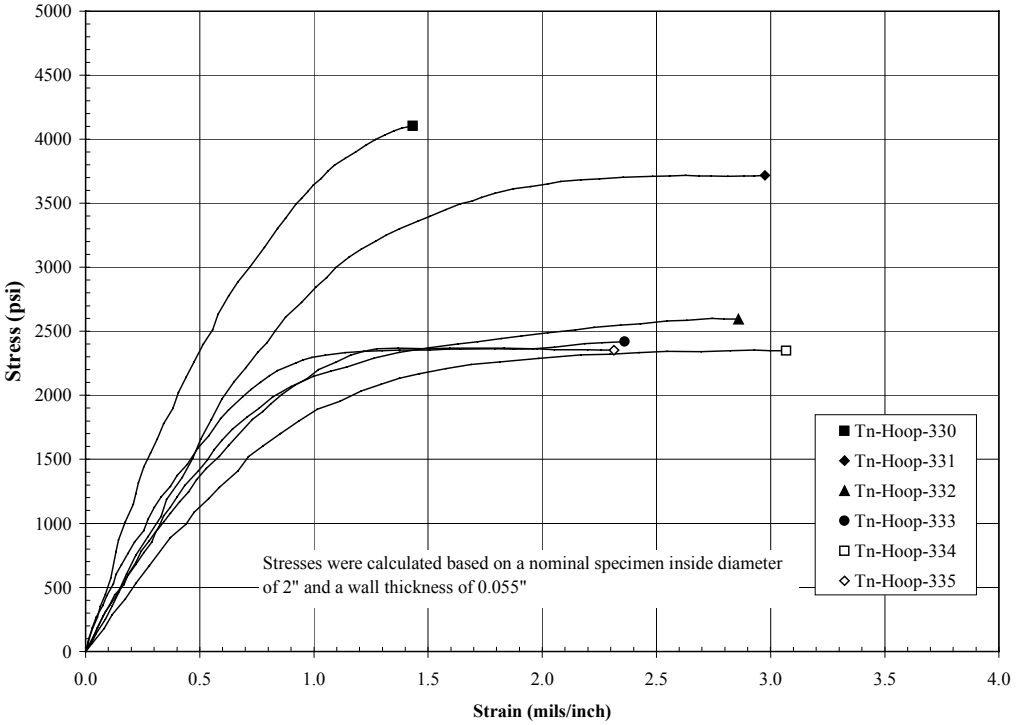

Figure 3.4-11 Hoop Tensile Stress-Strain Responses for 3M Oxide-Oxide After 1,420 Hours in Operation

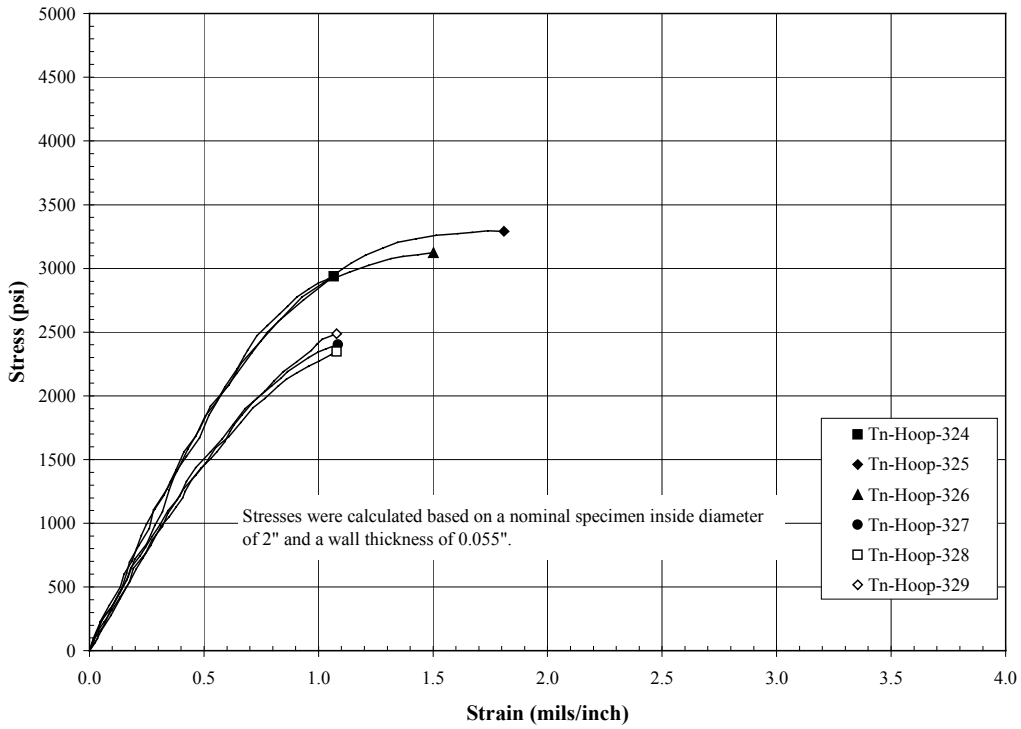

Figure 3.4-12 Hoop Tensile Stress-Strain Responses for 3M Oxide-Oxide After 1,982 Hours in Operation Including PCD Fire

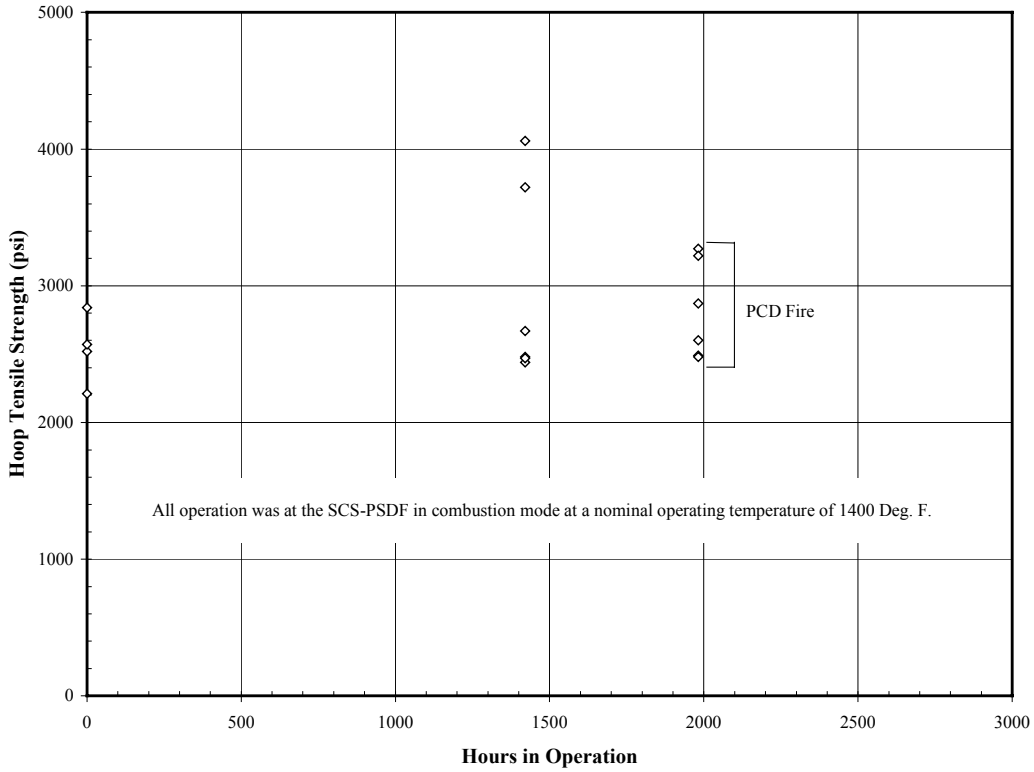

Figure 3.4-13 Hoop Tensile Strength Versus Hours of Operation for 3M Oxide-Oxide

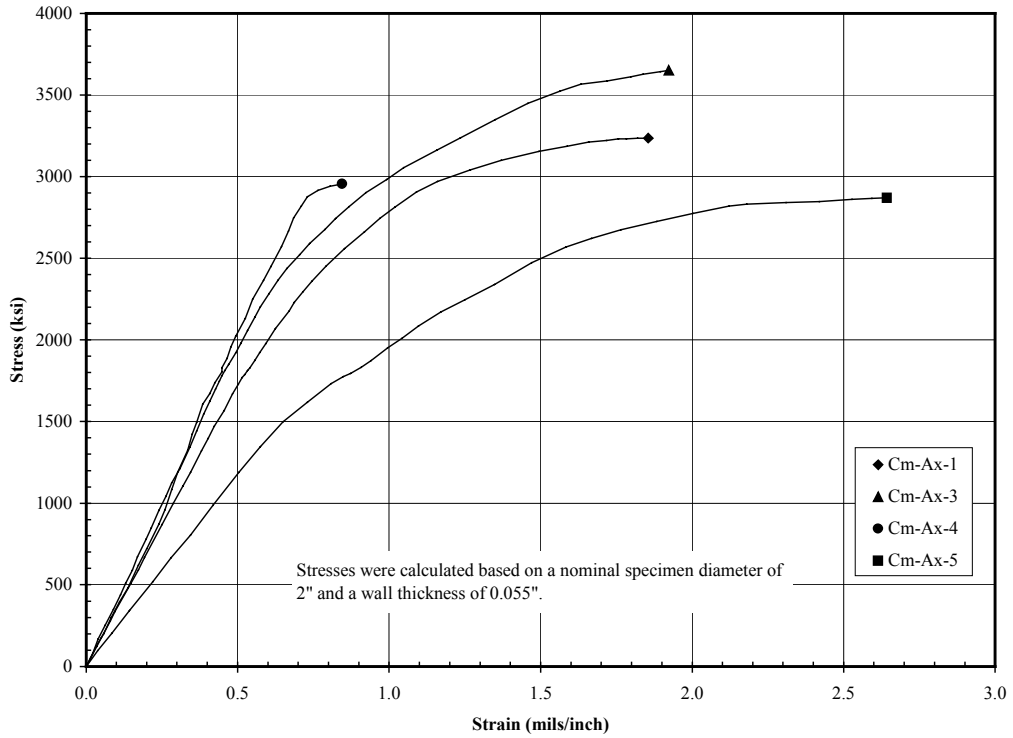

Figure 3.4-14 Axial Compressive Stress-Strain Responses for As-Manufactured 3M Oxide-Oxide

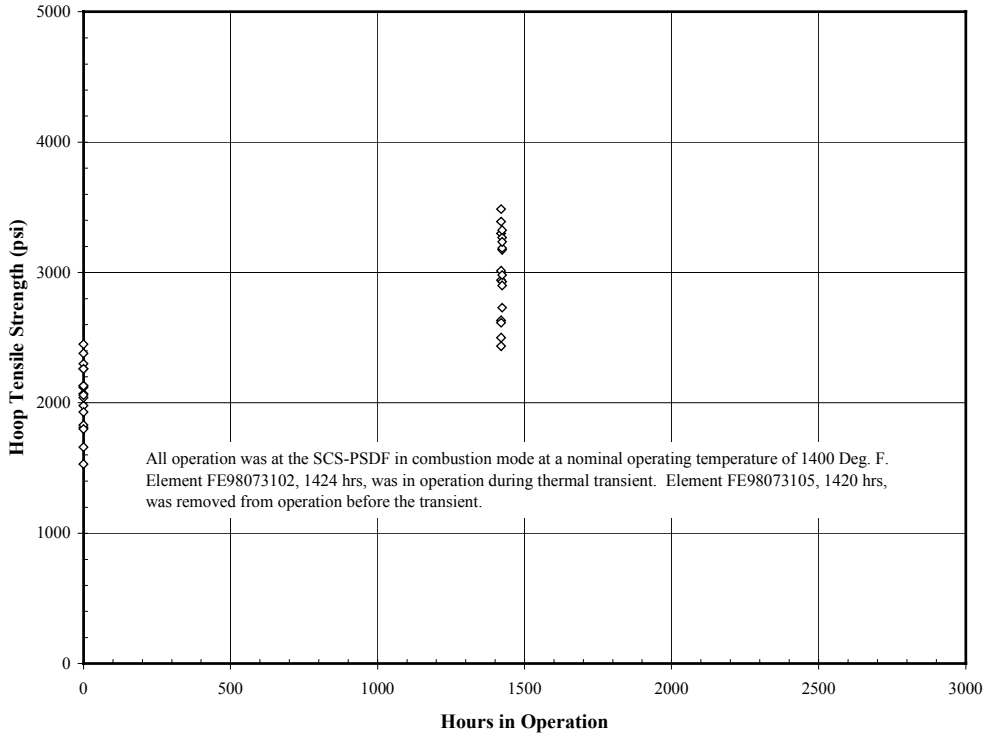

Figure 3.4-15 Hoop Tensile Strength Versus Hours of Operation for IF&P REECER™

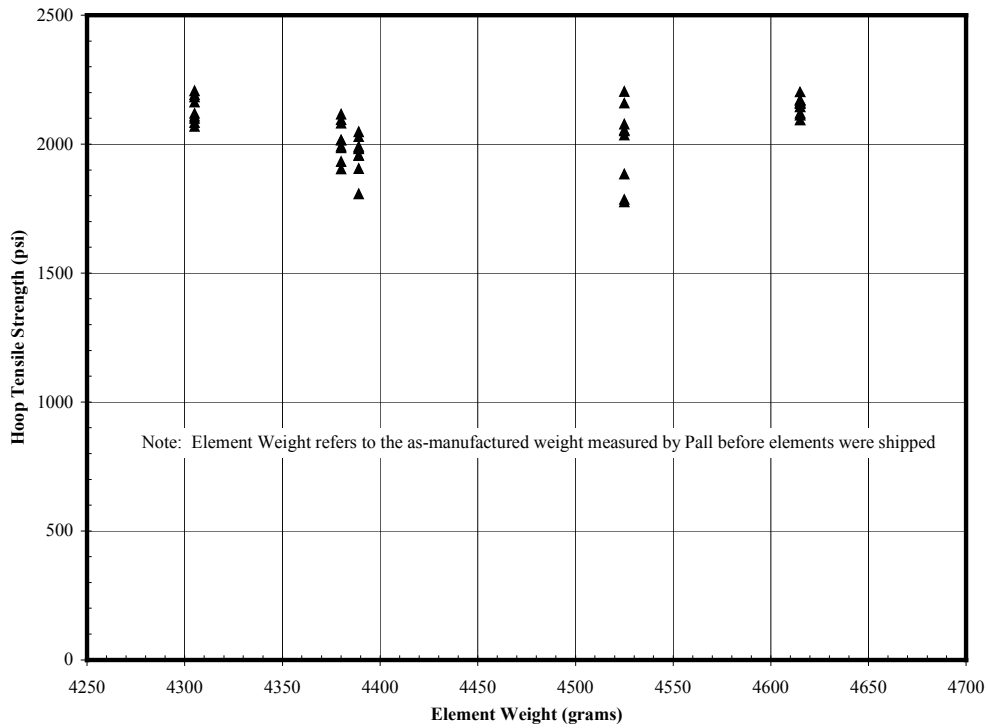

Figure 3.4-16 As-Manufactured Hoop Tensile Strength Versus Element Weight for Pall 326

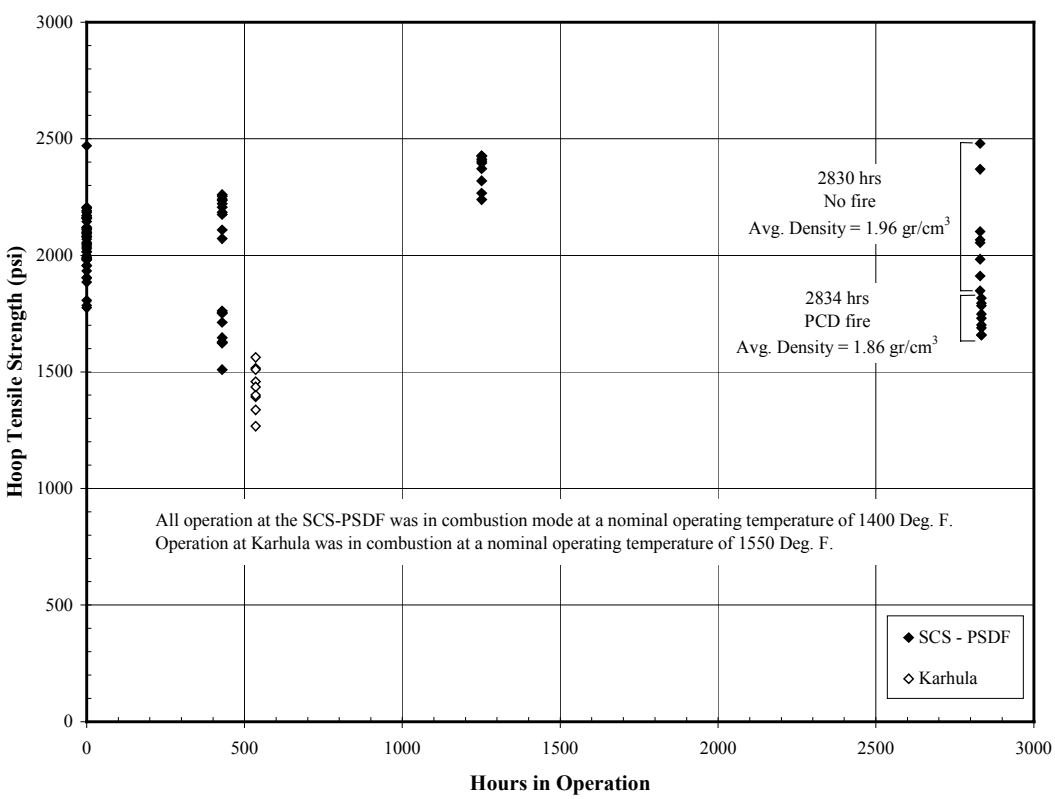

Figure 3.4-17 Hoop Tensile Strength Versus Hours of Operation for Pall 326

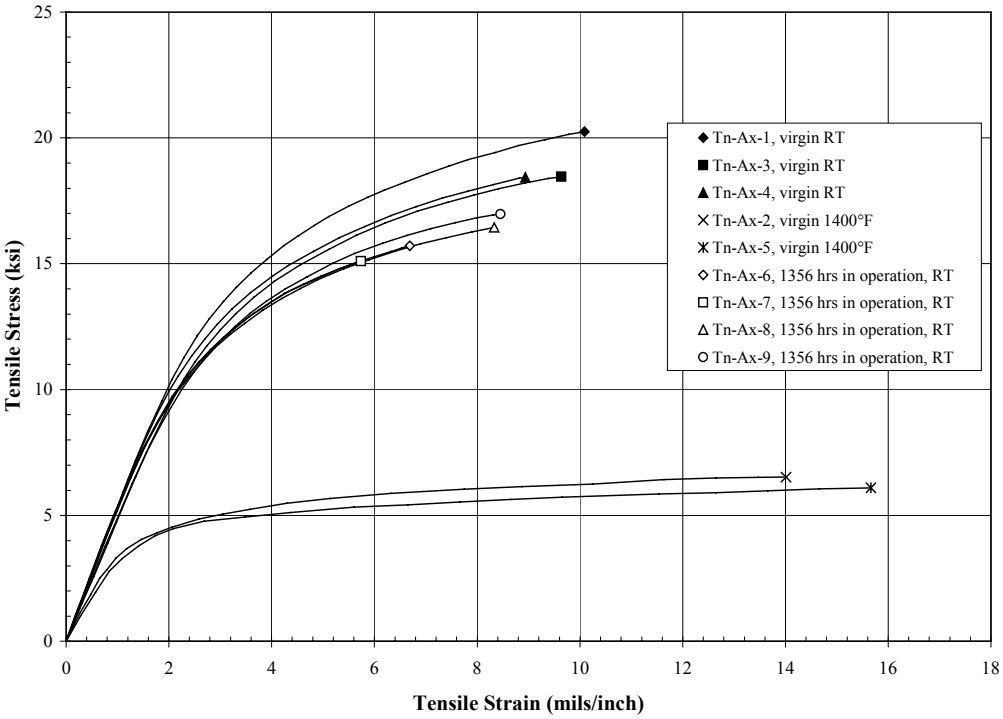

Figure 3.4-18 Axial Tensile Stress-Strain Responses for Pall FeAl

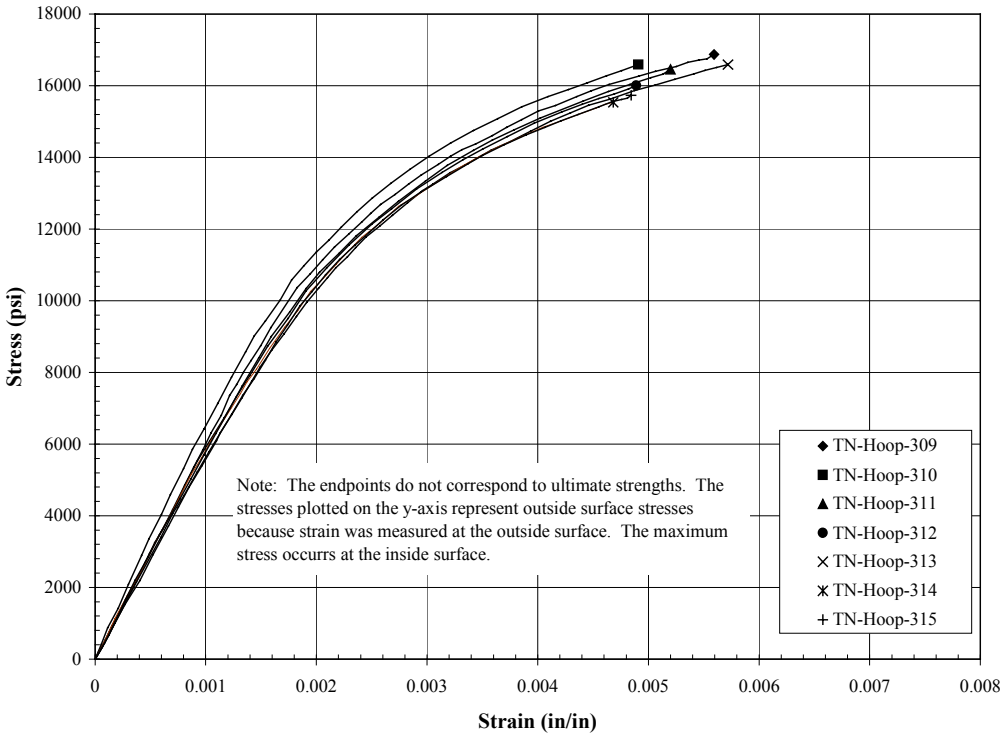

Figure 3.4-19 Room Temperature Hoop Tensile Stress-Strain Responses of As-Manufactured Pall FeAl

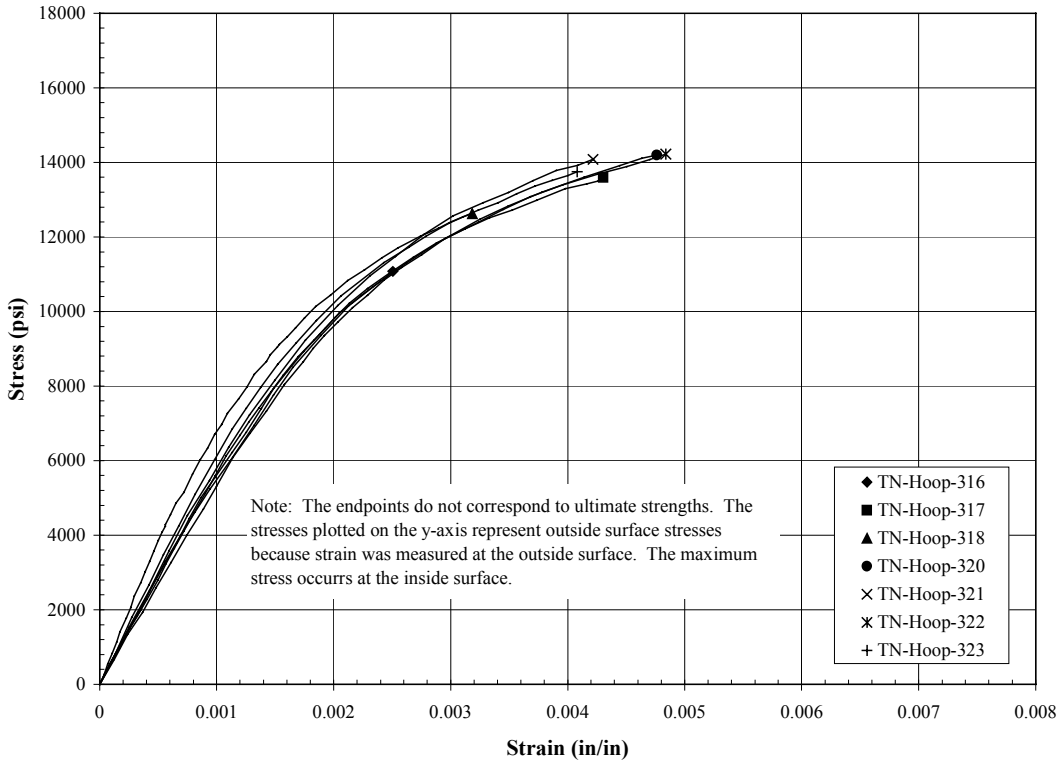

Figure 3.4-20 Room Temperature Hoop Tensile Stress-Strain Responses of Pall FeAl After 1,356 Hours in Operation

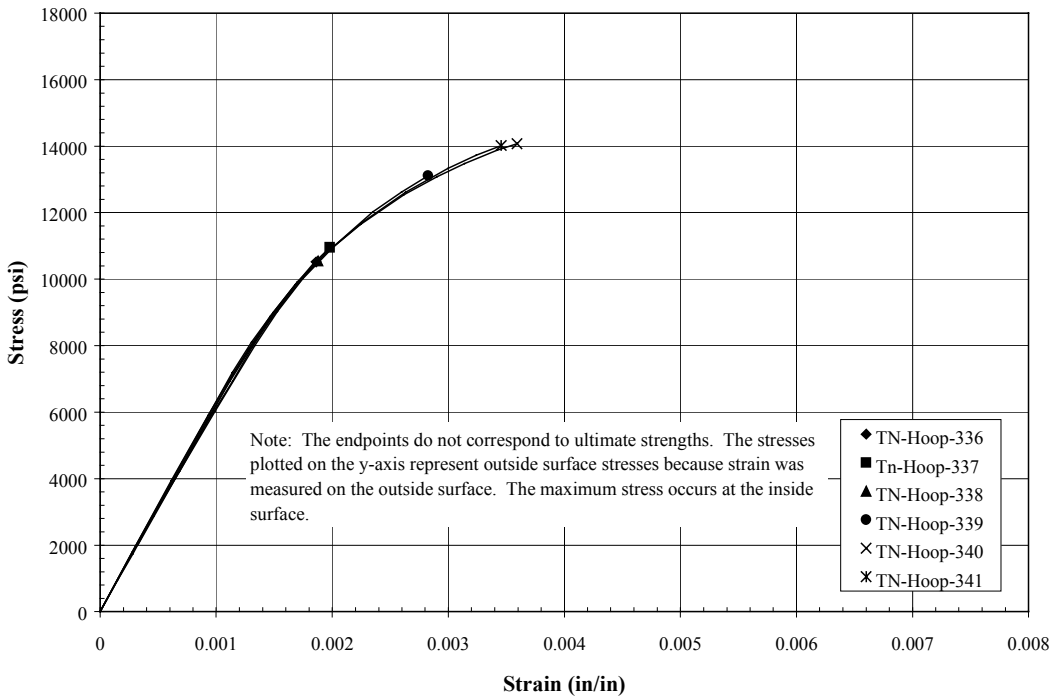

Figure 3.4-21 Room Temperature Hoop Tensile Stress-Strain Responses of Pall FeAl After 1,424 Hours in Operation

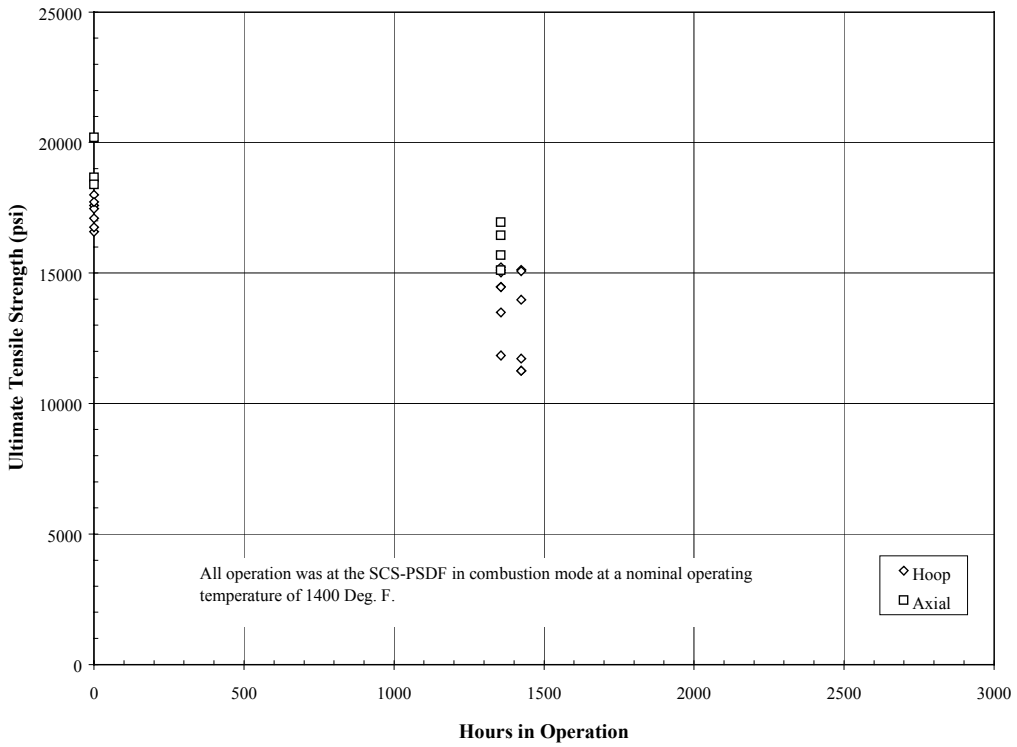

Figure 3.4-22 Room Temperature Tensile Strength Versus Hours of Operation for Pall FeAl

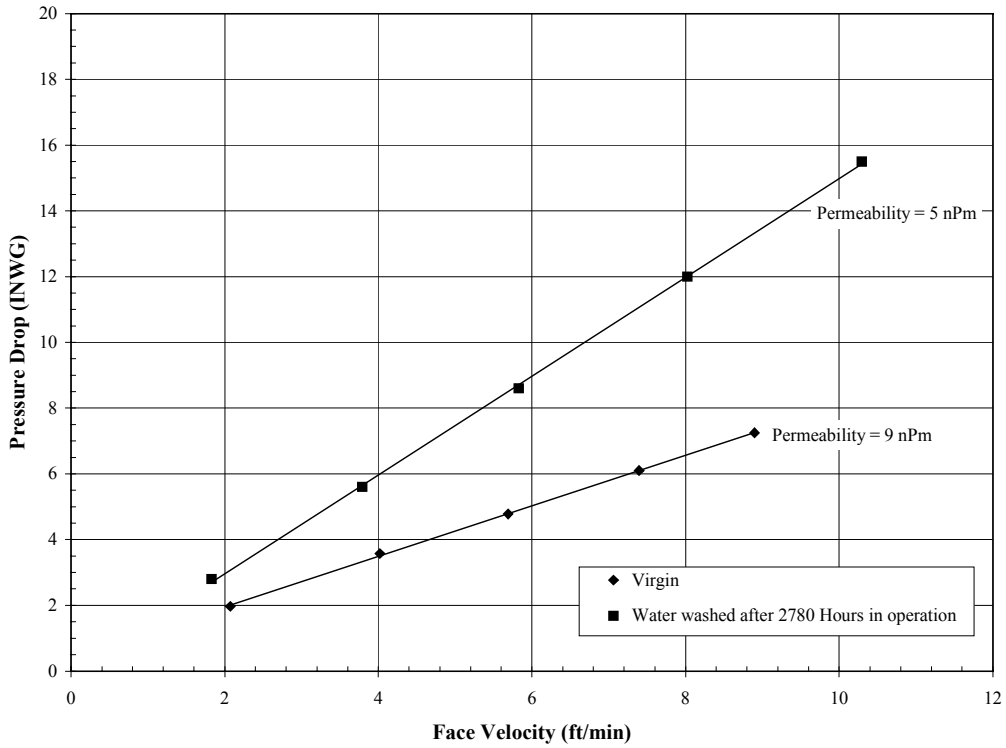

Figure 3.4-23 Pressure Drop Versus Flow Rate for Pall Iron Aluminide Element 034H005

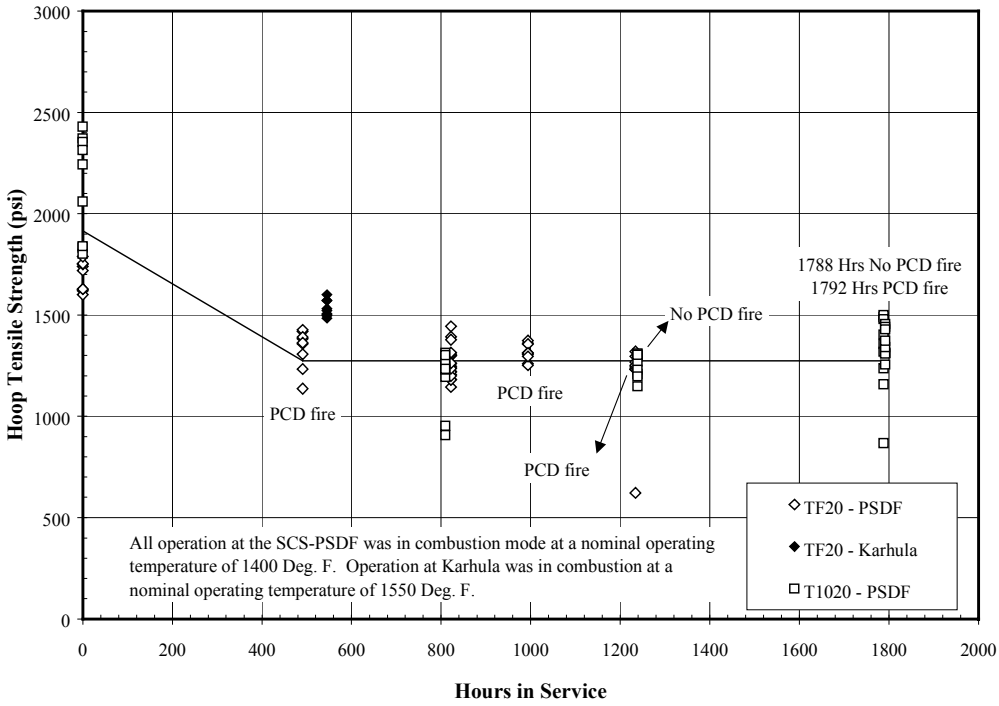

Figure 3.4-24 Tensile Strength Versus Hours of Operation for Schumacher TF20 and T10-20

3.5 THERMAL STRESS ANALYSIS

All types of monolithic ceramic filter elements, except IF&P REECER™, have failed in operation at the PSDF during thermal transients; however, some of the filter elements have proven more susceptible to thermal transient failure than others. A model has been developed to analyze the thermal and structural responses of the ceramic filters during thermal transients. The objectives of this effort include the following:

1. Explain the filter element failures that have occurred and why some elements have been more susceptible to failure during thermal transients than others.

2. Provide a means of evaluating potential filter materials, based on measured properties, to determine the likelihood of failure under thermal transient conditions.

3. Provide a better understanding of filter element performance during thermal transients.

Temperatures among the filter elements were calculated from a 1-dimensional (1-D) transient conduction model with appropriate boundary and initial conditions. The heat equation, which gives the temperature distribution in the elements, was discretized and solved numerically using the finite difference method. The stresses and strains generated due to this temperature profile were then calculated by the thermal stress equations as provided in reference 1. A numerical algorithm was written in the Visual Basic program to calculate the temperature profile using the finite difference equations and the corresponding thermal stresses and strains.

Filter element responses during thermal transients were also modeled using ANSYS finite element software. The ANSYS model provides refinement of the simple model by including the effects of axial and circumferential temperature gradients and more complex boundary conditions. Finally, the results from the 1-D finite difference model and the 3-D ANSYS model were compared.

3.5.1 Nomenclature

The following nomenclature is used throughout this section:

General-

T	Temperature
t	Time
r,θ,z	Radial, circumferential, and axial coordinates in cylindrical coordinate system
h	Convective heat transfer coefficient
σ	Normal stress
ε	Normal strain
l	element wall thickness

Material Properties-

k	Thermal conductivity
ρ	Bulk density
Cp	Specific heat
κ	Thermal diffusivity ($k/\rho Cp$)
α	Coefficient of thermal expansion
E	Young's modulus
ν	Poisson's ratio

Subscripts-

a	Inside radius
b	Outside radius
∞a	Free stream gas inside element
∞b	Free stream gas outside element
i	i^{th} point in the r-direction (i=0 at the inside surface)
ref	Reference conditions
r,θ,z	Radial, circumferential, and axial directions

Superscripts-

p	p^{th} time increment (p=0 at t=0)

3.5.2 Temperature Distribution in Filter Element

The temperature distributions in the filter elements were obtained from the solution of the heat equation subject to the following simplifying assumptions:

1. Heat transfer is by conduction only. Thermal effects of gas flow are neglected.

2. Heat flow is in the radial direction only with no axial or circumferential gradients.

3. Filter has infinite length.

4. Filter material is a continuum. Bulk material properties measured on the porous material were used in the analysis.

5. Filter material is isotropic with constant material properties.

Simplifying assumption numbers 2 and 5 are addressed by the ANSYS 3-D finite element model (see section 3.5.4). ANSYS results indicate that for low-conductivity materials, the largest stresses are generated due to the radial gradients calculated using this 1-D model but for high-conductivity materials, the largest stresses result from axial and circumferential gradients not considered here. The ANSYS model also has the capability to consider material property variations with temperature and anisotropic materials if necessary. The current materials considered are likely isotropic (although this has not been confirmed by testing) and the properties are nearly constant within the temperature range of interest here. Assumption 3, infinite length filter, means that end effects are not considered. If end effects need to be

considered, an ANSYS model can be constructed to do so. Analysis of the effect of gas flow through the elements, neglected in assumption number 1, and the actual material microstructure, not the continuum as assumed in number 4, will require more sophisticated modeling. Future efforts will be directed toward developing a model that includes these effects. With the assumptions above, this current model provides an understanding of which material properties control performance during thermal transients and helps explain why some elements have survived and others failed during the transients encountered at the PSDF. Understanding which properties control performance may help system operators select the filter elements with the greatest likelihood of success for the anticipated operating conditions.

With assumptions 1 through 5 (above), the heat equation in cylindrical coordinates becomes:

$$\frac{1}{\kappa}\frac{\partial T}{\partial t} = \frac{\partial^2 T}{\partial r^2} + \frac{1}{r}\frac{\partial T}{\partial r} \tag{1}$$

Solution to equation (1) requires one initial condition and two boundary conditions. The initial condition takes the form:

$$T(r,0) = f_1(r) \tag{2}$$

The boundary condition at the outside surface is given as a specified temperature as a function of time during a heat-up period (for example, a coal particle burning on the element surface) and then convective heat transfer from the surface to the free stream gas (for example, after the coal particle burns out). That is,

$$T(r_b,t) = f_2(t) \qquad \text{during heat-up phase}$$

and

$$-k\frac{\partial T}{\partial r}\Big|_{r=r_b} = h_b(T(r_b,t) - T_{\infty b}) \qquad \text{during cool-down phase} \tag{3}$$

At the inside surface, the boundary condition is given as convective heat transfer from the surface to the free stream gas. That is written as:

$$k\frac{\partial T}{\partial r}\Big|_{r=r_a} = h_a(T(r_a,t) - T_{\infty a}) \tag{4}$$

In order to calculate the temperatures in the filter elements during a particular thermal transient event the form of f_1(r) and f_2(t) were obtained from temperatures measured during operation. One Pall 326 and one Coors P-100A-1 element were instrumented with thermocouples at the outside and inside surfaces during one thermal transient (coal carryover into the PCD during TC02 (see reference 2, page 3.5-11). These thermocouple measurements were used to specify f_1(r) and f_2(t) for that particular transient. Nominal operating temperature when the thermal transient began was 750°F and a temperature increase of 315°F over a period of 55 seconds was measured at the outside surface of the Pall element. Using these measured values, a uniform initial temperature of 750°F was assumed and equation (2) is then written as:

$$T(r,0) = 750°F \tag{5}$$

and the boundary condition at the outside surface, equation (3), is written as:

$$T(r_b,t) = \frac{315°F}{55\sec}t + T_{init} = \frac{5.727°F}{\sec}t + 750°F \qquad \text{for t=0 to 55 sec}$$

and

$$-k\frac{\partial T}{\partial r}\Big|_{r=r_b} = h_b(T(r_b,t) - T_{\infty b}) \qquad \text{for t>55 sec} \tag{6}$$

The Visual Basic numerical algorithm which follows has the capability to handle the more complex initial condition which corresponds to a filter element operating at steady-state with free-stream gas temperatures of $T_{\infty a}$ on the inside and $T_{\infty b}$ on the outside. For this case, equation (2) becomes:

$$T(r,0) = \frac{T_a \ln\frac{r_b}{r} + T_b \ln\frac{r}{r_a}}{\ln\frac{r_b}{r_a}} \tag{7}$$

The wall temperatures Ta and Tb are calculated from the free-stream gas temperatures as shown in equations (8), (9), and (10)

$$T_b - T_a = \frac{T_{\infty b} - T_{\infty a}}{1 + \frac{k}{\ln\frac{r_b}{r_a}}\left(\frac{1}{h_b r_b} + \frac{1}{h_a r_a}\right)} \tag{8}$$

$$T_a = T_{\infty a} + \frac{k(T_b - T_a)}{h_a r_a \ln\frac{r_b}{r_a}} \tag{9}$$

and

$$T_b = T_{\infty b} + \frac{k(T_b - T_a)}{h_b r_b \ln\frac{r_b}{r_a}} \tag{10}$$

Closed form solutions to (the heat equation) equation (1), with the initial condition of equation (5) and boundary conditions of equations (4) and (6), could not be obtained; therefore, the equations were discretized and solved by the finite difference method. The finite difference model is illustrated in Figure 3.5-1. The finite difference approximations to the time and spatial derivatives of equation (1) are:

$$\frac{\partial T}{\partial t} = \frac{T_i^{P+1} - T_i^P}{\Delta t} \tag{11}$$

$$\frac{\partial T}{\partial r} = \frac{T_{i+1}^P - T_i^P}{\Delta r} \tag{12}$$

$$\frac{\partial^2 T}{\partial r^2} = \frac{T_{i+1}^P - 2T_i^P + T_{i-1}^P}{\Delta r^2} \tag{13}$$

Substitution of these into the heat equation and initial and boundary conditions gives the explicit finite difference form of the heat equation as follows:

$$T_i^{P+1} = \frac{\kappa \Delta t}{\Delta r^2}(1 + \frac{\Delta r}{r_i})T_{i+1}^P + \left(1 - 2\frac{\kappa \Delta t}{\Delta r^2} - \frac{\Delta r}{r_i}\frac{\kappa \Delta t}{\Delta r^2}\right)T_i^P + \frac{\kappa \Delta t}{\Delta r^2}T_{i-1}^P \tag{14}$$

$$\Delta t = \frac{t_{\max}}{m} \tag{15}$$

$$\Delta r = \frac{r_b - r_a}{n} \tag{16}$$

with i=1 to n-1 and p=0 to m-1. For all numerical calculations presented in this section, a uniform initial temperature of 750°F was used (instead of the steady-state initial temperature distribution). The explicit finite difference form of the initial and boundary conditions is then:

Initial condition $$T_i^0 = 750°F \tag{17}$$

Boundary condition at O.D. $T_n^{P+1} = 5.727(p+1)\Delta t + 750°F$ for t=0 to 55 sec

$$T_n^{P+1} = \frac{T_{\infty b} + \frac{k}{h_b \Delta r}T_{n-1}^P}{1 + \frac{k}{h_b \Delta r}} \quad \text{for t>55 sec} \tag{18}$$

Boundary condition at I.D. $$T_o^{P+1} = \frac{T_{\infty a} + \frac{k}{h_a \Delta r}T_1^P}{1 + \frac{k}{h_a \Delta r}} \tag{19}$$

A numerical algorithm was written in Visual Basic to calculate temperatures from equations (14) through (19). Thermal properties of the elements as required for the temperature calculations are summarized in Table 3.5-1. These properties were measured at SRI and reported previously (see references 3 and 4, page 3.5-12). The convective heat transfer coefficient was estimated to

be 2 Btu/hr-ft^2-°F and the free-stream gas temperature on the inside and outside of the elements was assumed to be 750°F.

Calculated temperature distributions are plotted in Figure 3.5-2 with the temperature shown throughout the element wall. The temperatures are plotted at t=55 sec., which is the time of the most severe temperature gradient. The heat equation, either equation (1) or the finite difference form in equation (14), clearly suggests that the temperature distribution at any particular time depends on the thermal diffusivity κ. The most similar closed-form solution available is given by Carslaw and Jaeger (see reference 5, page 3.5-12) for a flat plate initially at uniform temperature—one surface insulated and the other surface temperature increasing at a constant rate. This solution shows that the temperature distribution at any particular time depends on the quantity κ/l^2. For the current problem, the dependence of the temperature gradient on κ/l^2 is illustrated in Figure 3.5-3, which shows the gradient T_b-T_a at t=55 sec and κ/l^2 for each type of filter element. As κ/l^2 decreases from 0.082 sec^{-1} for REECER™ to 0.0017 sec.$^{-1}$ for Ensto the temperature gradient increases from ~34°F for REECER™ to ~300°F for Ensto.

3.5.3 Thermal Stresses and Strains

It is the thermal stresses and strains resulting from the temperature gradients calculated in the previous section (not the gradients themselves) which lead to element failures. For linear elastic materials (that is, materials governed by Hooke's Law) thermal stress can be calculated from the known temperature profiles by the following equations (see reference 1):

$$\sigma_r = \frac{\alpha E}{1-\nu}\frac{1}{r^2}\left[\frac{r^2 - r_a^2}{r_b^2 - r_a^2}\int_{r_a}^{r_b} Trdr - \int_{r_a}^{r} Trdr\right] \tag{20}$$

$$\sigma_\Theta = \frac{\alpha E}{1-\nu}\frac{1}{r^2}\left[\frac{r^2 + r_a^2}{r_b^2 - r_a^2}\int_{r_a}^{r_b} Trdr + \int_{r_a}^{r} Trdr - Tr^2\right] \tag{21}$$

$$\sigma_z = \frac{\alpha E}{1-\nu}\left[\frac{2}{r_b^2 - r_a^2}\int_{r_a}^{r_b} Trdr - T\right] \tag{22}$$

The mechanical component of the strains generated are then calculated from the stress-strain relations:

$$\varepsilon_r - \alpha(T - T_{ref}) = \frac{1}{\mathrm{E}}[\sigma_r - \nu(\sigma_\theta + \sigma_z)] \tag{23}$$

$$\varepsilon_\Theta - \alpha(T - T_{ref}) = \frac{1}{\mathrm{E}}[\sigma_\theta - \nu(\sigma_r + \sigma_z)] \tag{24}$$

$$\varepsilon_z - \alpha(T - T_{ref}) = \frac{1}{\mathrm{E}}[\sigma_z - \nu(\sigma_r + \sigma_\theta)] \tag{25}$$

The quantities given by equations (23) through (25) represent the mechanical components of the strain while the values of ε_r, ε_θ, and ε_z represent total strain. When the mechanical component of strain exceeds the strain capability of the material cracks will form. Since the temperature profile in the filter elements T(r) is known only as numerical values at discrete points and not in closed form, calculation of stress by equations (20) through (22) requires numerical integration. The Visual Basic program used to calculate the temperatures also performs the integrations required in equations (20) through (22) by use of Simpson's Rule and then calculates mechanical strains according to equations (23) through (25).

Calculated mechanical strains throughout the wall of the filter elements are plotted in Figure 3.5-4, which shows the largest strains in the aluminum oxide materials (especially Blasch and Ensto), which had the greatest temperature gradients. Note that although the magnitude of the compressive strains generated is 2 to 3 times greater than the magnitude of the tensile strains these elements are most likely to fail in tension because ceramic materials typically have a compressive strength of 8 to 10 times the tensile strength. Since it was shown in the previous section that the value κ/l^2 sets the magnitude of the temperature gradient, the tensile strain at the inside surface at t=55 sec (the location and time of the most severe tensile strain) is shown along with κ/l^2 in Figure 3.5-5. The trend of increasing tensile strain with decreasing κ/l^2 is seen; however, Ensto has a slightly lower strain than Blasch even with a lower κ/l^2 (higher temperature gradient) due to the effect of a lower coefficient of thermal expansion.

Because some elements can accommodate more strain than others these calculated strains must be compared to the measured strain-to-failure for each material to determine the likelihood of cracks forming during thermal transients. The ratios of calculated tensile strain during the thermal transient to measured strain-to-failure, $\varepsilon_{calc}/\varepsilon_f$, is shown in Figure 3.5-6, which shows that $\varepsilon_{calc}/\varepsilon_f$ is greater for the aluminum oxide materials. A horizontal line is drawn on Figure 3.5-6 at $\varepsilon_{calc}/\varepsilon_f = 0.25$: the values for all aluminum oxide materials are above the line and the values for all SiC materials are below the line. These results are consistent with operational experience at the PSDF where Blasch and Coors elements have failed "selectively" during thermal transients (that is, these elements have failed during thermal transients that the clay-bonded and REECER™ SiC elements survived). Ensto was in operation during only one thermal transient and it failed; however, all types of monolithic aluminum oxide and clay-bonded SiC elements failed during that particular event (REECER™ survived).

While the plot results shown in Figure 3.5-6 reveal that the monolithic aluminum oxide or alumina mullite filter elements are more likely to fail during thermal transients than the SiC materials, the tensile strain calculated for Coors during the 315°F/55 sec surface temperature increase was only ~28 percent of the measured tensile strain-to-failure; however, the Coors elements failed during that thermal transient. Several factors make crack initiation possible even with $\varepsilon_{calc}/\varepsilon_f \approx 0.28$. If the surface heating rate of 315°F/55 sec was measured inches away from a burning coal particle (assuming coal carryover into the PCD caused the transient), local conditions would have been much worse and gradients severe enough to initiate cracking would have been likely. Another important consideration is that the strain-to-failure values used to generate Figure 3.5-6 (and to calculate $\varepsilon_{calc}/\varepsilon_f \approx 0.28$ for Coors) were based on average properties of virgin material. Property degradation during operation could lower the strain-to-failure.

More importantly, cracking will initiate selectively at the weakest locations, or at least the locations where strain-to-failure is the lowest. At these locations, cracking will occur at gradients less severe than those calculated based on average properties.

If the data and analysis presented above indicate that cracks will initiate during thermal transients the question of whether the cracks will propagate and lead to failure remains. The clay-bonded SiC materials consist of individual SiC particles or clusters of SiC particles connected by bridges of clay binder material. When cracking occurs it is in the binder bridges. A large amount of energy is required to propagate a crack from one bridge to an adjacent bridge. The aluminum oxide and alumina-mullite filter elements have a much different microstructure. Although these materials are quite porous they are much closer to homogenous monolithic ceramics than the clay-bonded materials. If cracks start in these materials they propagate much more readily than clay-bonded SiC materials making failure more likely.

This 1-D analysis of filter elements under the thermal transient conditions measured at the PSDF indicates that failure of Schumacher and Pall clay-bonded SiC or IF&P REECER™ recrystallized SiC elements is less likely than the monolithic aluminum oxide or alumina mullite elements from Blasch, Ensto, or Coors. It must be noted, however, that the clay-bonded SiC materials have failed during at least two thermal transients at the PSDF.

3.5.4 ANSYS Finite Element Model Results

In order to verify that the ANSYS 3-D model and the 1-D finite difference model give consistent results for similar boundary conditions and material properties, the temperatures and resulting thermal stresses and strains were calculated for Coors elements using the ANSYS finite element model illustrated in Figure 3.5-7. Boundary conditions for this model are the same as the 1-D model except that this model has a length of 6 inches with appropriate boundary conditions at the ends, whereas the 1-D model has infinite length. In the middle of the 4-inch length, the effect of the end conditions should be minimal. Results obtained from the ANSYS and 1-D models are compared in Figures 3.5-8 and -9. These plots show that for a uniform temperature on the outside surface, the ANSYS and 1-D models give nearly identical temperature and strain distributions.

Next, the elements were analyzed using the ANSYS 3-D model illustrated in Figure 3.5-10. This model represents a refinement over the 1-D model by applying the temperature increase on the outside surface only to a “hot spot” approximately 3 inches in diameter. The rest of the outside surface is subject to convective heat transfer to the free-stream gas with a convection coefficient $h=2$ Btu/hr-ft^2-°F. With the temperature increase applied to only a 3-inch diameter region, axial and circumferential heat transfer will affect the temperature gradients and thermal stresses and strains generated.

The temperature distribution at the center of the 3-inch diameter hot spot as calculated by the ANSYS 3-D model is plotted in Figure 3.5-11. Previously presented results from the 1-D model are shown as dashed lines in this figure. The temperatures predicted by the two models are nearly identical. Mechanical strains generated at the center of the hot spot due to these temperature distributions are plotted in Figure 3.5-12. Strains calculated by the 1-D model are

included as dashed lines. The strains calculated by the ANSYS 3-D model include those generated due to the temperature gradient across the element wall as the 1-D model predicts, plus another component. Free thermal expansion of the material in the hot zone would tend to increase the radius of curvature; however, this free expansion is resisted by the material outside of the hot zone, and a circumferential load and a bending moment result as illustrated in Figure 3.5-13. A bending moment that decreases the radius of curvature, or in this case resists an increase in radius of curvature, results in compressive strain at the inside surface and tensile strain at the outside surface. This is reflected in the calculated strains plotted in Figure 3.5-12. The tensile strain at the inside surface has been decreased although all elements remain in tension at that location. The compressive strain at the outside surface has also been decreased for all elements. In fact, for REECER™ the ANSYS 3-D model predicts tension throughout the element all the way to the outside surface. Another noticeable difference between the strains calculated by the ANSYS and 1-D models is that for REECER™, Schumacher, and Pall the high-conductivity materials (the maximum strain calculated by ANSYS) is not at the inside surface. Instead, the maximum tensile strain was calculated near the center of the wall for REECER™ and 0.075 to 0.10 inch from the inside surface for Pall 326 and Schumacher TF20.

Strains calculated by the ANSYS 3-D model are compared to the strains calculated by the 1-D finite difference model in Table 3.5-2. Comparison of strain at the inside surface shows good agreement between the two models for materials with low κ/l^2. For the aluminum oxide materials, tensile strains predicted by the 1-D and ANSYS models are within less than 20 percent of each other. For Blasch and Ensto, which have the lowest κ/l^2, the models agree within 10 percent. The difference between the two models increases as κ/l^2 for the elements increases. For REECER™ the 1-D model predicts 3 times as much strain at the inside surface as the ANSYS model. Maximum tensile strains calculated for the SiC materials by the ANSYS model did not occur at the inside surface. The maximum values compared better to the strains obtained by the 1-D model; however, for a different geometry, different heating rate, different size hot spot, etc., the agreement between maximum strain predicted by ANSYS and the 1-D model may change. The results indicate that either the 1-D or the ANSYS 3-D model is capable of giving good results for elements with low κ/l^2 where temperature gradients through the walls control the strains generated. For high-κ/l^2 elements, axial and circumferential temperature gradients are significant in setting the strain levels and the 1-D model gives a considerable error. For these materials a refinement that includes the multidimensional effects is needed for accurate strain prediction. The strains calculated by the ANSYS model for high-κ/l^2 materials also depend on how the surface temperature increase is input. For example, how large is the hot spot? Is the temperature uniform over the hot spot? Better definition of the thermal loading and boundary conditions during thermal transients is needed to get accurate strain calculations from the ANSYS model for high-κ/l^2 materials. For this purpose more detailed temperature measurements are needed to better represent the modeling parameters.

The bending moments and circumferential loads illustrated in Figure 3.5-13 generate strains (and stresses) in the elements at locations far from the center of the hot spot. For high-κ/l^2 elements, these strains were greater than the strains at the center of the hot spot. Strains calculated by ANSYS throughout the element are shown in Figures 3.5-14 through -16 for REECER™, Schumacher TF20, and Blasch 4-270. The maximum tensile strain calculated for Blasch

elements was the value shown above (0.35 mils/inch) at the center of the hot spot on the inside surface, but for REECER™ and Schumacher TF20 the maximum tensile strain occurs outside of the hot zone. For REECER™ the maximum calculated tensile strain was 0.097 mils/inch and occurred at three locations: (1) at the same axial location as the center of the hot spot but ~138° away (location 1 in Figure 3.5-14), (2) a similar location on the other half of the element not included in the model due to symmetry, and (3) at the same circumferential location as the center of the hot spot but ~1.87 inches away (location 2 in Figure 3.5-14). For Schumacher TF20 the maximum calculated tensile strain was 0.091 mils/inch and occurred at approximately the same axial and circumferential locations as in the REECER™ elements. For REECER™, this maximum strain is 75 percent of the measured strain-to-failure and for TF20 this maximum strain is 22 percent of the measured strain-to-failure. Strains of that magnitude would likely cause failure; therefore, the actual strains during operation were probably less than this. The stresses and strains calculated at these locations outside of the hot zone depend strongly on how the temperature increase is input to the ANSYS model. Hot spot size, shape, temperature distribution (uniform or varying within the hot spot), and other factors will affect the resulting stresses and strains. The hot spot shape used in these calculations was assumed but no experimental measurements have been made to allow accurate modeling of the hot spot.

The ANSYS 3-D model results show that for elements with low κ/l^2—the aluminum oxide materials in this analysis—the temperature gradients through the thickness of the element wall control the tensile strains generated during thermal transients. For these elements, good agreement between the 1-D finite difference model and ANSYS 3-D model was obtained; either model will predict temperature gradients and thermal stresses and strains with reasonable accuracy. For elements with high κ/l^2—the SiC materials in this analysis—axial and circumferential gradients have a significant effect on the thermal stresses and strains; a 3-D model is required to predict element response. For these elements, bending loads alter the stress and strain profile at the center of the hot spot and can lead to even greater stresses and strains outside of the hot spot. The strains predicted by the current analysis are probably not accurate for elements with high κ/l^2; however, the analysis shows the effect of axial or circumferential temperature gradients. Accurate prediction of the thermal stresses and strains in these elements will require better modeling of the hot spot. The ANSYS results, even without enough information to accurately model the hot spot, confirm the major conclusion of the 1-D model: elements with low κ/l^2 will experience greater temperature gradients and strains during thermal transients than elements with high κ/l^2. Whether the larger strains will lead to element failure depends on tensile strain-to-failure and toughness.

These results do not consider the effect of coefficient of thermal expansion on strains generated. Because the thermal conductivity of these materials varied over a much greater range than thermal expansion, the effect of thermal conductivity was much greater. Thermal expansion will, however, affect the strains produced during thermal transients. Higher thermal expansion will lead to higher strain.

It was stated in the section 3.5.3 that a surface temperature increase much greater than the 315°F/55 sec measured during the thermal transient may have occurred if the thermocouple was located inches away from the burning coal particle. The same ANSYS 3-D model was used to

investigate this, except that a surface temperature increase of 1,300°F/55 sec (from 700 to 2,000°F) was specified over a 3-inch diameter hot spot and the resulting temperatures throughout the element were calculated. Temperature-dependent material properties of Coors elements were used in the model for this study. The calculated surface temperatures at t=55 sec are plotted versus distance from the center of the hot spot in Figure 3.5-17. At a distance of only 0.15 inch from the edge of the hot spot the surface temperature increase was only 300°F. This indicates that if the thermocouple that measured the temperature increase of 315°F was farther from the hot spot than this the temperature increase indeed would have been much more severe.

3.5.5 Conclusion

The performance of several monolithic ceramic filter elements during thermal transients was studied in this effort. The filters evaluated were IF&P REECER™, Schumacher TF20, Pall 326, Coors P-100A-1, Blasch 4-270, and Ensto. A 1-D finite difference model was developed to calculate the temperature profiles in the elements under conditions measured during one thermal transient at the PSDF. A refinement to this 1-D model was developed using an ANSYS 3-D finite element model. The ANSYS considers the effects of axial and circumferential temperature gradients and more complex boundary conditions.

The results presented here show that elements with low κ/l^2, including monolithic aluminum oxide elements, will develop greater temperature gradients and thermal stresses and strains during thermal transients than elements with high κ/l^2. Thermal expansion will also have an effect, but for the filter elements considered here κ/l^2 is the most important factor in determining the thermal-stress and -strain level. Mechanical properties including tensile strain-to-failure and "toughness" will determine whether these strains lead to crack formation and whether cracks propagate and lead to element failure.

From the results obtained in this effort some areas to be addressed in future efforts have been identified. These include:

- Development of a model that includes gas flow through the wall.
- Modeling of the actual microstructure of the elements instead of the continuum assumed here.
- More detailed temperature measurements to obtain better definition of the thermal loading and boundary conditions during thermal transients.

3.5.6 References

1. Timoshenko, S. P., and Goodier, J.N., Theory of Elasticity, McGraw-Hill, 1951.
2. "Technical Progress Report for Kellogg Brown and Root Transport Reactor Train With Siemens-Westinghouse Particulate Control Device TC02: April 1998 – May 1998," DOE Cooperative Agreement Number DE-FC21-90MC25140, June 1999.

3. Spain, J. D., and Starrett, H.S., "Mechanical and Thermal Evaluation of Several Element Filter Materials," Report to Southern Company Services, purchase order number C-97-001785.
4. Spain, J. D., and Starrett, H.S., "Physical, Mechanical, and Thermal Properties of Coors Alumina Mullite Filter Material," Report No. SRI-MME-94-480-6938.20.1-I-F, Prepared for DOE/FETC, Contract DE-AC21-89-MC26233.
5. Carslaw, H. S., and Jaeger, J.C., Conduction of Heat in Solids, Oxford University Press, 1948.

Table 3.5-1

Filter Element Properties Used in Thermal Model

Material	ID (in.)	OD (in.)	E (Msi)	ν	$\alpha(10^{-6})$ (1/°F)	k (Btu/ hr-in-°F)	ρ (lb/in^3)	Cp (Btu/ lb-°F)
REECER™	1.70	2.40	17.0	0.15	2.70	0.87	0.083	0.26
Schumacher TF20	1.58	2.36	3.2	0.10	2.35	0.36	0.069	0.27
Pall 326	1.58	2.36	3.8	0.10	3.03	0.27	0.067	0.27
Coors P-100A-1	1.58	2.36	3.3	0.10	2.85	0.077	0.058	0.27
Blasch 4-270	1.52	2.36	0.8	0.10	4.10	0.036	0.064	0.27
Ensto	1.45	2.40	2.3	0.10	4.00	0.042	0.068	0.27

Nomenclature:
ID Inside diameter
OD Outside diameter
E Young's modulus
ν Poisson's ratio
α Coefficient of thermal expansion
k Thermal conductivity
ρ Bulk density
Cp Specific heat

Table 3.5-2

Comparison of Tensile Strains Calculated by 1-D Model and ANSYS 3-D Model

Material	Tensile Strain at Inside Surface by 1-D Model (mils/inch)	Tensile Strain at Inside Surface by ANSYS Model (mils/inch)	Maximum Tensile Strain by ANSYS Model (mils/inch)
Blasch 4-270	0.38	0.35	0.35
Ensto	0.37	0.34	0.34
Coors P-100A-1	0.22	0.18	0.18
Pall 326	0.11	0.069	0.080
Schumacher TF20	0.063	0.036	0.047
REECER™	0.029	0.0094	0.032

Tensile strains calculated by ANSYS model were at the center of the hot spot.

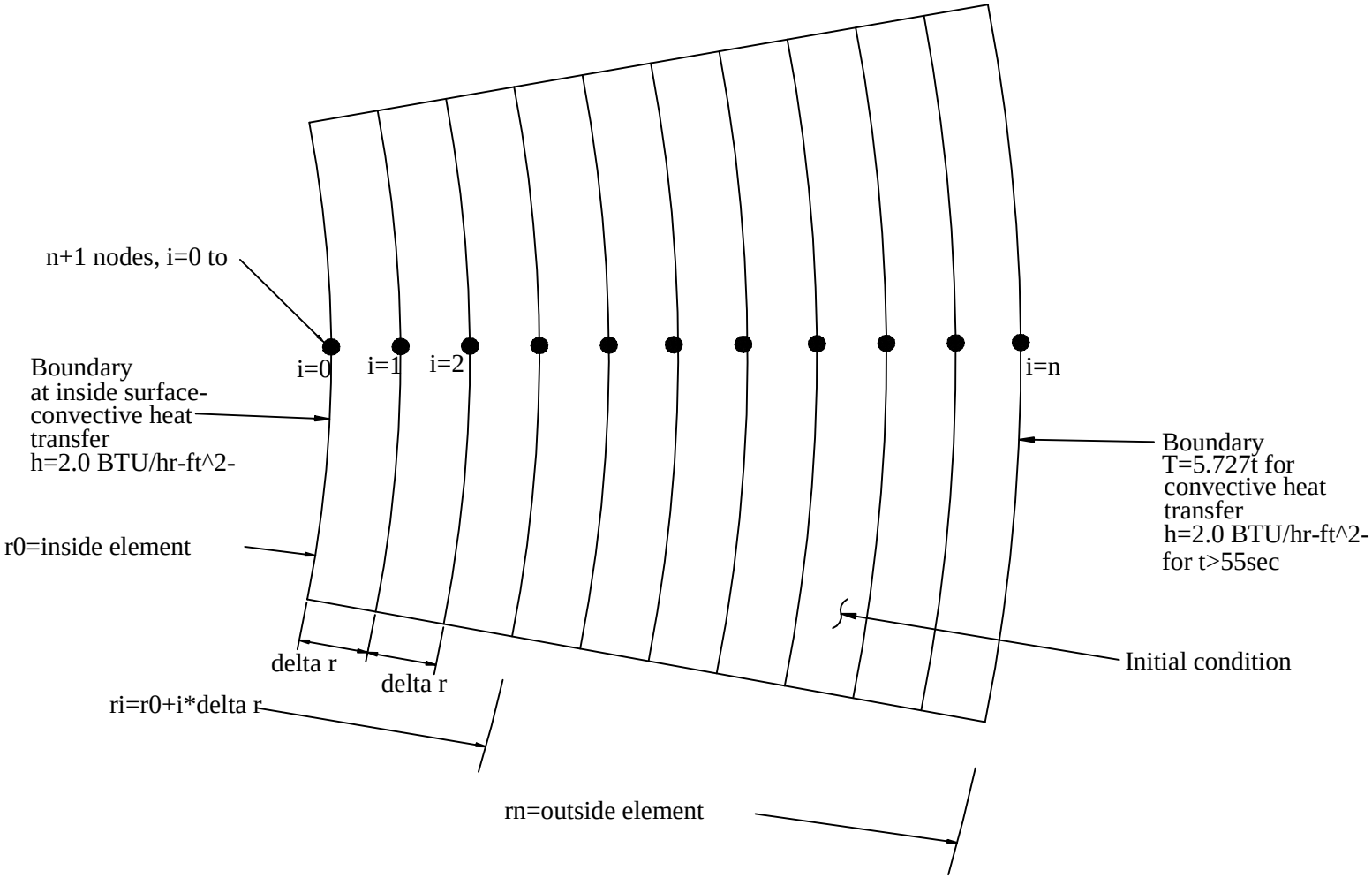

Figure 3.5-1 Finite Difference Model for Thermal Transient Temperature and Stress Calculations

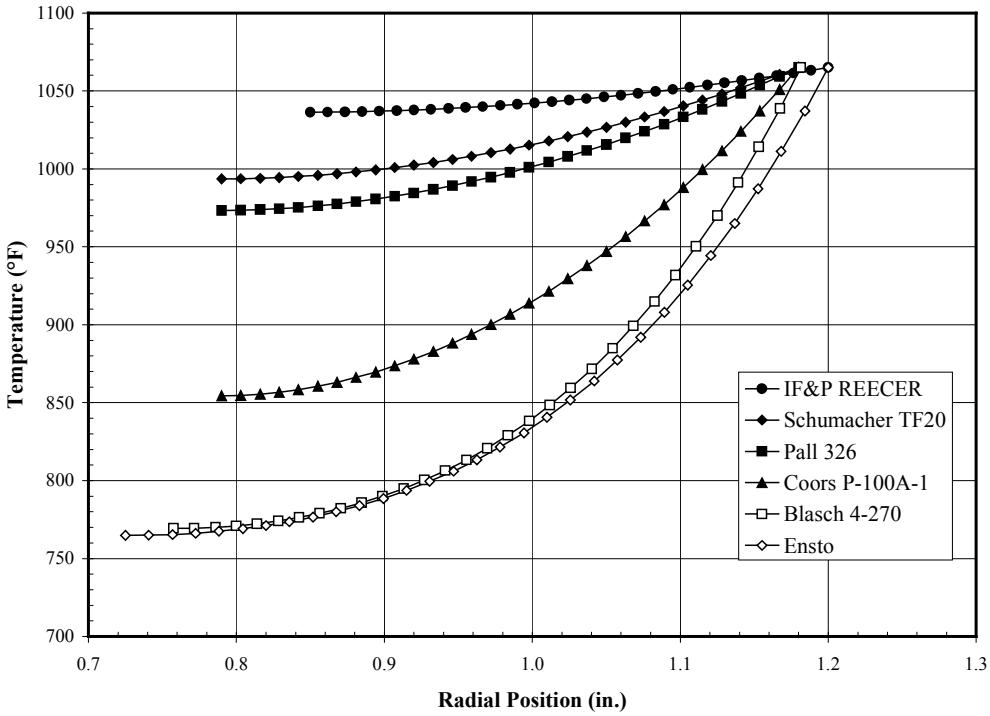

Figure 3.5-2 Temperature Distribution Calculated From Thermal Model for a Temperature Increase of 315°F/55 sec at the OD

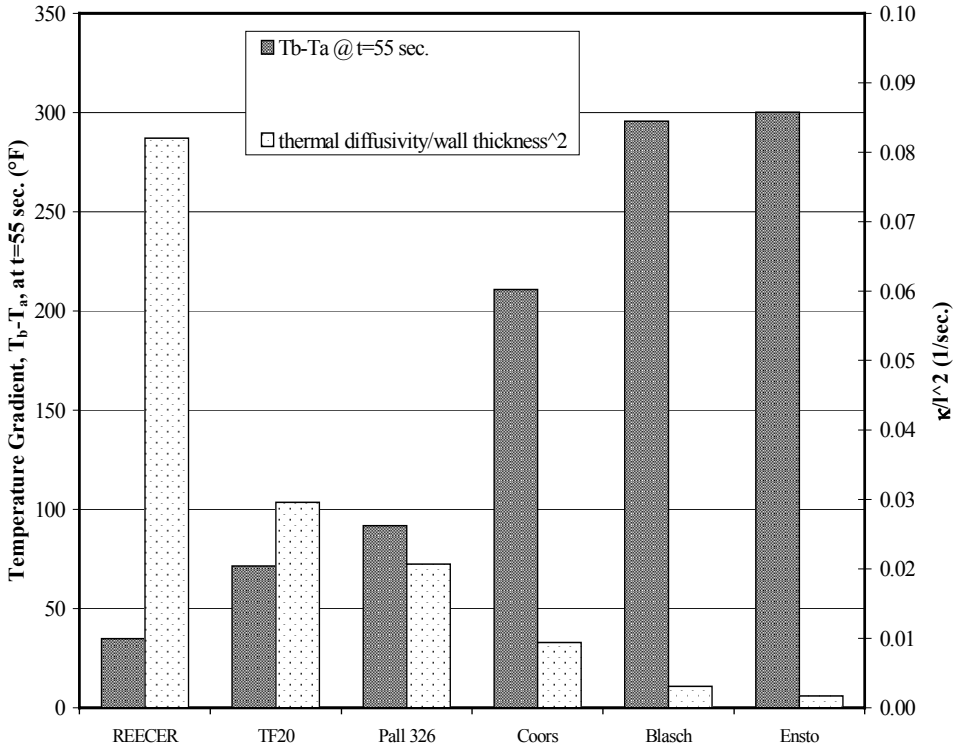

Figure 3.5-3 Temperature Gradient During Thermal Transient and κ/l^2 for Ceramic Filter Elements

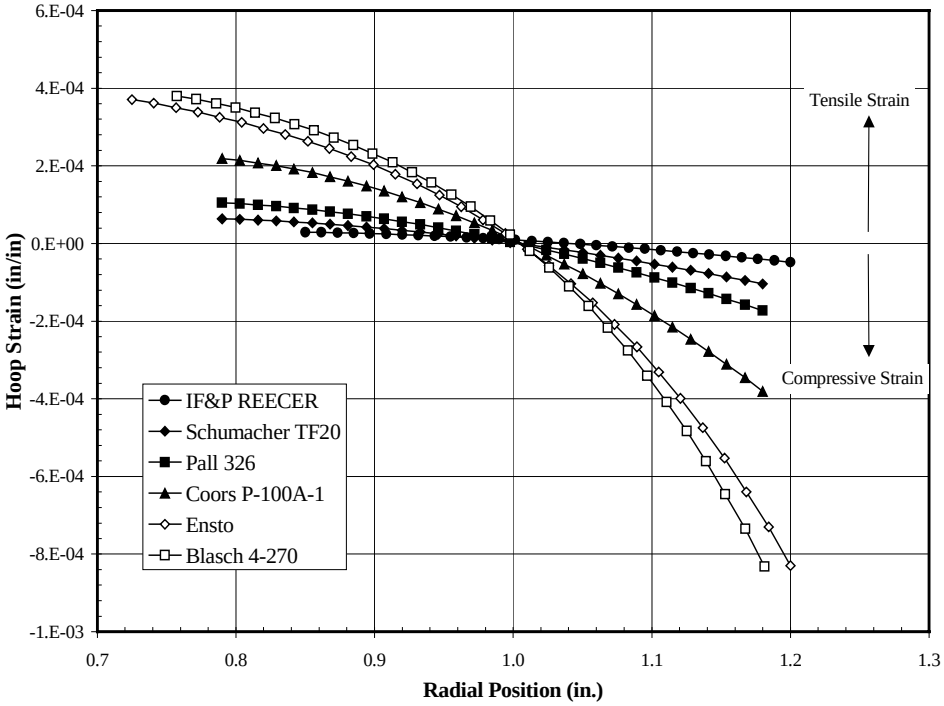

Figure 3.5-4 Strain Distribution Calculated From Thermal Model for a Temperature Increase of 315°F/55 sec at the OD

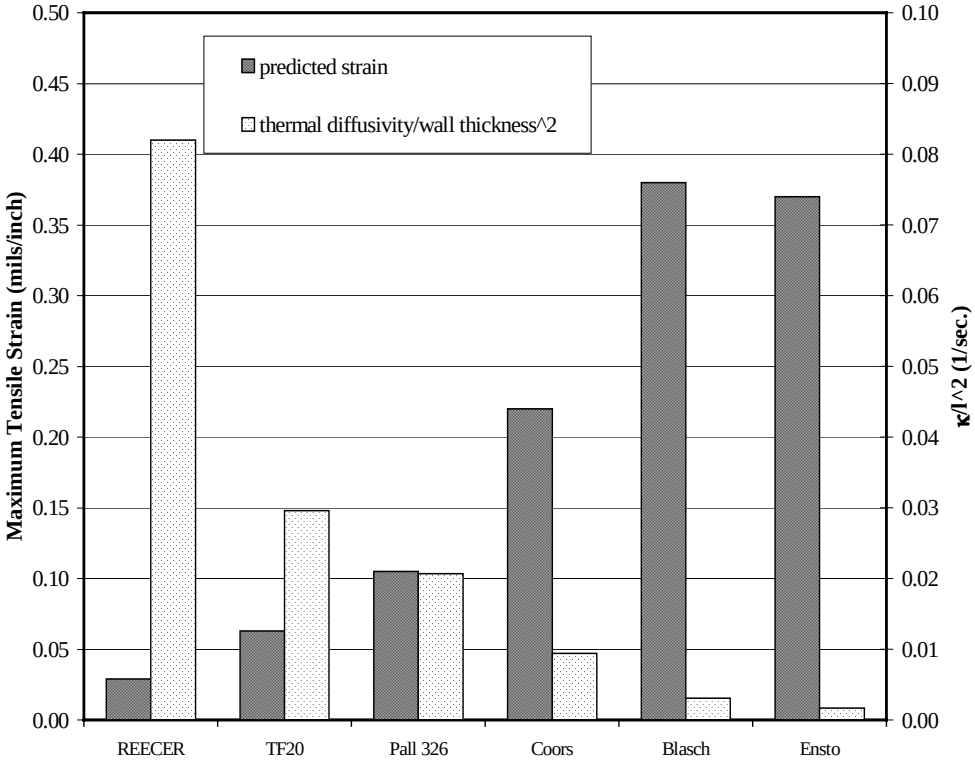

Figure 3.5-5 Tensile Strain During Thermal Transient and κ/l^2 for Ceramic Filter Elements

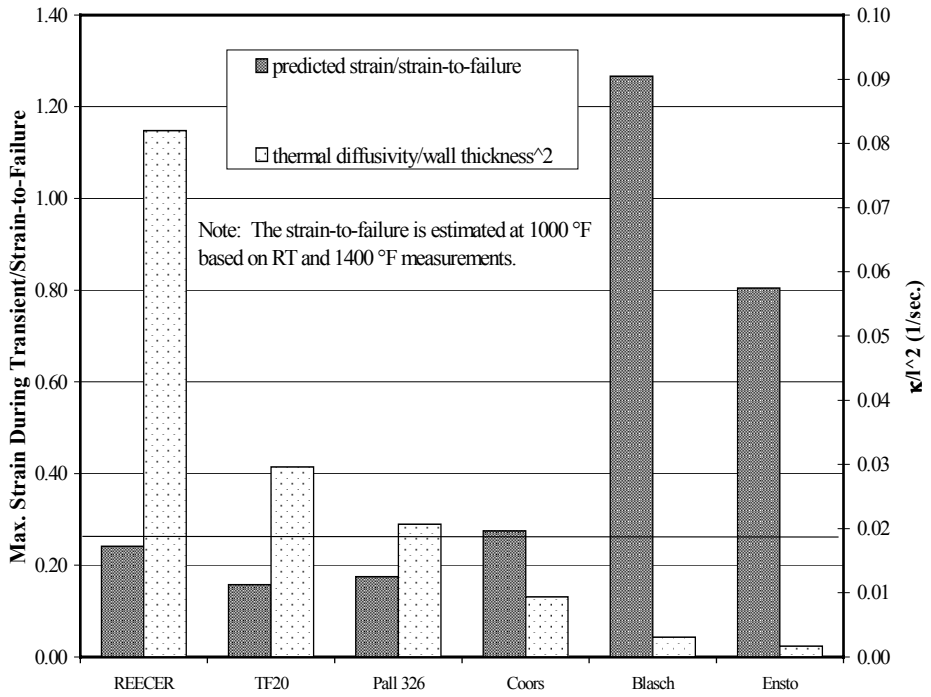

Figure 3.5-6 Tensile Strain During Thermal Transient/Strain-to-Failure and κ/l^2 for Ceramic Filter Elements

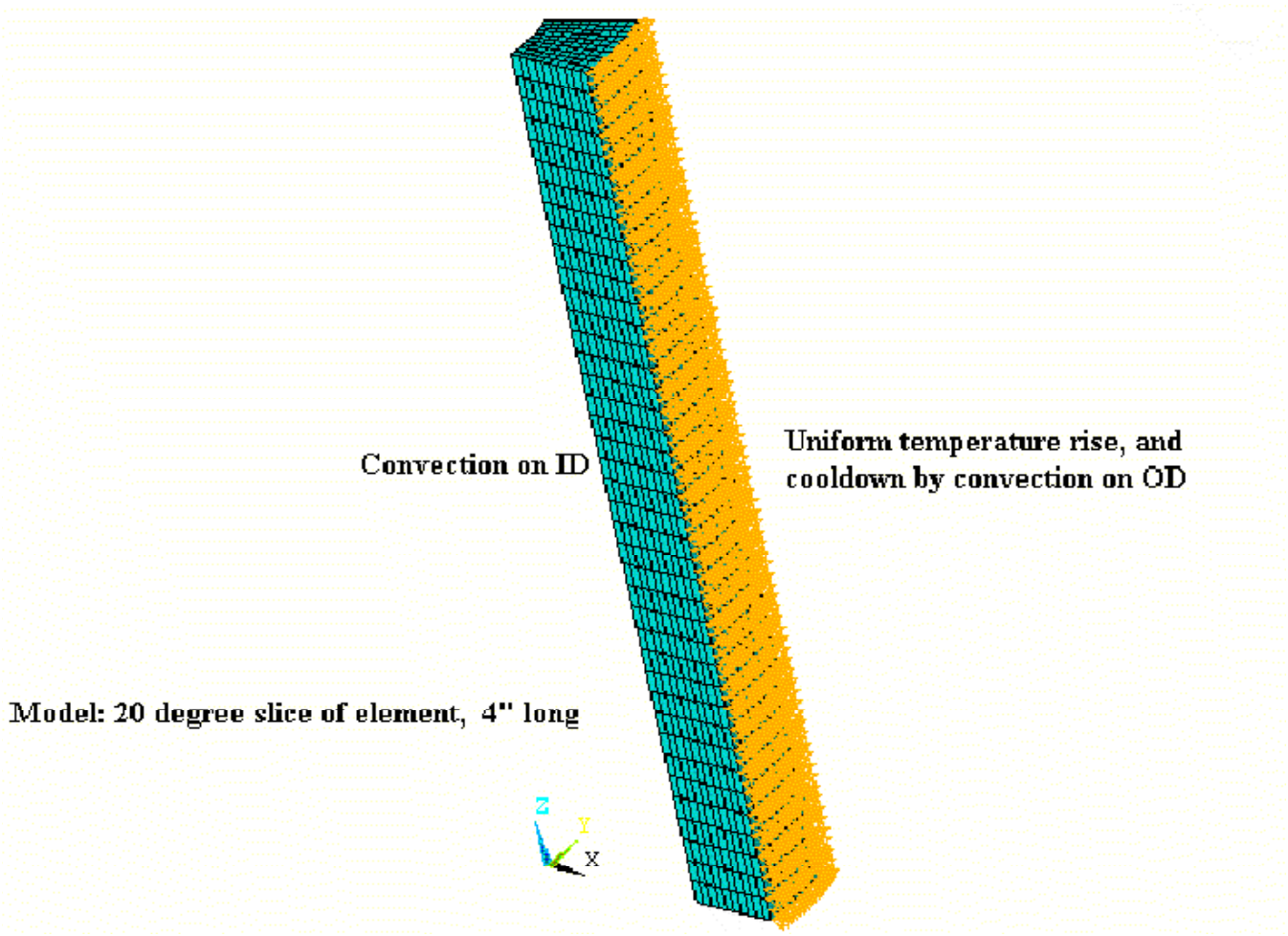

Figure 3.5-7 ANSYS Finite Model With Uniform Temperature Increase on Outside Surface

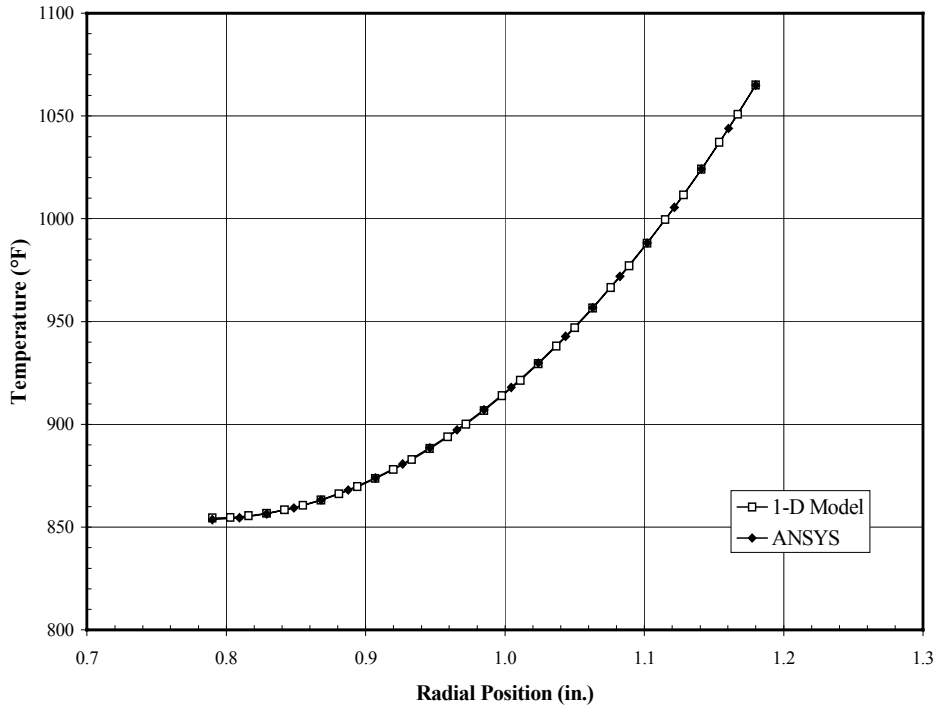

Figure 3.5-8 Temperature Distribution With a Uniform Temperature Increase on the Outside Surface

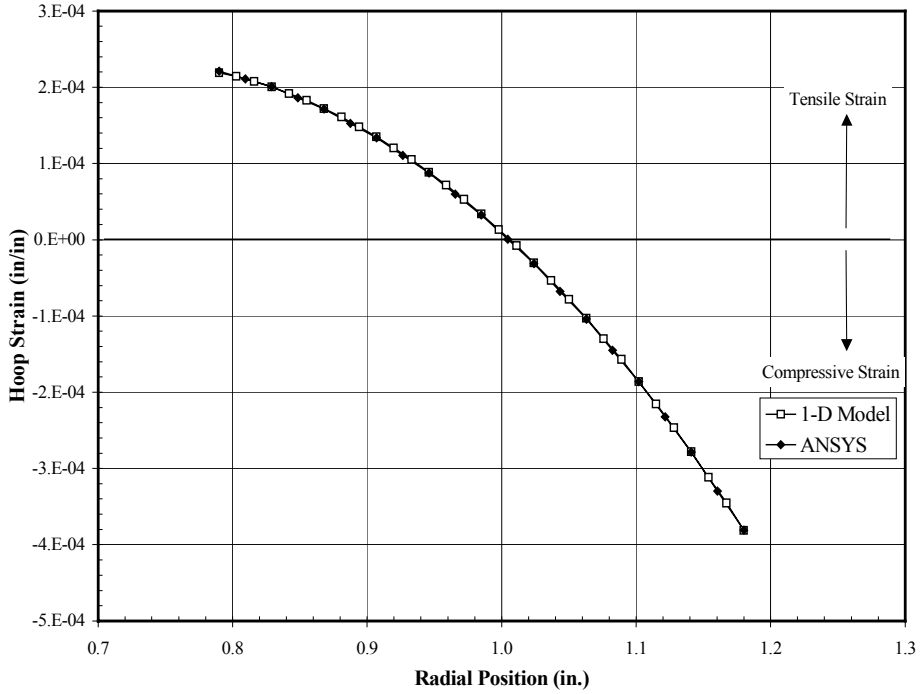

Figure 3.5-9 Strain Distribution With a Uniform Temperature Increase on the Outside Surface

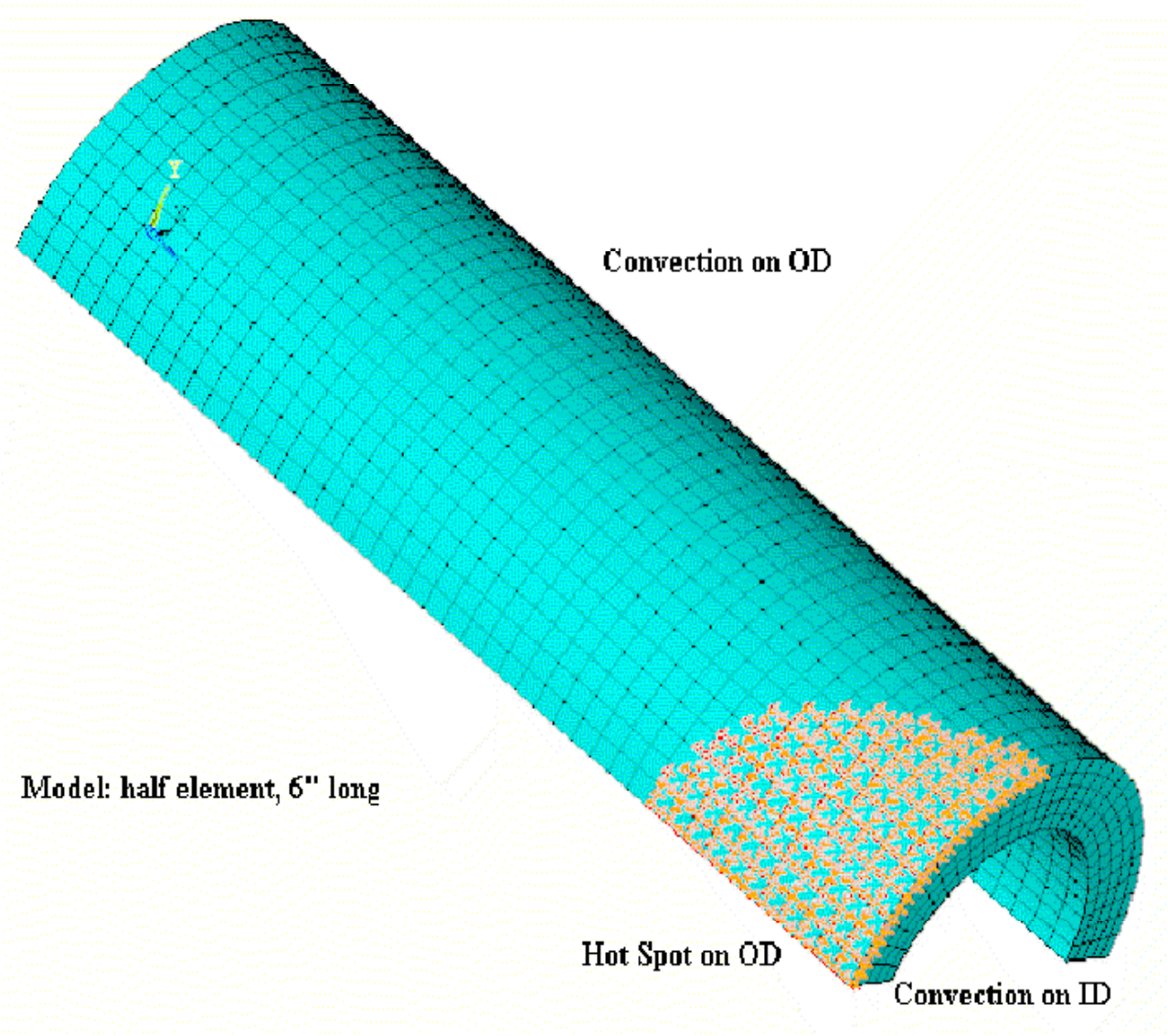

Figure 3.5-10 ANSYS 3-D Model With Temperature Increase Over a 3-Inch Hot Spot on Outside Surface

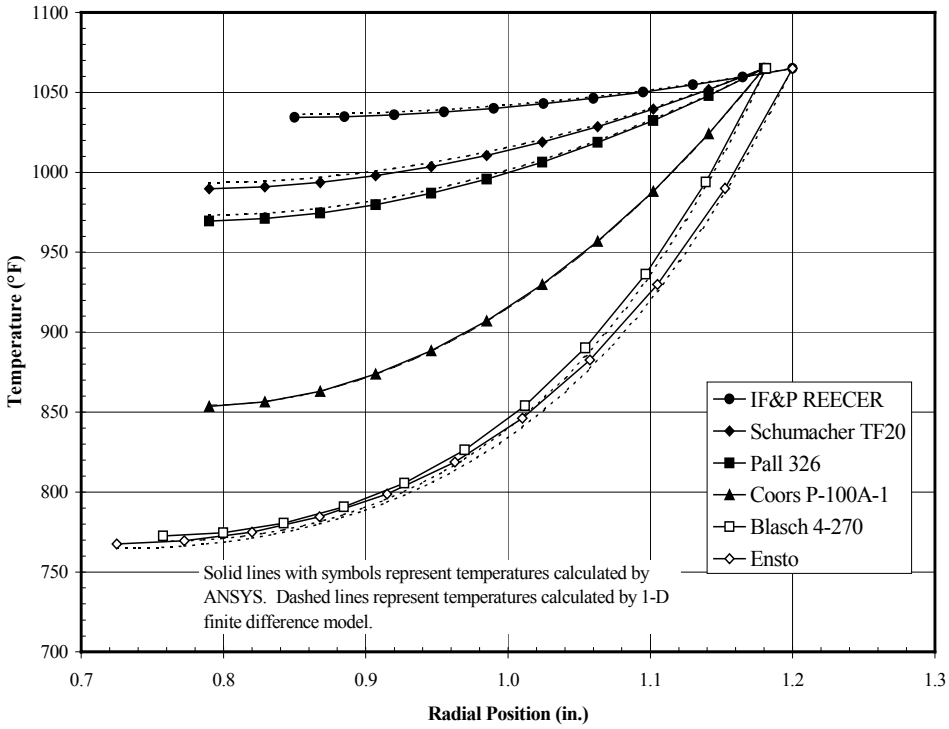

Figure 3.5-11 Temperature Distribution With an Increase of 315°F/55 sec Applied to a 3-Inch-Diameter Hot Spot

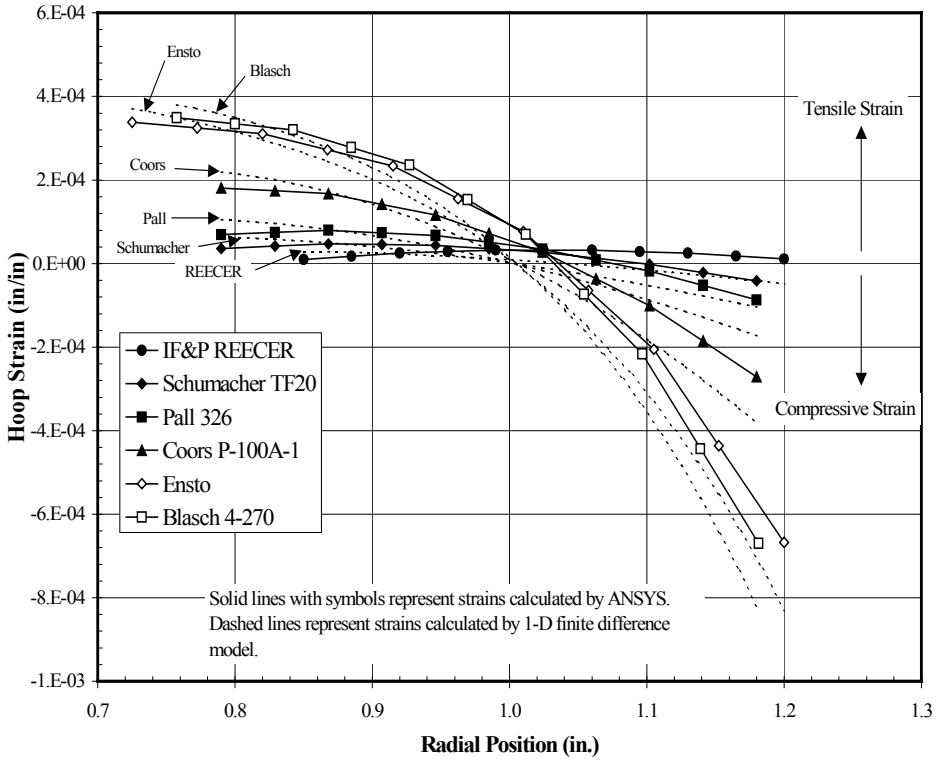

Figure 3.5-12 Strain Distribution With a Temperature Increase of 315°F/55 sec Applied to a 3-Inch-Diameter Hot Spot

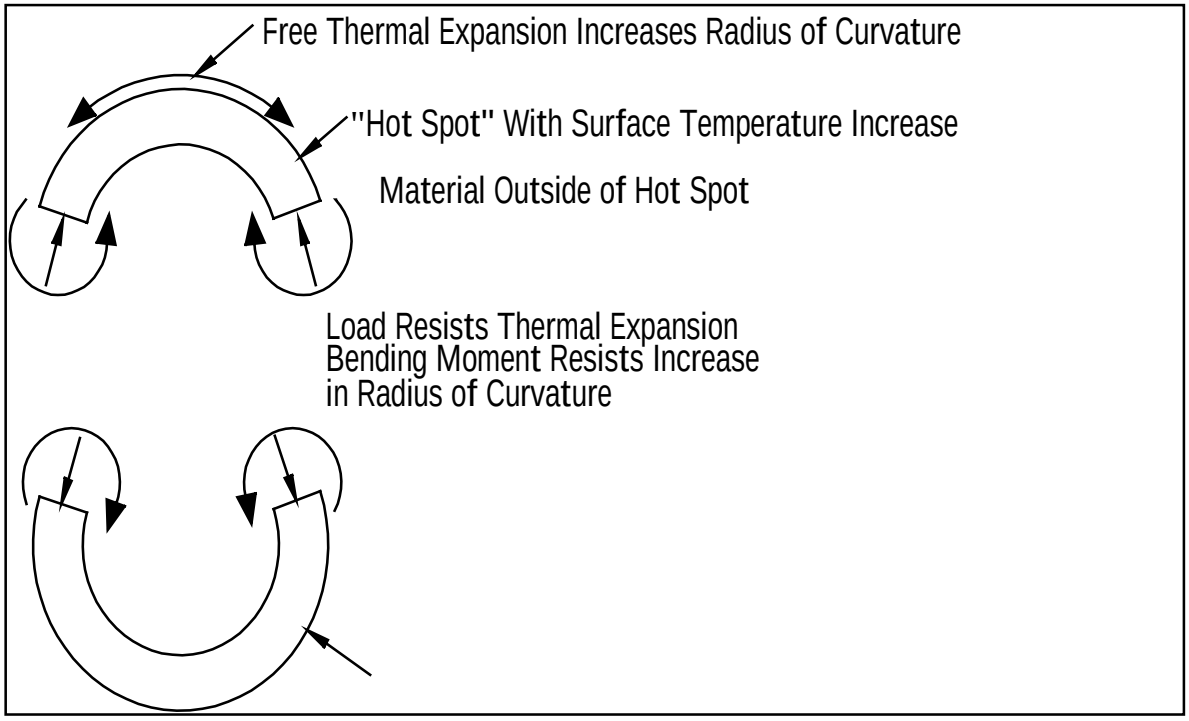

Figure 3.5-13 Loads Produced on Elements by Circumferential Temperature Gradients

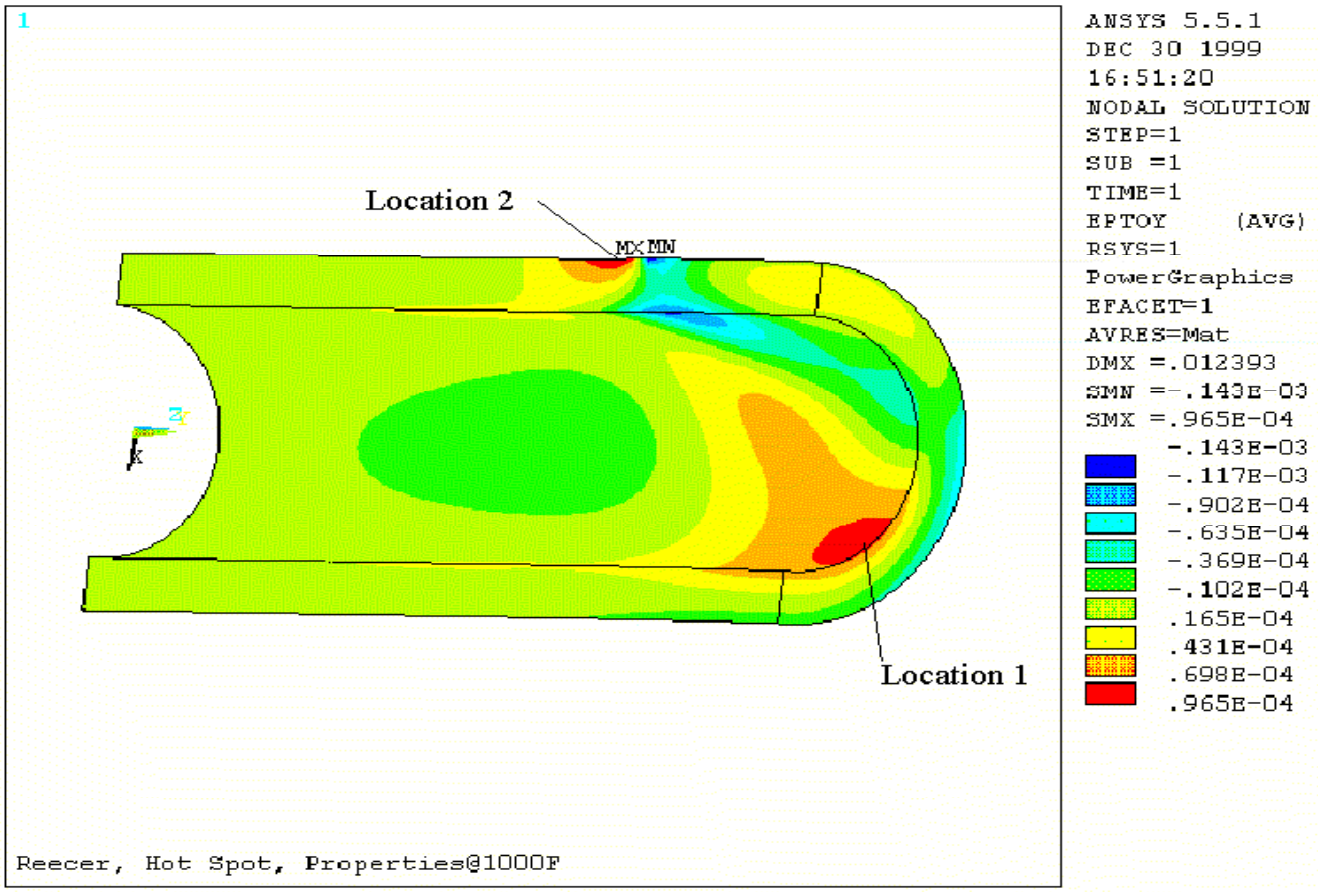

Figure 3.5-14 Strain Distribution in IF&P REECER™ Element With 3-Inch-Diameter Hot Spot

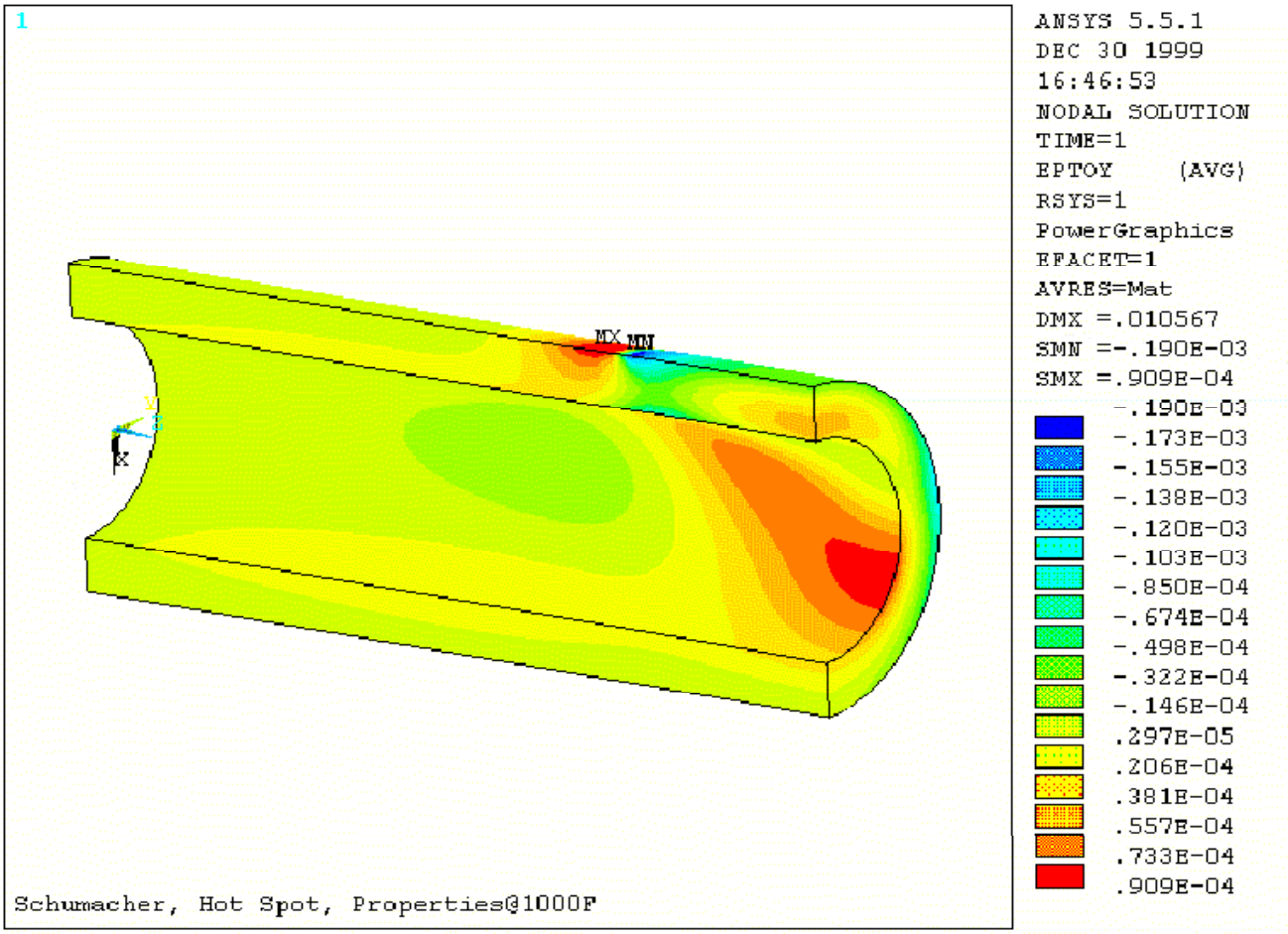

Figure 3.5-15 Strain Distribution in Schumacher TF20 Element With 3-Inch-Diameter Hot Spot

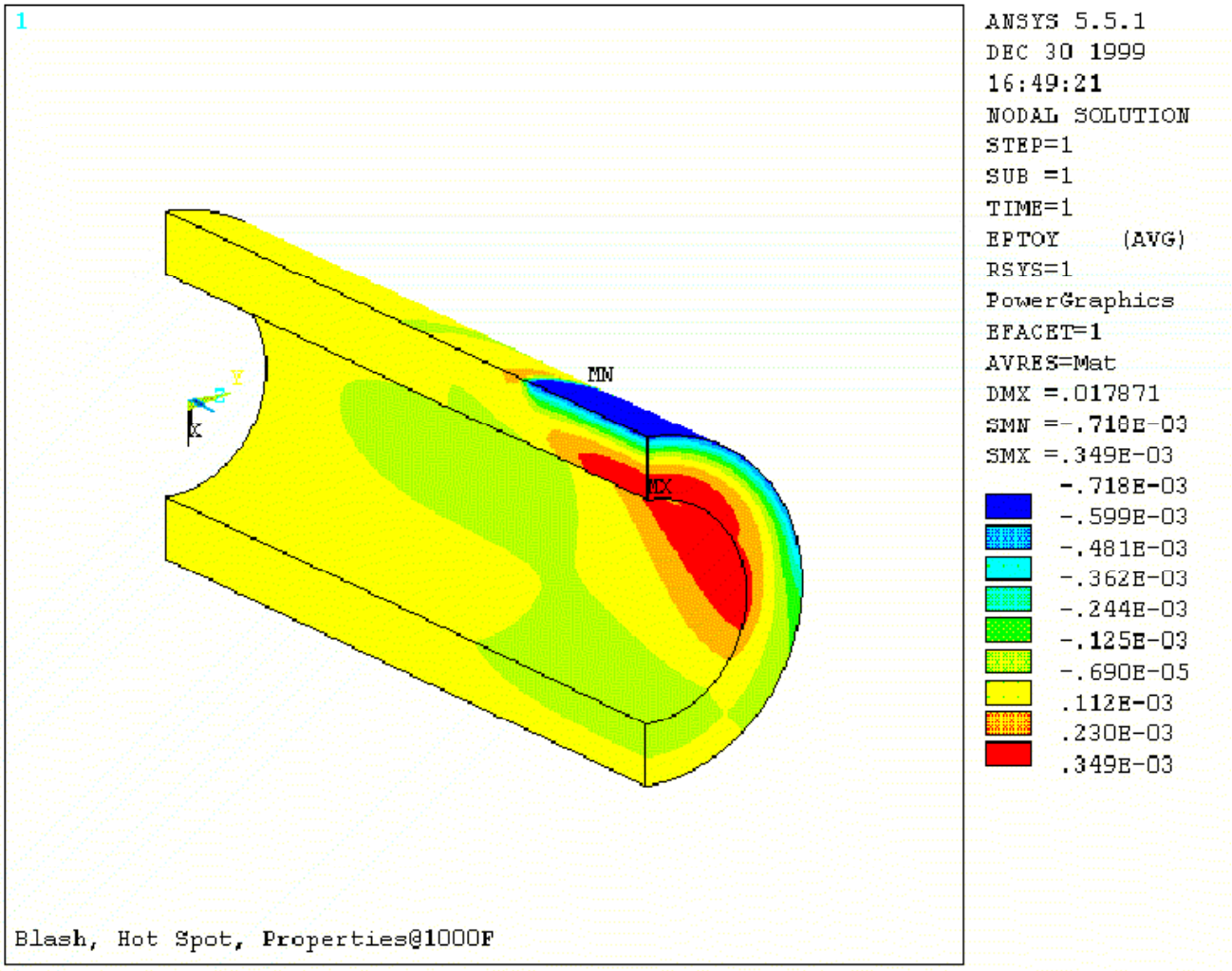

Figure 3.5-16 Strain Distribution in Blasch 4-270 Element With 3-Inch-Diameter Hot Spot

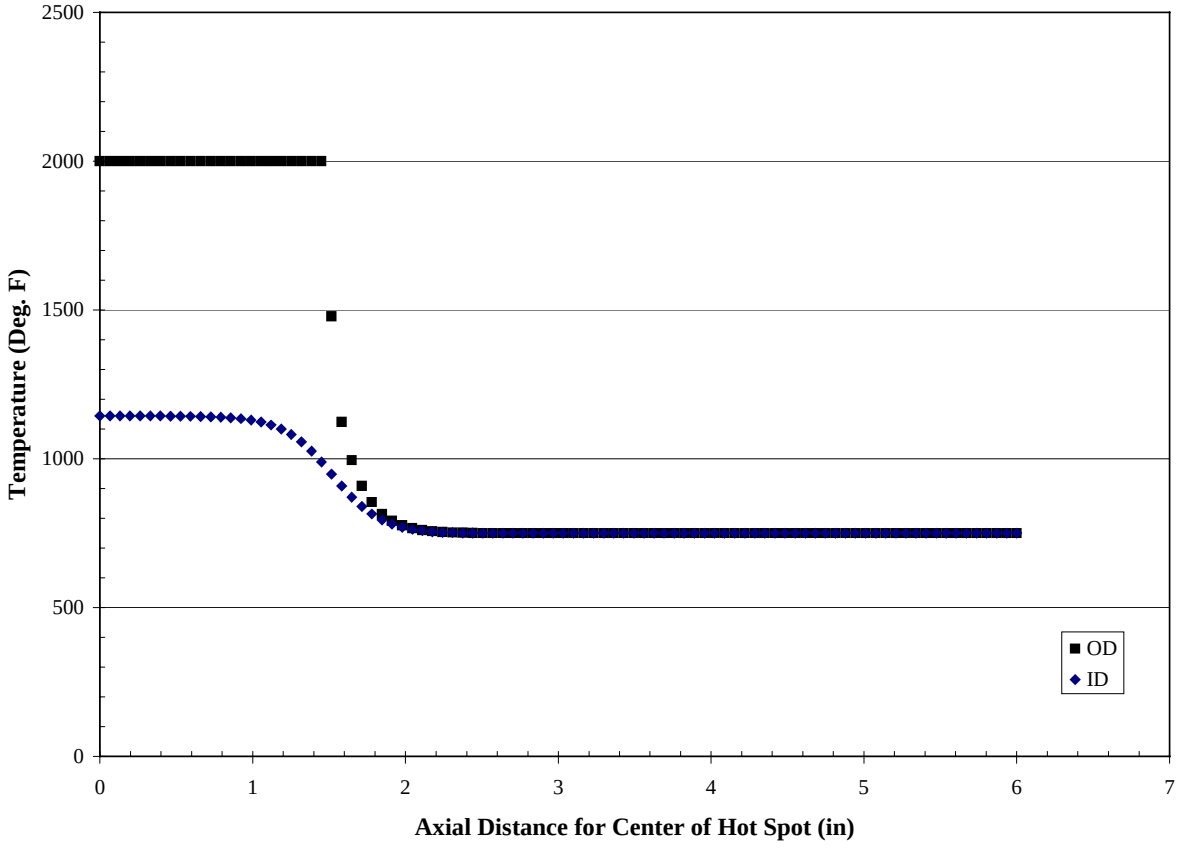

Figure 3.5-17 Axial Temperature Distribution in Coors Element With Hot Spot, 1,300°F/55 sec Temperature Increase

TERMS

Listing of Abbreviations

AAS	Automated Analytical Solutions
ADEM	Alabama Department of Environmental Management
APC	Alabama Power Company
APFBC	Advance Pressurized Fluidized-Bed Combustion
ASME	American Society of Mechanical Engineers
AW	Application Workstation
BFI	Browning-Ferris Industries
BFW	Boiler Feed Water
BMS	Burner Management System
BOC	BOC Gases
BOP	Balance-of-Plant
BPIR	Ball Pass Inner Race, Frequencies
BPOR	Ball Pass Outer Race, Frequencies
BSF	Ball Spin Frequency
CAD	Computer-Aided Design
CEM	Continuous Emissions Monitor
CFB	Circulating Fluidized Bed
CFR	Code of Federal Regulations
CHE	Combustor Heat Exchanger
COV	Coefficient of Variation (Standard Deviation/Average)
CPC	Combustion Power Compay
CPR	Cardiopulmonary Resuscitation
CTE	Coefficient of Thermal Expansion
DC	Direct Current
DCS	Distributed Control System
DOE	U.S. Department of Energy
E & I	Electrical and Instrumentation
EERC	Energy and Environmental Research Center
EPRI	Electric Power Research Institute
EDX	Energy-Dispersive X-Ray
ESCA	Electron Spectroscopy for Chemical Analysis
FCC	Fluidized Catalytic Cracker
FCP	Flow-Compacted Porosity
FFG	Flame Front Generator
FI	Flow Indicator
FIC	Flow Indicator Controller
FOAK	First-of-a-Kind
FTF	Fundamental Train Frequency
FW	Foster Wheeler
GBF	Granular Bed Filter
GC	Gas Chromatograph
GEESI	General Electric Environmental Services, Inc.
HP	High Pressure

HRSG	Heat Recovery Steam Generator
HTF	Heat Transfer Fluid
HTHP	High-Temperature, High-Pressure
I/O	Inputs/Outputs
ID	Inside Diameter
IF&P	Industrial Filter & Pump
IGV	Inlet Guide Vanes
IR	Infrared
KBR	Kellogg Brown & Root
LAN	Local Area Network
LIMS	Laboratory Information Management System
LOC	Limiting Oxygen Concentration
LOI	Loss on Ignition
LPG	Liquefied Propane Gas
LSLL	Level Switch, Low Level
MAC	Main Air Compressor
MCC	Motor Control Center
MS	Microsoft Corporation
NDIR	Nondestructive Infrared
NETL	National Energy Technology Laboratory
NFPA	National Fire Protection Association
NO_X	Nitrogen Oxides
NPDES	National Pollutant Discharge Elimination System
NPS	Nominal Pipe Size
OD	Outside Diameter
OSHA	Occupational Safety Health Administration
OSI	OSI Software, Inc.
P&IDs	Piping and Instrumentation Diagrams
PC	Pulverized Coal
PCD	Particulate Control Device
PDI	Pressure Differential Indicator
PDT	Pressure Differential Transmitter
PFBC	Pressurized Fluidized-Bed Combustion
PI	Plant Information
PLC	Programmable Logic Controller
PPE	Personal Protection Equipment
PRB	Powder River Basin
PSD	Particle Size Distribution
PSDF	Power Systems Development Facility
ΔP	Pressure Drop
PT	Pressure Transmitter
RFQ	Request for Quotation
RO	Restriction Orifice
RSSE	Reactor Solid Separation Efficiency
RT	Room Temperature
SCS	Southern Company Services, Inc.
SEM	Scanning Electron Microscopy

SMD	Sauter Mean Diameter
SRI	Southern Research Institute
SUB	Start-up Burner
TCLP	Toxicity Characteristic Leaching Procedure
TR	Transport Reactor
TRDU	Transport Reactor Demonstration Unit
TSS	Total Suspended Solids
UBP	Uncompacted Bulk Porosity
UND	University of North Dakota
UPS	Uninterruptible Power Supply
UV	Ultraviolet
VFD	Variable Frequency Drive
VOCs	Volatile Organic Compounds
WPC	William's Patent Crusher
XRD	X-Ray Diffraction
XXS	Extra, Extra Strong

Listing of Units

acfm	actual cubic feet per minute
Btu	British thermal units
°C	degrees celsius or centigrade
°F	degrees fahrenheit
ft	feet
FPS	feet per second
gpm	gallons per minute
g/cm^3	grams per cubic centimeter
g	grams
GPa	gigapascals
hp	horsepower
hr	hour
in.	inches
inWg	inches, water gauge
°K	degrees kelvin
kg	kilograms
kJ	kilojoules
kPa	kilopascals
ksi	thousand pounds per square inch
m	meters
MB	megabytes
mm	millimeters
MPa	megapascals
msi	million pounds per square inch
MW	megawatts
m/s	meters per second
MBtu	Million British thermal units
m^2/g	square meters per gram
μ or μm	microns or micrometers
nPm	nanoperm (1 nPm = $10^{-9}cm^2$)
dp_{50}	particle size distribution at 50 percentile
ppm	parts per million
ppm (v)	parts per million (volume)
ppm (w)	parts per million (weight)
lb	pounds
pph	pounds per hour
psia	pounds per square inch
psig	pounds per square inch gauge
ΔP	pressure drop
rpm	revolutions per minute
s or sec	seconds
scf	standard cubic feet
scfm	standard cubic feet per minute
V	volts
W	watts